

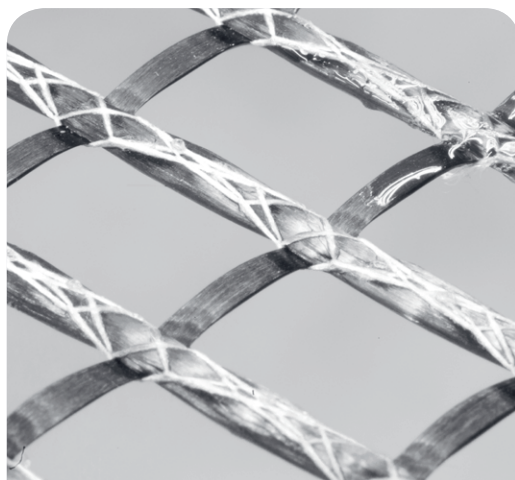


12. CARBON- UND TEXTILBETONTAGE



22. UND 23.
SEPTEMBER 2020
DRESDEN

TAGUNGSBAND





12. CARBON-UND TEXTILBETONTAGE

**„WENN DER WIND DER VERÄNDERUNG
WEHT, BAUEN DIE EINEN MAUERN UND DIE
ANDEREN WINDMÜHLEN.“**

Chinesische Weisheit

Die Veranstaltung wird gesponsert von:

CARBOCON

Inhalt >



Grußwort Manfred Curbach 6

VORTRÄGE TUDALIT 9

Ökobilanz der Carbonbetonbrücke in Ebingen 10

Carbonbeton für den Rosensteig II 12

Vorspannung als Mittel zum wirtschaftlichen und ressourcenschonenden Bauen mit Carbonbeton 14

Innovative Kanalhauben aus Carbonbeton für den Wärmeleitungsbau 16

Brückenverstärkung mit Textilbeton – Einblick in ein österreichisches Pilotprojekt 18

CUBE: Carbonbeton im Planungsalltag 20

Anwendung von vorgespannten CFK-Textilien zur Entwicklung dünnwandiger Betonbauteile 22

Dünne Verbundwerkstofffassaden in der Umsetzung im Fertigteilwerk – ein Erfahrungsbericht 24

Betonbewehrung für Anwendungen in tropischen Klimabedingungen 26

Carbonbeton im Brückenbau – aktuelle ZiEs beim Verstärken und Neubau 28

Verstärkung von Brücken spannungsrissskorrosionsgefährdetem Spannstahl im Carbonbeton 30

Neue Carbonfaserbewehrung für Beton-3D-Druck und andere digitale Betonbauverfahren 32

VORTRÄGE C³ 37

Shear Strengthening of RCT-Beams with CRC 38

Serviceability limit state design for carbon reinforced concrete structures 42

Mechanical model for the calculation of the splitting forces in textile-reinforced concrete 48

Bearing behaviour of Carbon-Textile-Reinforced Concrete Beams 54

Corrosion tests for hybrid construction with concrete, metal and carbon 60

Durability of FRP rebars in concrete structures – current test methods and approaches 70

Effect of Tension Forces on Shear Capacity of Thin Slab Segments 76

Carbon Textile Reinforced Concrete at ambient and high temperatures 82

Positioning aids for textile reinforcements 90

Strut-and-Tie Models for Carbon Reinforced Concrete Members 96

Bond behavior of carbon rebars and concrete 102

What can we learn from sustainability assessment: the case of carbon concrete composite structures 110

PARTNER & IMPRESSUM 120

Übersicht der C³-Partner 120

Impressum 125

Notizen 126

Grußwort >



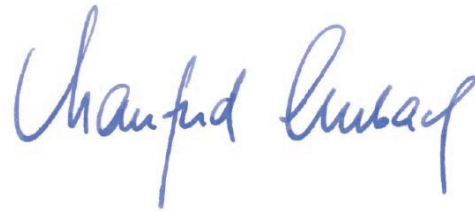
Liebe Teilnehmende,

das Jahr 2020 ist nicht nur durch Einschränkungen aufgrund der Corona-Pandemie und deren Folgen geprägt, sondern auch durch positive Dynamik in der Unternehmenskultur. Homeoffice, digitale Konferenzen und Videochats gehören mittlerweile zum Arbeitsalltag vieler Branchen und eröffnen fast unbegrenzte Möglichkeiten in der Digitalisierung. Auch wir gehen neue, digitale Wege und präsentieren uns im neuen Gewand. Dieses Jahr finden unsere Carbon- und Textilbetontage auf virtueller Bühne statt. In weniger als zwei Monaten hat das Organisationsteam Großartiges geleistet und ein digitales Format erschaffen, zu denen jeder von Ihnen, egal ob Referent, Aussteller oder Teilnehmer einen wesentlichen Beitrag geleistet hat. Besonders stolz sind wir darauf, dass die Konferenz nicht in irgendeiner digitalen Umgebung stattfindet, sondern im C³-Ergebnishaus CUBE. So präsentieren sich die Aussteller im Foyer des CUBE und die Vorträge werden in den realen Vortragsräumen gehalten. Die Teilnehmenden erhalten somit einen exklusiven Einblick in das Gebäudeinnere des weltweit ersten Hauses, das vollständig aus Carbonbeton errichtet wird und aktuell auf dem Campus der TU Dresden entsteht.

Die zukunftsweisende Carbonbeton-Technologie schreitet unaufhaltsam voran und findet bereits Einzug in den Markt. Sowohl im Neubau als auch im Bereich der Sanierung erlaubt die Alternative zum Stahlbeton eine wirtschaftliche, flexible und ressourcenschonende Bauweise. In den zahlreichen Vorträgen aus den Bereichen des Carbon- und Textilbetons wird das umfangreiche Repertoire an verschiedenen Referenzobjekten kurz und prägnant dargestellt. Zudem gewähren renommierte Wissenschaftlerinnen und Wissenschaftler Einblicke in die neuesten Ergebnisse.

Der C³ – Carbon Concrete Composite e. V. lobt zum ersten Mal einen „BEST PAPER AWARD“ für Forschende aus, deren herausragender wissenschaftlicher Beitrag zur Weiterentwicklung des Verbundmaterials Carbonbeton oder der Carbonbeton-Bauweise maßgeblich beitragen.

Freuen Sie sich auf einen spannenden Austausch mit Teilnehmenden aus 20 Nationen, eine Podiumsdiskussion mit erstklassigen Experten sowie eine abwechslungsreiche Themenagenda.



Prof. Dr.-Ing. Dr.-Ing. E.h.

Manfred Curbach

CPC-Technologie – die neue Betonbauweise

CPC-Betonplatten basieren auf der «**carbon prestressed concrete**»-Technologie, die aus einem langjährigen Forschungsprojekt der Zürcher Hochschule für Angewandte Wissenschaften Winterthur (ZHAW) und der Silidur AG, Andelfingen, hervorging.

Die filigranen und dennoch belastbaren Platten eignen sich für zahlreiche Anwendungen im Bauwesen und im Landschaftsbau.

Mit CPC-Platten können zahlreiche Bauprodukte realisiert werden:

- Fuß- und Radwegbrücken
- Verkehrsbrücken
- Brückenbeläge
- Balkonplatten
- Treppen
- Bodenplatten
- Fassadenelemente
- Betonmöbel



✓ CPC ist robust.

✓ CPC ist leicht einzubauen.

✓ CPC ist leicht.

✓ CPC ist unterhaltsarm.

✓ CPC ist ökologisch.

✓ CPC ist kostengünstig.



Für die Fabrikation der Carbonbewehrung wie auch der Betonplatten wurden eigene Verfahren und verschiedene Fertigungsmaschinen entwickelt. Die Herstellung dieser Platten wurde patentrechtlich geschützt. In einem eigens eingerichteten Bearbeitungszentrum werden aus diesen Halbfabrikaten beliebige Plattenformate geschnitten und konfektioniert.



In Deutschland erfolgen die Herstellung und der Vertrieb der CPC-Platten durch die Vetra Betonfertigteilwerke GmbH. Diese ist ein 100-prozentiges Tochterunternehmen der Holcim (Deutschland) GmbH. Kerngeschäft von Vetra ist die Herstellung und der Vertrieb von individuell geplanten und qualitativ hochwertigen Betonfertigteilen für den Industrie- und Hausbau sowie den Agrarbau.

Beratung und Kontakt

Simon Liebl
Holcim (Deutschland) GmbH
Leiter Business Development
(+49) 172 6118814
simon.liebl@lafargeholcim.com

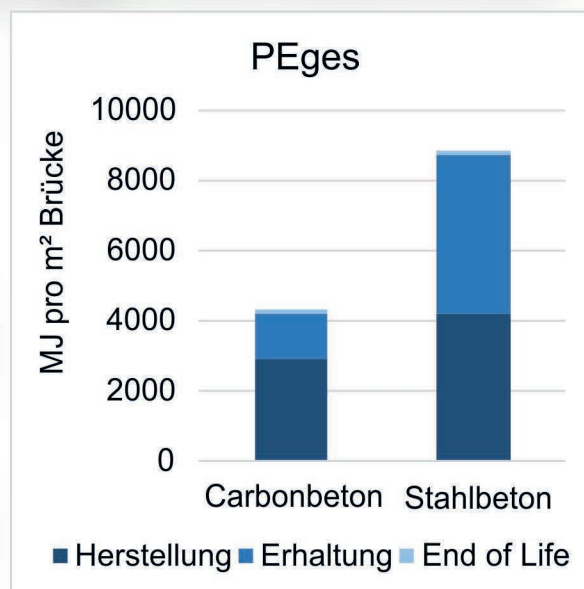
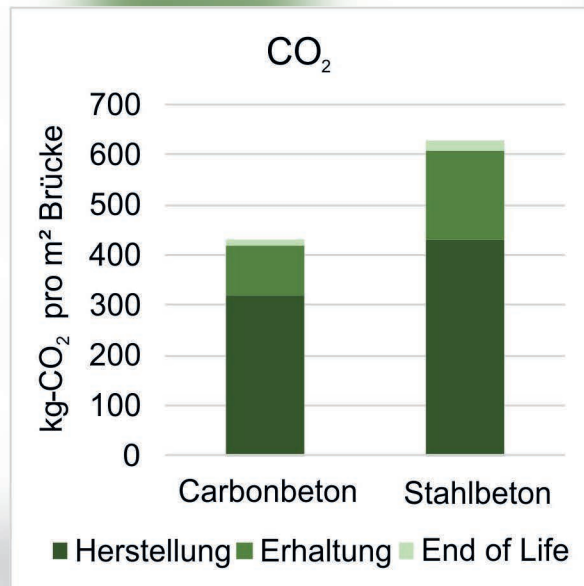
Stefan Gramberg
VETRA Betonfertigteilwerke GmbH
Geschäftsführer
(+49) 49 549283-10
stefan.gramberg@vetra.de

VORTRÄGE ✓

TUDALIT®

Leichter bauen – Zukunft formen

Ökobilanz der Carbonbetonbrücke in Ebingen



Die erste Carbonbetonbrücke in Deutschland wurde in dem Jahr 2015 in Albstadt errichtet. Hierbei wurde anstelle der herkömmlichen Stahlbewehrung eine Carbonbewehrung verwendet. Diese innovative Bewehrung hat zwei maßgebende Vorteile. Zum einen können Zugbruchspannungen von über 4000 N/mm² erreicht werden und zum anderen ist eine hohe Korrosionsbeständigkeit gegeben. Dank dieser Eigenschaften können geringe Betondeckungen realisiert und auf die zusätzliche Schutzschicht verzichtet werden. Dadurch entsteht ein nachhaltiges Brückenbauwerk, dessen Ökobilanz im Vergleich zu einem äquivalenten Stahlbetontyp positiver ausfällt.

Die Carbonbetonbrücke in Albstadt ist eine 15,5 m lange Brücke mit einem 3 m breiten Trogquerschnitt. Aufgrund der korrosionsresistenten Bewehrung konnten Wandstärken von 7 cm und eine Plattendicke von 9 cm realisiert werden. Für diese Brücke wurde eine Ökobilanz erstellt. Die Ökobilanz wurde mit einer Stahlbetonbrücke verglichen. Hierfür wurden die gleichen Spannweiten und Querschnittstypen gewählt. Aufgrund der erforderlichen Betondeckung für die Stahlbewehrung ergaben sich eine Wand- und Plattenstärke von 25 cm.

Bei einer genaueren Betrachtung der beiden Varianten fällt besonders die benötigte Betonmenge für den Oberbau auf. Während die Carbonbetonbrücke 6,2 m³ Beton mit der Güte C70/85 benötigt, wird für die Stahlbetonvariante 18,9 m³ C30/37 verwendet. Die Masse der Bewehrung kann schwer verglichen werden, da zwei verschiedene Baustoffe eingesetzt wurden. Die Stahlbetonvariante benötigt ca. 2.650 kg Stahlbewehrung und die Carbonbetonbauweise ca. 210 kg Carbongelege mit Epoxidharztränkung.

Bei der Erstellung der Ökobilanz wurde der gesamte Herstellungsprozess der untersuchten Brückenkonstruktionen betrachtet. Dazu gehören sowohl der Überbau als auch die Widerlager und das Geländer. Es wurden die Rohstoffgewinnung, der Transport der Rohstoffe zum Produktionsort und die Produktionsprozesse berücksichtigt. Des Weiteren umfassen die Untersuchungen ebenfalls die vorhandenen Transportwege zur Baustelle. Der dritte berücksichtigte Punkt ist die Nutzungsphase und umfasst die Instandhaltung, die Instandsetzung, den Austausch und die Modernisierung. Es wurde ein Zeitraum von 100 Jahren festgelegt. Abschließend wurde die Entsorgungsphase (End of Life) betrachtet und die Abfallbehandlung oder alternativ die Beseitigung integriert. Somit liegt eine

Ökobilanz von der „Wiege bis zur Wiege“ für die betrachteten Bauwerke vor.

Die Ergebnisse der Ökobilanz sind wie folgt (Bild 1):

- Bei der Betrachtung des ersten ökobilanziellen Leitindikators des Treibhauspotentials (GWP) stellt sich hier heraus, dass über den gesamten Lebenszyklus bzw. den 100 Jahre-Betrachtungszeitraum bei der Carbonbetonbrücke ca. 30 % weniger CO₂ freigesetzt werden als bei der Stahlbetonvariante.
- Bei der Betrachtung des zweiten ökobilanziellen Leitindikators des Gesamtprimärenergiebedarfs (PEges) liegt der Verbrauch bei der Carbonbetonbrücke über den gesamten Lebenszyklus 50 % unterhalb des Stahlbetonquerschnitts.

Eine Ursache dafür ist der geringere Materialaufwand, insbesondere beim Beton, sowohl für die Bauwerksgründung wie auch für den Oberbau. Maßgebend sind allerdings die geringeren Instandhaltungsarbeiten und die dafür notwendigen Materialien. Hier sollte insbesondere die Asphaltdeckschicht erwähnt werden. Nach der Nutzungsdauer von 25 Jahren wird diese bei der Stahlbetonvariante erneuert. Das freigesetzte CO₂ und die Primärenergie haben einen enormen Einfluss auf die Gesamtbetrachtung der Ökobilanz.

Sergej Rempel studierte Bauingenieurwesen an der RWTH Aachen. Anschließend war er ab 2011 im Ingenieurbüro HS&P in Köln als Tragwerksplaner tätig. Ab 2012 arbeitete er als wissenschaftlicher Mitarbeiter am Institut für Massivbau der RWTH Aachen, wo er das Tragverhalten und die Zuverlässigkeit von Textilbetonbauteil untersuchte. Seit 02/2018 ist er als Projektleiter bei solidian GmbH angestellt und unter anderem für die Bemessung von Textilbetonbauteilen sowie Brücken verantwortlich. Anfang 2020 erhielt er den Ruf an die Hochschule Augsburg und ist dort Professor für das Lehrgebiet Massivbau.



Carbonbeton für den Rosensteinsteg II



Durch den Wiederaufbau des Rosensteinstegs II erhält die Stuttgarter Öffentlichkeit eine der für das Stadtbild so charakteristischen Brücken in Leichtbauweise zurück. Der erstmals 1977 errichtete Seilbindersteg musste im Jahr 2014 dem Ausbau des Verkehrsknotens B10/B14 am Mineralbad Leuze weichen und konnte schließlich 2019 oberhalb der fertiggestellten Tunnelsegmente wiederaufgebaut werden. Da die schlanken Überbauplatten mit einer Stärke von lediglich 10 cm schon etliche Jahre vor ihrem Abbau erhebliche Korrosionsschäden aufwiesen, entschieden sich Planer und Bauherr für den Wiederaufbau für ein Bewehrungsmaterial ohne Korrosionsrisiko.

Entsprechend der ursprünglichen Planung in den 1970er-Jahren wurden die Betonplatten des Überbaus damals mit gewöhnlicher Stahlbewehrung und einer Betondeckung von nur 30 mm auf der Oberseite und 20 mm auf der Unterseite ausgebildet. Wie bei zahlreichen Projekten aus jener Zeit wurde auch hier in den darauffolgenden Jahren deutlich, dass eine solch geringe Betondeckung bei weitem keinen dauerhaften Korrosionsschutz über die geplante Lebensdauer sicherstellen kann. Bis zum Abbau des Steges bildeten sich erhebliche Korrosionsschäden mit großflächigen Abplatzungen an der Bauteilunterseite aus.

Da für den Wiederaufbau des Steges eines der alten Widerlager wiederverwendet wurde, sollten auch die Auflagerbeanspruchungen und folglich das Eigengewicht des Überbaus nicht nennenswert erhöht werden. Aus diesem Grund wurde als Alternative zu einer Stahlbetonplatte mit größerer Betondeckung auch erstmals ein alternatives Bewehrungsmaterial in Erwägung gezogen. In der Wahl zwischen verzinktem Bewehrungsstahl, Edelstahlbewehrung und textiler Bewehrung aus glasfaser- oder carbonfaserverstärktem Kunststoff (GFK bzw. CFK) konnte sich eine textile Mattenbewehrung aus CFK aufgrund der geringen erforderlichen Betondeckung und eines günstigen Tragverhaltens in der Platte durchsetzen.

Im Rahmen des Zustimmungsverfahrens wurden vier Überbauplatten an der TU Berlin in zerstörender Prüfung auf ihre Querkraft- und Biegetragfähigkeit sowie die Tragfähigkeit des Geländerschlusses überprüft. Die Biegetragfähigkeit wurde einmal unter statischer Last (Belastung bis zum Bruch) und einmal unter zyklischer Last (15 Lastwechsel bis zur Bemessungslast, anschließend Belastung bis zum Bruch) untersucht. Die exper-

imentellen Bauteilversuche liefern konservative Ergebnisse im Grenzzustand der Tragfähigkeit sowie der Gebrauchstauglichkeit und bestätigen die in der statischen Berechnung ermittelten Bauteilwiderstände sowie das angenommene Bauteilverhalten [1]. In den Biegeversuchen zeigte sich weiterhin eine deutlich wahrnehmbare Bauteildurchbiegung, welche als ausreichende Versagensvorankündigung gewertet werden kann.

Mit der Carbonbewehrung der Firma solidian und der Betonage im Werk der Firma informbeton in Schwepnitz konnte eine durchgehend hohe Qualität der Betonelemente erreicht werden. Der Seilbindersteg inklusive aller Betonelemente sowie Geländer und Berührschutz wurden innerhalb von einem Wochenende bei Außerbetriebnahme der U-Bahn von der Firma Stahlbau Urfer im Auftrag des Generalunternehmers Ed. Züblin AG montiert. Durch die gute Zusammenarbeit zwischen dem Bauherrn (Tiefbauamt Stuttgart), den Planern (schlaich bergemann partner), Prüfern (Peter und Lochner Ingenieure) und Gutachtern (FG Entwerfen und Konstruieren – Massivbau, TU Berlin) sowie allen beauftragten Firmen konnten die Vergabe, Herstellung und Prüfung der Überbauelemente aus Carbonbeton ohne Verzögerungen im Gesamtzeitplan durchgeführt werden und der Steg konnte zum Ende des Jahres 2019 eröffnet werden.

[1] Rettinger M.; Hückler A.; Andelfinger J.: Der Wiederaufbau des Rosensteinstegs II in Stuttgart mit Überbauelementen aus Carbonbeton. In: Bauingenieur 95 (2020), Heft 7-8, S. 243-253.

Martin Rettinger, M.Sc.

studierte Bauingenieurwesen an der TU Darmstadt mit einem einjährigen Aufenthalt an der University of Sheffield, wo er erstmals in der Lehre mit carbonfaserverstärkten Kunststoffen in Kontakt kam. Von 2016 bis 2020 war er als Tragwerksplaner bei schlaich bergemann partner tätig und bearbeitete dort unter anderem das in diesem Beitrag vorgestellte Projekt. Seit Anfang 2020 ist er Mitarbeiter am Fachgebiet Entwerfen und Konstruieren - Massivbau an der TU Berlin und forscht über modulare Tragstrukturen und Carbonbeton.



Vorspannung als Mittel zum wirtschaftlichen und ressourcenschonenden Bauen mit Carbonbeton



Carbonbeton verspricht extrem dauerhafte und belastbare Bauwerke, weil die Bewehrung nicht korrodieren kann. Die hohe Festigkeit des Carbons wird oft mit der Erwartung verbunden, gleichzeitig dünnwandig, schlank bzw. allgemein ressourcensparend bauen zu können. Die Konstruktionspraxis zeigt jedoch, dass diese Erwartungen teils an klare technische Grenzen stoßen. Anwendungsfälle, bei denen die Bauteilabmessungen vorrangig aus der erforderlichen Betondeckung resultieren, können wegen der geringeren erforderlichen Betondeckung der Carbonbewehrung nennenswerte Einsparungen bei der Betonmenge realisieren. Dies gelingt jedoch nur, solange diese Bauteile im Grenzzustand der Gebrauchstauglichkeit (GZG) ganz oder überwiegend ungerissen bleiben. Zu diesen Anwendungsfällen zählen dünnwandige Fassadenelemente, also eher gering belastete Bauteile.

Bei Anwendungen mit höherer Belastung, bei denen im GZG mit Rissbildung zu rechnen ist, lässt sich Carbonbewehrung hingegen kaum wirtschaftlich ausnutzen. Und auch schlankere Konstruktionen als mit herkömmlichen Stahlbetonbeton sind kaum realisierbar. Dies ergibt sich regelmäßig im Rahmen der Querschnittsbemessung aus den Grenzdehnungen von Carbon und Beton. Versucht man die sehr hohe Zugfestigkeit der Carbonbewehrung im Grenzzustand der Tragfähigkeit (GZT) auszunutzen, sieht man sich mit sehr großen Bauteilverformungen im GZG konfrontiert, die nur in wenigen Anwendungsfällen akzeptabel sind. Zudem führen hohe Dehnungen der Zugzone zur Überlastung der dann zunehmend eingeschnürten Druckzone. Dieser Effekt kann durch hochfeste Betone teilweise kompensiert werden, führt aber generell zu einer nur geringen Ausnutzung der Carbonbewehrung oder verhindert schlanke Bauteilabmessungen.

Die Anwendung der Vorspanntechnik bietet eine Lösung für diese Problematik. Vorspannung ermöglicht eine vollständige Ausnutzung und damit wirtschaftlichere Anwendung der Carbonbewehrung. Gleichzeitig reduziert die Vorspannung die Verformungen soweit, dass trotz der hohen Materialdehnungen sehr schlanke und damit materialsparende und elegante Konstruktionen möglich werden. Dabei kann grundsätzlich auf jahrzehntelange Erfahrungen mit Spannbeton zurückgegriffen werden.

Bei der Vorspannung von Carbon muss allerdings noch geklärt werden, wie trotz des spröden und unangekündigten Versagens von Carbon am Bau-

teil ein unangekündigtes Versagen vermieden werden kann. Denn der Anteil der Vordehnung an der rechnerischen Bruchdehnung steht für eine Versagensankündigung nicht mehr zur Verfügung. Die Vordehnung sollte mindestens so hoch gewählt werden, dass die Verformungsgrenzen im GZG eingehalten werden können. Andererseits sollte die Vordehnung nur so hoch gewählt werden, dass im GZT eine hinreichende Ankündigung eines drohenden Versagens durch eine ausgeprägte Rissbildung bzw. Verformung gewährleistet werden kann, wobei aktuelle Regelwerke hier keine konkreten, auf Carbonbewehrung übertragbaren Vorgaben enthalten. Die Vorspannung könnte z.B. so gewählt werden, dass ein Verlassen des Lastniveaus des GZG durch eine deutlich sichtbare Rissbildung angezeigt wird. Diese Überlegungen führen je nach Anwendung zu einer eher moderaten Vordehnung in Höhe von nur 20-40 % der Materialfestigkeit. Dies entspricht dem in Deutschland bisher nur vereinzelt umgesetzten Konzept der Teilvorspannung. Um ein Verlassen des GZG sichtbar anzuzeigen, liegt es nahe, auf eine Oberflächenbewehrung teils bewusst zu verzichten, was die Wirtschaftlichkeit einer Carbonbetonkonstruktion signifikant verbessert.

Die wirtschaftlichste Art der Vorspannung ist die Vorspannung im sofortigen Verbund, weil keine aufwendigen Ankerkonstruktionen nötig sind. Wiederverwendbare, robuste und zuverlässige Verankerungen zur Einleitung der Vorspannkraft vorausgesetzt, ermöglicht diese Art der Vorspannung ein sehr wirtschaftliches und damit automatisch ressourcenschonendes Konstruieren und Bauen mit Carbonbeton.

Dr.-Ing. Frank Jesse

studierte Bauingenieurwesen an der TU Dresden. Die anschließende Promotion am Institut für Massivbau wurde zum Ausgangspunkt einer intensiven Beschäftigung mit dem vielseitigen Material Carbonbeton. Später wechselte er zu der in Bautzen ansässigen Hentschke Bau GmbH und arbeitet dort an der praktischen Realisierung von Carbonbeton unter industriellen Bedingungen. Das Bauunternehmen konzentriert sich vor allem auf wirtschaftliche und technologische Aspekte unter den üblichen Bedingungen einer werkmäßiger Herstellung und im Ortbetonbau.



Innovative Kanalhauben aus Carbonbeton für den Wärmeleitungsbau

MASSE [t]
GESAMT

3,98

MASSE [t]
GESAMT

1,85

MASSE [kg]
STAHL

214

MASSE [kg]
CARBON

8



Die Anwendungsmöglichkeiten für Carbonbeton liegen beim Neubau in den Bauteilgruppen Fassaden, Außenwände, hochbelastete Unterzüge und Decken sowie bei Modulbauten. Des Weiteren finden sich Anwendungsmöglichkeiten in der Instandsetzung und Verstärkung bestehender baulicher Anlagen. Bautechnologisch scheint die Fertigteilbauweise besonders prädestiniert für schlanke Carbonbetonbauteile zu sein und wird daher aktuell vorrangig angewendet. Ein Grund dafür ist, dass in Fertigteilwerken gleichbleibend optimale Rahmenbedingungen (Witterung, Schalung und Rüstung, spezialisierte Fertigungsgruppen) vorliegen, so dass die Herstellung filigraner und qualitativ hochwertiger Bauteile mit geringerem Aufwand zu realisieren ist als in der Ortbetonbauweise.

Für die vorteilhafte Substitution von Stahlbeton durch Carbonbeton eignen sich generell Einsatzgebiete, in denen hohe Expositionsanforderungen vorherrschen. Der Fernwärmeleitungsbau ist ein Anwendungsszenario dafür. Für den Transport von innerstädtischer Fernwärme werden u. a. Rohrleitungen eingesetzt, die streckenweise mit einem überdeckenden Bauwerk geschützt sind. Die Leitungen werden entlang der Trasse mit Kanalhauben, bisher als Stahlbetonfertigteile ausgeführt, abgedeckt mit dem Vorteil der Revisionierbarkeit. Durch den dauerhaften Kontakt mit dem Erdreich sind die Kanalhauben aus Stahlbeton korrosionsgefährdet. Neben möglichen oberirdischen Nutzungsänderungen mit höheren Auflasten stellt daher vor allem die Korrosion der Stahlbewehrung ein Hauptproblem dar. Im Havariefall können für den Betreiber hohe Kosten durch die auftretenden Versorgungsstörungen und die erforderliche Sanierung der ober- und unterirdischen Infrastruktur entstehen. Deshalb werden bestehende Kanalhauben häufig vorsorglich durch neue Stahlbetonhauben ersetzt. Bei diesen sehr massiven Kanalhauben mit 5 Tonnen und mehr Bauteilgewicht besteht jedoch erneut die Gefahr der Korrosion.

In einer abgeschlossenen Machbarkeitsstudie – gefördert von der Sächsischen Aufbaubank (SAB) – wurde die bestehende Bauweise für Kanalhauben auf das Einsatzpotenzial durch den Einsatz von Carbonbeton untersucht. Im Vergleich zur Stahlbetonbauweise ist neben den Kriterien der Bauteilqualität, der Ressourceneinsparung, den Herstellungsbedingungen und dem Arbeitsschutz die Wirtschaftlichkeit das entscheidende Kriterium für den Einsatz von Carbonbeton. Ziel war u. a. die

Wirtschaftlichkeitsuntersuchung am Beispiel einer carbonbewehrten Kanalhaube für nicht begehbare Fernwärme Kanäle. Für die monetäre Untersuchung beider Bauarten war es notwendig, Kostenansätze für Material-, Lohn-, Schalungs- und Gerätekosten zu ermitteln. Grundlage für die Bestimmung der Aufwandswerte und Kostenansätze der Stahlbetonbauweise bildeten belastbare Angaben in der Literatur, validierte Erfahrungswerte und spezifische Vorgaben aus konkreten Angeboten von externen Leistungserbringern. Für die Ermittlung der Lohnkosten waren die Aufwandswerte für die herstellungsrelevanten Vorgänge erforderlich. Aufwandswerte für die Herstellung von Stahlbetonbauteilen sind allgemein bekannt. Für die Herstellung von Carbonbetonbauteilen wurden die Aufwandswerte abgeschätzt und unter Zuhilfenahme der Ergebnisse aus anderen Forschungsprojekten validiert. Die Vergleichsbasis stellten in dieser Betrachtung funktionsgleiche Bauteile aus Carbon- und Stahlbeton in Fertigteilbauweise dar, welche für gleiche statische Lastfälle bemessen wurden. Bei gleicher Funktionalität ergaben sich für die Bauteile aufgrund unterschiedlicher Baustoffkennwerte signifikant unterschiedliche Abmessungen.

Mit der entwickelten Carbonbeton-Kanalhaube konnten bei gleicher statischer Tragwirkung ca. 50 % der Bauteilmasse eingespart werden. Im Wirtschaftlichkeitsvergleich wurde zudem die monetäre Vorteilhaftigkeit der Carbonbetonbauweise nachgewiesen.

Dr.-Ing. Jan Kortmann

studierte von 2005 bis 2010 an der TU Dresden Bauingenieurwesen und war im Anschluss als Planungsingenieur in einem Consultingbüro angestellt. Seit Mai arbeitet er als wissenschaftlicher Mitarbeiter am Institut für Baubetriebswesen der TU



Dresden und ist dort seit Ende 2019 als Oberassistent tätig. Der Promotionsabschluss erfolgte 2020 zum Thema „Recyclingfähigkeit von Carbonbeton“. Herr Dr. Kortmann ist als Vorhabenleiter für die Forschungsschwerpunkte Herstellung, Recyclingfähigkeit und Gesundheitsschutz im Zusammenhang mit Carbonbeton verantwortlich.

Brückenverstärkung mit Textilbeton – Einblick in ein österreichisches Pilotprojekt



In Österreich gibt es circa 36.300 öffentlich verwaltete Brücken. 43 % davon wurden zwischen 1960 und 1990 errichtet. Steigende Verkehrsbelastungen, erhöhte Dauerhaftigkeitsprobleme und Veränderungen im Normungswesen stellen dabei Erhalter, Ingenieure und Baufirmen gleichermaßen vor große Herausforderungen. Es stellt sich die Frage, wie auch zukünftig ein sicheres und stabiles Verkehrsnetz garantiert werden kann. Dabei zeigt speziell die Bauweise Textilbeton ein großes Potential, um Betontragwerke zeitgemäß zu verstärken und sanieren. Eine dauerhafte und leistungsfähige Bewehrung, ein geringes Konstruktionseigengewicht und der Einbau mittels praxiserprobter Bauabläufe sind besondere Vorteile. Jedoch gibt es in Österreich für die Bauweise noch kein Regelwerk. Daher ist der Einsatz bei Pilotanwendungen ein wesentlicher Entwicklungsschritt.

In diesem Zusammenhang wird aktuell anhand einer Brücke in Österreich die Verwendung von Textilbeton zur Querkraft- und Torsionsverstärkung eines Plattenbalken-Tragwerks untersucht. Die Krumbachbrücke ist eine dreifeldrige, längs vorgespannte Stahlbetonbrücke und wurde 1983 für den Verkehr freigegeben. Sie ist eine wichtige Verbindungsbrücke für den Tourismusort Damüls in Vorarlberg. Die Brücke liegt in einem Kreisbogen mit einem mittleren Radius von 100 m und hat eine Länge von 120 m. Beide Randfelder, mit jeweils einer Spannweite von 36 m, sind mit einem 4-stegigen Plattenbalkenquerschnitt ausgeführt. Aktuell zeigen sich dort starke Verformungen und Schrägrissbildungen an den Stegflächen. Ziel ist es ein Konzept zu erarbeiten, welches eine Restlebensdauer von ca. 50 Jahren zulässt. Das Konzept zur Aufnahme der Defizite der Plattenbalken besteht in Abhängigkeit der Belastung aus 2 bis 3 cm dünnen Textilbeton U-Schalen. Zusätzlich wird ein Textilbetonkragen über eine Länge von 60 cm, seitlich der Stegflächen, auf der Unterseite der Fahrbahnplatte weitergeführt. In Kombination mit einem Verankerungssystem, bestehend aus einer Ankerplatte und einem Verbundankersystem, wird somit die Endverankerung des Textils ermöglicht. Eine Besonderheit bei der Bewehrung selbst ist, dass sie im Stickprozess hergestellt werden soll. Sie besteht aus ebenen sowie formangepassten Carbon-Gitterstrukturen.

Die Herstellung der Textilbetonschicht vor Ort ist lagenweise, im Dichtstrom-Nassspritzverfahren, geplant. Die Entscheidungsgrundlagen eines solchen Technologie-Einsatzes wurden in unterschiedlichen Planungs- und Entwicklungsphasen

erarbeitet. Ausgangspunkt war eine Machbarkeitsstudie. Danach folgten die weiteren Schritte: Brückenerkundung, statische Nachrechnung, Konzeptentwicklung, Untersuchungen an Klein- und Großbauteilversuchen, Kostenschätzung, Lebenszykluskostenermittlung sowie Risikomanagement mittels Identifikation von Chancen und Bedrohungen. Darüber hinaus wurde ein Variantenvergleich mit einer konventionell stahlbewehrten Spritzbetonschicht erarbeitet. Die Arbeiten wurden vom Ingenieurbüro Prof. Feix Ingenieure GmbH und vom Arbeitsbereich Massivbau und Brückenbau der Uni Innsbruck in den letzten beiden Jahren durchgeführt. Im Zuge der Bearbeitung sind zusätzliche Schäden und Defizite am Quertragwerk der Fahrbahnplatte bekannt geworden. Grundsätzlich haben sich die Projektbeteiligten gemeinsam für den Einsatz von Textilbeton auf Basis der Projektausarbeitung entschieden, nun muss jedoch zuerst ein Lösungskonzept für das Defizit der Fahrbahnplatte erarbeitet werden. Sodann soll einer Ausführungsplanung nichts mehr im Wege stehen. Für den Einsatz einer neuen Technologie braucht es Mut, Ehrgeiz und Engagement. Deshalb bedanken wir uns bei allen Projektbeteiligten für die tolle Zusammenarbeit. Spezielle Anerkennung möchten wir an die Landesverwaltung Vorarlberg, vertreten durch die Abteilung Straßenbau (VIIb), Herrn DI Armin Wachter (Fachbereichsleiter) und Herrn Ing. Norbert Plattner (Projektleiter) richten.

Matthias Egger und **Christoph Waltl** studierten beide Bauingenieurwesen.

Neben Ingenieurertätigkeiten in der Praxis arbeiten sie seit 2014 am AB für Massiv- und Brückenbau der Uni Innsbruck. Zu deren Forschungsschwerpunkte zählen Themen im Brücken- und Textilbetonbau. Seit 2018 sind sie im FFG Projekt Spin-Off-Fellowship „concreteX“ tätig. Gemeinsam mit Prof. Feix verfolgen sie das Ziel, die Voraussetzungen für ein FTI (Forschung, Technologie und Innovation) orientiertes Unternehmen im Bereich des Textilbetonbaus zu schaffen. Damit sollen die gewonnenen Erkenntnisse in der Praxis umgesetzt werden.



TUDALIT®
Leichter bauen – Zukunft formen

carbon
concrete
composite

CUBE: Carbonbeton im Planungsalltag



In der bisherigen Forschung und Entwicklung wurde der Nachweis erbracht, dass mit Carbonbeton tragende Konstruktionen modelliert, berechnet, und hergestellt werden können. Mit dem Projekt CUBE stellen wir uns nun den Herausforderungen des öffentlichen Baurechts und der vertragsgebundenen Bauplanung, besonders der Kostenermittlung, des Tragwerksnachweises sowie der Ausschreibung von Bauleistungen.

Die Kostenermittlung im Bau stützt sich üblicherweise auf allgemein verfügbare Kennwerte, Erfahrungen des Planers sowie Bieterpreise in der Angebotsphase. Für Carbonbetongebäude sind Kostenkennwerte und Erfahrungen jedoch nicht verfügbar. Für die Kostenschätzung wurden deshalb Kennwerte für vergleichbare Gebäude mit einem von uns eingeschätzten prozentualen Aufschlag versehen und in der Kostenberechnung für die geplanten Carbonbeton-Konstruktionen Materialpreise ermittelt sowie Arbeitszeit und Geräteaufwand eingeschätzt. Nach erfolgter Ausführungsplanung wurden dann erste Bieterangebote eingeholt, in denen deutlich wurde, dass wir die Risiken einer nicht genormten Bauweise, besonders in der Gewährleistung stark unterschätzt hatten. Durch vorgezogene Technologietests und genauere Definition der Anforderungen in Zusammenarbeit mit den Bietern sollen diese Risiken minimiert und damit die berechneten Baukosten eingehalten werden. Nach Abnahme der Bauleistungen stehen erstmals tatsächliche Baukosten zur Verfügung, die zukünftig für die Planung mit Carbonbeton genutzt werden können.

Mit der Tragwerksplanung sind die Nachweise einer ausreichenden Gebäude- und Bauteilstandsicherheit zu erbringen, in geltenden Vorschriften und Richtlinien werden dafür verbindliche Materialkennwerte und Berechnungsalgorithmen ausgewiesen. Für die Verwendung von Carbon als Betonbewehrung gibt es bisher keine allgemein gültigen Normen oder Bewehrungskriterien, auch die Produkte am Markt weisen unterschiedliche Eigenschaften auf. Für alle relevanten Bauteile und Materialien im Vorhaben war deshalb eine Zustimmung im Einzelfall zu erwirken. Grundlage dafür bildeten statische Vorabberechnungen, experimentelle Untersuchungen sowie die Durchführung von Technologietests. Da in der Projektlaufzeit kein allgemein gültiger Berechnungsalgorithmus zum Querkraftnachweis aufgestellt werden konnte, wurden alle relevanten Betonquerschnitte ohne Querkraft-Bewehrung nachgewiesen und teilweise konstruktiv mit Carbon-Stäben als offene Bügel bewehrt. Um die hohen Zugfestigkeiten des

Carbons auszunutzen, wurde weitestgehend die Betonfestigkeitsklasse C50/60 gewählt. Nach Erhalt der ZIE konnten die statische Berechnung und die Ausführungsplanung erstellt, bauaufsichtlich geprüft und zur Ausführung freigegeben werden. Mit der gelungenen Nachweisführung für CUBE steht ein Beispiel für zukünftige Planungen zur Verfügung, aufgrund der Komplexität des Baustoffes Carbonbeton aber noch kein allgemein zugelassenes Bauverfahren.

Für die Ausschreibung von Bauleistungen werden Texte des Standardleistungsbuchs oder konkreter Anbieter verwendet, die auf anerkannten Regeln der Technik basieren und eindeutige Beschreibungen der auszuführenden Leistungen in Menge und Qualität ermöglichen. Solche standardisierten Beschreibungen, Normen und Richtlinien liegen für Carbonbeton-Bauteile nicht vor. Im Projekt wurden deshalb frühzeitig in einer funktionalen Leistungsbeschreibung Zielkriterien für die zu erbringenden Bauleistungen formuliert und in der laufenden Projektentwicklung mit den Festlegungen aus der Zustimmung im Einzelfall fortgeschrieben sowie die Bieter fachlich eingebunden, um technologisch und wirtschaftlich umsetzbare Lösungen zu erarbeiten. Nach Abschluss der Baumaßnahmen werden anhand der umgesetzten Leistungen Ausschreibungstexte erstellt, die zukünftig zur Einholung von Angeboten und zur Qualitätssicherung in der Carbonbetonbauweise verwendet werden können.

Dipl.-Ing. Marén Kupke

ist Prokuristin bei der AIB GmbH. Sie ist als Architektin, Energieberaterin, Sachverständige Nachhaltiges Bauen und Sachverständige Brandschutz tätig. Seit 2008 arbeitet sie in der Textilbeton-Forschung und -Entwicklung mit und war von 2009 bis 2010 Managerin des Netzwerks TEXTON.



Dipl.-Ing. Hendrik Ritter

ist Tragwerksplaner bei der ASSMANN Beraten+Planen GmbH am Standort Dresden. Seit dem Studium ist er ununterbrochen in der Tragwerksplanung tätig, vor allem in der Betonfertigteil- und Hochbauplanung, seit 2014 auch in der Textilbeton-Forschung und -Entwicklung.



Anwendung von vorgespannten CFK- Textilien zur Entwicklung dünnwandiger Betonbauteile



Die Erfolgsgeschichte von Spannbeton basiert auf der Verwendung von hochfestem Spannstahl, mit dem große Druckkräfte in den Beton eingebracht werden können. Dünnwandige Betonkonstruktionen erfordern jedoch häufig erhebliche Dicken, um die Korrosion der Stahlbewehrung zu vermeiden. In dieser Arbeit wird kurz die Verwendung von vorgespanntem kohlefaserverstärktem Polymer (CFK) als Textilstruktur für die Entwicklung dünnwandiger Betonbauteile vorgestellt.

Mit vorgespannter Carbonbewehrung kann die Haltbarkeit von Betonkonstruktionen erheblich erhöht werden. Insbesondere, wenn sie Umgebungsbedingungen wie Frost- und Tausalz oder zyklischen Belastungen ausgesetzt sind. Da die Betondeckung nur zur Kraftübertragung und nicht zum Korrosionsschutz benötigt wird, kann kohlefaserverstärkter Beton extrem schlank, leicht und damit ressourcenschonend sein. Betonelemente mit schlaffer Carbonbewehrung, die einer Biegung ausgesetzt sind, können jedoch im Allgemeinen die hohe Zugfestigkeit von CFK nicht ausnutzen, ohne große Krümmungen und damit Risse aufzuweisen. Eine elegante Option, um dem entgegenzuwirken, ist die Verwendung der Vorspannungstechnik. Durch das Vorspannen werden Verformungen der schlanken kohlefaserverstärkten Betonelemente reduziert und Risse im Gebrauchszustand zumeist vermieden. Darüber hinaus ermöglicht die Verwendung von hochfestem Beton die Einführung besonders hoher Vorspannkräfte. Vorgespannte CFK-Elemente führen zu schlankeren und damit wirtschaftlicheren und haltbareren Strukturelementen.

Im Vergleich zur Vorspannung mit CFK-Stäben oder -Litzen können durch die Verwendung von CFK-Textilien die Querschnitte weiter reduziert werden.

Vorspannungstechnologien wurden für verschiedene Anwendungen wie Platten und doppelt gekrümmte Betonschalen entwickelt und angepasst und durch experimentelle Tests validiert. In Zusammenarbeit mit den Projektpartnern TU Berlin, GINKGO, Solidian und Kneitz wurden mehrere vorgespannte CFK-Textilbetonelemente mit unterschiedlichen Geometrien und Textilien hergestellt. Infolgedessen wurden an der TU Berlin Belastungstests an diesen Probekörpern durchgeführt. Sie zeigten die erwartete Verbesserung des Verformungsverhaltens.

Einige der entwickelten Bauelemente wurden in realen Konstruktionen eingesetzt. Ein Beispiel ist eine

Garage (in Figur 1), die ILC-Wände (Infralichtbeton) und ein Dach aus vorgespannten, CFK-verstärkten gefalteten Platten kombiniert. Das Dach besteht aus 5 gefalteten Deckenelementen und jedes Element hat eine Breite und Spannweite von 1,20 m bzw. 8,71 m. Das gesamte Bausystem ist leicht zerlegbar, so dass es leicht zu recyceln und umweltfreundlich ist.

In diesem Fall des Vorspannens von Carbondextilstreifen unterschiedlicher Breite bei welchem gleichzeitig die gesamte Textilstruktur eines Bauteils nach dem patentierten Verfahren von GINKGO vorgespannt wurde, entstand eine dünne Deckenplatte mit einer Dicke von nur 4 cm.

Als weiteres Beispiel wurden lange, schmale Hyperboloidschalen mit vorgespannten Carbon-Textilstreifen hergestellt. Die Methode ist grundsätzlich bekannt, da Silberkuhl und Müller in den 50er bis 70er Jahren des letzten Jahrhunderts ähnliche Schalen herstellten. Die Verwendung dieser Elemente erfolgte hauptsächlich für Dachkonstruktionen. Der Trick besteht darin, dass die Vorspannungslinien bei hyperboloiden Schalen linear sind.

Ginkgo produzierte hyperboloide Schalen mit den Abmessungen 4,30 m x 0,80 m x 0,03 m mit einseitiger Schalung unter Verwendung derselben Herstellungsmethode mit einem Paar sich kreuzender vorgespannter CFK-Textilstreifen. Für die Zukunft werden größere Strukturen für den Einsatz als elegante, organische Außenwartebereiche zum Beispiel in Bahnhöfen oder Bushaltestellen möglich sein.

Dipl.-Ing. Osman-Letelier

beschäftigt sich seit 2016 im Rahmen seiner Doktorarbeit mit der Analyse des Tragverhaltens sowie Versuchen an Flächentragwerken, die mit Carbondextilien vorgespannt sind.

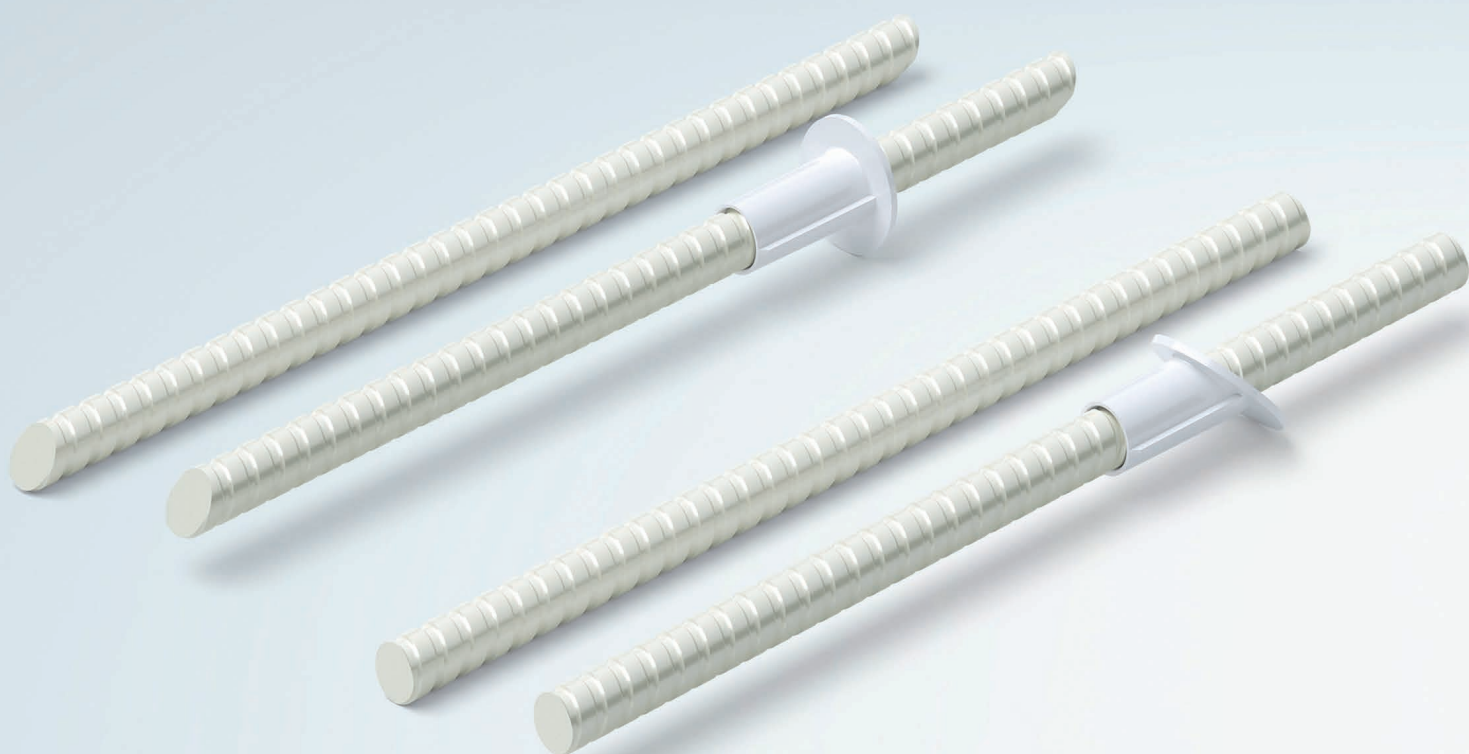


Dipl.-Ing. T. Lenz

konnte bereits 2012 in ersten Versuchen die Wirkung der Vorspannung von Gelegen in Carbonbetonteilen nachweisen. Es wurden daraufhin ein Patent für eine Vorspannvorrichtung für mehrere Geleeebenen erteilt



Dünne Verbundwerkstofffassaden in der Umsetzung im Fertigteilwerk – ein Erfahrungsbericht.



Das Ziel ist es dünne Verbundkonstruktionen in nahezu gleichen Vorgängen im Fertigteilwerk wie Standard-Elementbetonwände zu produzieren.

Die Umsetzung einer Elementwand ist heute ein standardisierter und sehr komplexer Vorgang. Die Anlagentechnik, häufig roboterunterstützt neben einer hohen Automation und Prozesse, die eine hohe Qualitätsstufe haben, werden täglich in sehr großer Quadratmeteranzahl hergestellt.

Heutige Betonfassaden werden bei Elementwänden ab 70 mm sicher und ökonomisch hergestellt. Die Elementplanung erfolgt in Programmen der Planungsabteilungen in den jeweiligen Werken, die mit der Anlagensteuerung eng verknüpft sind und diese steuern. Sie stellen den Anspruch und die Messlatte dar. Bedingt durch neue Möglichkeiten und das Weglassen von Stahl, besteht nun die Möglichkeit, Vorsatzschalen deutlich in der Dicke zu reduzieren. Sprechen wir „nur“ von einer Gewichtseinsparung? Sicher nicht, da diese Reduktion von Materialdicke auch einige Konsequenzen zur Folge hat, die sich sowohl im Umgang mit dem Werkstoff als auch im Verfahren innerhalb der Produktion ergeben. Neue Materialien im Fassaden und Elementwandbau ermöglichen eine Reduzierung des Transportgewichtes. Mehr Wände auf den Straßen zu transportieren ist effizienter und schlägt sich auch in Kosten und CO₂ Einträgen nieder. Dieser Mehrfachnutzen ist offensichtlich, Materialeinsparung und ökologischer Beitrag. Bewährte beim DIBt zugelassene Verankerungselemente aus Glasfaserwerkstoffen, beispielsweise als Fassadenanker Isolink® aus dem Hause Schöck Bauteile GmbH, sollen mit dünnen Verbundwerkstoffen aus Carbon und Beton zu einer neuen Bauweise führen. Der beim DIBt und weiteren Zulassungsbehörden im Ausland zugelassene Glasfaserverbundwerkstoff Schöck Combar®, eine Entwicklung der Fa. Schöck, wird heute schon millionenfach im Bereich von Fassaden aus Beton mit dem Namen Isolink® sowohl im Elementwand- als auch im Sandwichwandmarkt eingesetzt. Der Isolink® ist die statische Verbindung und die thermische Trennung der Fassade mit ihren Dilationen. Die zugelassene Passivhauskomponente ist die sichere statische Verbindung zur Tragwand unter geringstem Lambda Wert.

Welche Schritte sind bei der praktischen Umsetzung notwendig? Der Einbau soll einfach und im Fertigteilwerk ohne große Störungen des Umlaufbetriebes funktionieren, und damit gegen die her-

kömmliche Bauweise austauschbar werden. Es handelt sich um eine praktische Umsetzung von einer Standardanwendung hinzu einer neuen Methode im Fertigteilwerk - von der Idee zur Umsetzung und letztlich zur Automatisierung. Welche Tragfähigkeiten können bei dünnen Fassadenplatten aus Carbon-Beton erzielt werden? Wie wirken sich die dünnen Schalen im Handling eines Fertigungsprozesses aus?

Qualitätssicherung im Fertigteilwerk: Die Pull-out-Tests werden direkt im Werk begleitend durchgeführt, kontrolliert und dokumentiert. Auszugstests bestätigen die Ausziehlasten und geben Sicherheit bei der Verarbeitung. Wie verhält sich die Elementwand in der Umsetzung bei der Produktion im Fertigteilwerk und im folgenden Einbau?

Welche Hürden sind in der praktischen Umsetzung zu überwinden?

- 30-40 mm Vorsatzschalendicke
- Auf der Außenseite darf das Verbindungsmittel nicht sichtbar sein
- Carbon-Gewebe innerhalb des Betons; Einbringung des Isolink® Ankers mit 13,5 mm Durchmesser; Lagefixierung des Gewebes in der Schalenmitte
- Fixierung des Ankers in der Dämmschicht
- Weiterverarbeitung der Außenschale zu einer Elementwand
- Transport zur Baustelle
- In situ Betonage der Elementwand
- Raus aus der Theorie, rein in die laufende Fertigung eines Bauvorhabens. Die Antworten auf Fragen erfahren Sie im Vortrag. Viel Spaß beim Zuhören.

Dipl. Ing. Architekt Andreas Decker

Geboren am 12. August 1960 in Stuttgart; Schulweg, anschließendem Studium mit Diplomabschluss; Eingetragenes Mitglied der Architektenkammer; Bürotätigkeit in Frankfurt und Stuttgart; Über 10-jährige Tätigkeit in allen Leistungsphasen der HOAI; Projekte im Bereich öffentliche Gebäude, Wohn- und Gewerbebau; Seit 1996 in der Industrie, Kalksandstein Bauberatung Bereich Südwest; Seit 1999 bei der Schöck Bauteile GmbH; Bereiche Produkt- und Key Account Management



Betonbewehrung für Anwendungen in tropischen Klimabedingungen



Tropische Wetterbedingungen stellen eine besondere Herausforderung für den in verschiedenen Anwendungen verwendeten Stahlbeton dar. Eine der größten Herausforderungen bei herkömmlicher Betonbewehrung ist die Korrosion der Bewehrung. Das Problem der Korrosion der Bewehrung ist in Ländern wie Indien, mit sehr hoher Luftfeuchtigkeit bis zu 95 % bei Temperaturen bis zu 50 °C, sehr stark geprägt. Fasern und textilbasierte Bewehrungen bieten eine optimale Lösung.

Zurzeit werden diese Bewehrungen für nicht-strukturelle Bauteile sowie semi-strukturelle Bauteile eingesetzt. Fasern und Textilien werden für sehr dekorative Architekturfassaden sowie Straßenmöbel und Toiletten in Indien eingesetzt. Die Anforderungen an die Bauteile sind komplex. Bei Fassaden werden Materialien gesucht, die ca. 15–40 kg pro m² wiegen, ca. 10–30 mm dünn sind und wo die Bewehrung die Kräfte von den Befestigungselementen tragen kann. Auch bei den Straßenmöbeln sollen die Bauteile je nach Größe max. 100 kg wiegen, gut transportierbar sein und das Gewicht von 3–5 Personen tragen können. Die Bauteile müssen ca. 50 Jahre ohne Sanierung oder Instandhaltung aushalten.

Faser- und Textilbewehrung führen zu sehr dünnwandigen Strukturen sowie keine Bauteilbeschädigung beim Transport und leichte Bauteile. Die Berechnung der Menge an Fasern und Textilschichten werden gemeinsam mit den Faserherstellern bzw. in iterativen Versuchen festgelegt. Virgin AR-Glas-Fasern und Carbon-Gewebe-Randabschnitte werden als Bewehrung eingesetzt. Für bestimmte Anwendungen werden auch profilierte Polypropylen-Fasern eingesetzt. Als Einsatzgebiet im Strukturbauteilbereich werden C-Fasermatten für die Ummantelung von Betonsäulen verwendet. Weitere Anwendungen in Strukturbauteilbereichen werden gerade erforscht.

Die technischen Eigenschaften für die genannten Anwendungen erfordern bestimmte grundlegende Anforderungen wie eine Druckfestigkeit von etwa 40 bis 120 MPa und eine Biegefestigkeit von etwa 20 bis 24 MPa nach 28 Tagen. Die Wasseraufnahme des Betons wird voraussichtlich etwa 5–8 % betragen. Neben der Art der Bewehrung ist auch die Art der Anwendung von großer Bedeutung. Für Fasern ist das Verfahren einfach und eine vorgeschriebene Dosierung kann während der Anwendung mit dem Beton gemischt werden. Bei Textilien und der Anzahl der Schich-

ten ist dies jedoch kompliziert. Die Verträglichkeit der Betonmatrix mit der Bewehrung spielt ebenfalls eine entscheidende Rolle. Das Hinzufügen der Fasern oder Textilien als Verstärkung sollte die Eigenschaften des Betons aus Sicht der Verarbeitbarkeit nicht beeinträchtigen. Eine Betonmischung mit einer Dichte von 2.400 kg/m³ und selbstverdichtenden und selbstnivellierenden Eigenschaften sowie einem Slump von über 600 erfordert eine kalkulierte Dosierung der Fasern, um mit der zusätzlichen Textilverstärkung kompatibel zu sein. Darüber hinaus spielen die Kosten eine sehr wichtige Rolle bei der Entwicklung einer Betonmischung mit Fasern und Textilien. In Indien betragen die konventionellen Betonkosten ca. 90 € pro Kubikmeter und die konventionelle Bewehrung ca. 70 € pro Kubikmeter. Diese Kosten müssen angepasst werden, um nicht korrosive Verstärkungen verwenden zu können.

Unter Berücksichtigung von Kosten, Qualität und technischen Anforderungen muss das Betonmischungsdesign für jede einzelne Anwendung geprüft und entsprechend vorgeschlagen werden.

Dr. Mohit Raina absolvierte sein Studium am IIT Delhi in Indien und ging dann nach Deutschland, um dort zu promovieren. Hr. Raina begann ab November 2006 an der RWTH Aachen im Fachbereich Spinnerei. Ab Oktober 2010 leitete Herr Raina die Abteilung Produktionstechnologien und Textilmaschinen bei der ITA. Dr. Raina leitete auch die EU-Forschungskoordination am Institut und war persönlich an einer Reihe von EU- und deutschen Projekten beteiligt. 2013 hat Hr. Raina auch seinen Executive MBA an der RWTH Aachen und in St. Gallen erfolgreich abgeschlossen. Nach dem MBA arbeitete er als leitender Experte für fortschrittliche Verbundbaustoffe – textilbasierte Beton. Im Oktober 2014 kehrte Hr. Raina nach einem etwa 10-jährigen Aufenthalt in Deutschland nach Indien zurück, um sein eigenes Unternehmen mit dem Namen Raina Industries Pvt. Ltd. zu gründen. Raina Industries Pvt. Ltd. stellt vorgefertigten Glasfaserbeton und textilverstärkten Beton her. Hr. Raina ist Mitglied des Forschungsbeirats der ITA, RWTH Aachen. Dr. Raina ist auch in verschiedenen Ausschüssen bei NITI Aayog, Government of India und dem Textilministerium, Government of India, tätig.



Carbonbeton im Brückenbau – aktuelle ZiEs beim Verstärken und Neubau



Knapp 40.000 Brücken sind aktuell im Bestand der Bundesfernstraßen Deutschlands. Davon bestehen ca. 85 % aus Stahl- oder Spannbeton. Von allen Bundesfernbrücken können über 45 % in die Kategorie „noch ausreichender Bauwerkszustand“ oder schlechter eingestuft werden, wobei sogar 12 % einen „ungenügenden Bauwerkszustand“ aufweisen.

Viele der Betonbrücken in Deutschland, die in eine der unteren Zustandsbereiche eingeordnet werden können, haben die bekannten Probleme der Spannungsrisskorrosion bei Spannbetonbrücken mit älteren Spannstählen oder ein normatives Defizit an Robustheitsbewehrung. Diese Differenzen entstehen u. a. infolge von Normenänderungen und/oder durch höhere Verkehrslasten und sind durch die Bauherren und Planer aufgrund der Relevanz der funktionierenden Infrastruktur in kurzer Zeit zu beheben. Viele der bisher bekannten Baumaßnahmen zur Ertüchtigung sind aufwendig, ressourcenintensiven, und häufig auch bestandsschädigend (z. B. Teilabriss und Neubau). Die konventionellen Maßnahmen zur Erneuerung und Modernisierung von relevanten Brückenbauwerken beeinflussen die Volkswirtschaft von erheblichen Maß.

Eine zukunftsweisende Alternative in diesem Bereich bietet der Carbonbeton, sowohl im Gebiet der Verstärkung als auch im Neubau. Durch die hohe Tragfähigkeit in Kombination mit der guten Dauerhaftigkeit der verwendeten Carbonbewehrungen überzeugt der noch relativ junge Werkstoff gegenüber herkömmlichen Maßnahmen im Brückenbau schon jetzt. Durch das im Vergleich zu anderen Baumaterialien noch „junge Alter“ des Verbundwerkstoffs unterliegt der Carbonbeton in Deutschland noch keiner normativen Regelung und somit sind i. d. R. Zustimmungen im Einzelfall bzw. vorhabenbezogene Bauartgenehmigungen nötig. In den vergangenen zwei Jahren war und ist die CARBOCON an insgesamt sechs Brückenbauwerken hinsichtlich der Planung und experimentellen Nachweisführung beim Neubau und der Verstärkung aus und mit Carbonbeton beteiligt gewesen. Entsprechend den gegebenen Randbedingungen (zeitlicher und monetärer Aspekte) des Projektes und den Anforderungen der Bauherren sowie der beteiligten Institute konnten dabei vereinzelt auch schon Zustimmungen im Einzelfall für die Anwendung des Carbonbetons innerhalb weniger Monate erlangt werden, wodurch die vorgegebene Zeitschiene inklusive des ZIE-Prozesses gehalten

werden konnte. Die Erlangung einer ZIE kann bei entsprechender Planung in den Bauprozess integriert werden und stellt folglich keine Hürde dar.

Im Rahmen des Vortrages werden die planerischen und gutachterlichen Leistungen beim Erlangen und Umsetzen einer ZIE für die Anwendung des Carbonbetons in Verbindung mit den beteiligten Projektpartnern gezeigt. Hierbei werden neben den Bearbeitungsinhalten bei jetzigen Planungsprojekten auch auf aktuelle Ausführungsbeispiele eingegangen.

Dipl.-Ing. Sebastian May

studierte Bauingenieurwesen von 2009 bis 2012 an der Bauhaus-Universität (B. Sc.) und von 2013 bis 2016 an der TU Dresden (Diplom). Von 2016 bis 2020 war er als wissenschaftlicher Mitarbeiter am Institut für Massivbau der TU Dresden tätig und forschte in den Bereichen des Neubaus und der Verstärkung mit Carbonbeton. Von 2018 bis 2020 war er als Projektleiter bei der CARBONCON angestellt. Seit 2020 teilt er sich mit Dipl.-Ing. Alexander Schumann die Geschäftsführung der CARBOCON.



Verstärkung von Brücken mit spannungsrisskorrosionsgefährdetem Spannstahl mit Carbonbeton



Bis etwa 1993 wurde in Deutschland bei zahlreichen Brücken spannungsrissskorrosionsgefährdeter Spannstahl verbaut. Da ein Großteil des Brückenbestandes als Spannbetonkonstruktionen ausgeführt sind und in den 1960er bis 1980er Jahren gebaut wurden, ist eine große Anzahl von Brücken betroffen. Zahlreiche dieser Brücken können jedoch durch die Applikation von Carbonbeton gezielt verstärkt und somit weiterhin genutzt werden.

Bei der Spannungsrissskorrosion handelt es sich bis heute um ein Phänomen. So zeigen Spannstähle, trotz ähnlicher chemischer Zusammensetzung, eine unterschiedliche Anfälligkeit hinsichtlich Spannungsrissskorrosion. Kritisch ist hierbei, dass der Spannstahl infolge einer Versprödung sukzessive ausfällt und damit die Tragsicherheit des Bauteils herabsetzt. Im ungünstigen Fall bleibt der Ausfall des Spannstahls unbemerkt und kann bei einem entsprechenden Schädigungsgrad zu einem plötzlichen Versagen des Tragwerks führen. In diesem Fall spricht man von einem Bauteil ohne ausreichendem Ankündigungsverhalten. Infolge von Schadensfällen in den 1960er und 1970er Jahren im Hochbau sowie der Tatsache, dass diese Tragwerke ein Sicherheitsrisiko darstellen, wurde mit der sogenannten -Handlungsanweisung Spannungsrissskorrosion- seitens des BMVI in den 1990er Jahren ein erstes Konzept für die rechnerische Bewertung der Tragsicherheit von Brücken mit spannungsrissskorrosionsgefährdeten Spannstahl entwickelt und stetig fortgeschrieben. Das rechnerische Verfahren sieht vor, dass sich der Ausfall von Spannstahl durch Rissbildung an der gezogenen Randfaser des biegebeanspruchten Bauteils zeigt, bevor eine vorgeschriebene Mindesttragsicherheit unterschritten wird.

Dabei wird bei diesem Verfahren rechnerisch die Spannstahlfläche soweit reduziert, bis die Zugfestigkeit des Betons bei einer üblichen Verkehrsbelastung überschritten wird. Die beginnende Rissbildung kann somit bei Inspektionen im Rahmen der Bauwerksprüfung erkannt werden. Die Tragfähigkeit des geschädigten Querschnittes wird anschließend einer erforderlichen Tragfähigkeit gegenübergestellt und das Sicherheitsniveau ermittelt (Riss vor Bruch-Kriterium). Neben der verbleibenden Spannstahlfläche wird hierbei die Betonstahlbewehrung als zusätzlich tragendes Element angesetzt. Die zeitgenössischen Ausführungen von Spannbetonkonstruktionen jener Zeit als voll vorgespanntes Tragwerk, beziehungsweise das Fehlen einer normativen Forderung nach einer

schaffen Mindestbewehrung bei der Ausführung, führten meist mit zu geringen Bewehrungsgraden. Die Resttragfähigkeit ist häufig nicht in allen Nachweisquerschnitten gegeben. In einem zweiten Schritt sind weiterführende Nachweise auf Systemebene mit stochastischen Betrachtungen möglich, doch für zahlreiche Tragwerke ist auch damit kein ausreichendes Ankündigungsverhalten nachweisbar. Das fehlende Ankündigungsverhalten aufgrund zu geringer Bewehrungsmengen in Verbindung mit einem unbemerkten Spannstahlausfall, kann durch die Applikation einer Carbonbetonverstärkung kompensiert werden.

Im Rahmen des Beitrages wird die erstmalige Anwendung einer Carbonbetonverstärkung an Spannbetonbrücken mit spannungsrissskorrosionsgefährdetem Spannstahl zur Sicherstellung eines ausreichenden Ankündigungsverhaltens vorgestellt. Das Bauvorhaben befindet sich aktuell in der Umsetzung. Im Konkreten handelt es sich um zwei Teilbauwerke mit jeweils drei Feldern und einer Gesamtlänge von etwa 66 m. Für die Sicherstellung eines ausreichenden Ankündigungsverhaltens werden die Spannbetonüberbauten in den Randfeldern sowie im Stützbereich mit Carbonbeton verstärkt. Durch die geringen Schichtdicken der Verstärkung sind die Einschränkungen für den Raum unter den Bauwerken minimal – an den Oberseiten kann die nur wenige Zentimeter dicke Verstärkungsschicht ohne Gradientenanhebung unter dem Fahrbahnaufbau integriert werden.

Dipl.-Ing. Oliver Steinbock seit 11/2014: Wiss. Mitarbeiter am Institut für Massivbau der TU Dresden sowie seit 09/2018: Projektleiter bei Curbach Bösche Ingenieurpartner Beratende Ingenieure PartG mbB



Prof. Dr.-Ing. Thomas Bösche seit 2005: Partner bei Curbach Bösche Ingenieurpartner Beratende Ingenieure PartG mbB sowie seit 2017: Professor HTW Dresden – Lehrgebiet Stahlbeton und Spannbeton; Zuvor: 1997-2004: Projektleiter bei Köhler+Seitz



TUDALIT®
Leichter bauen – Zukunft formen

carbon
concrete
composite

Neue Carbonfaserbewehrung für Beton-3D-Druck und andere digitale Betonbauverfahren



Der 3D-Druck mit zementgebundenen Materialien erfordert geeignete Lösungen für die Integration der Bewehrung während des Herstellungsprozesses. In diesem Tagungsbeitrag wird eine neue Technologie vorgestellt, die mineralisch imprägnierte Carbonfasergarne (engl: mineral-impregnated carbon-fibre, MCF) für diesen Zweck verwendet.

Die Basis für mineralisch getränkte Carbonfasergarne bildet das Carborgarn SIGRAFIL von der SGL-Group mit 50.000 Einzelfilamenten, welches durch ein eigens entwickeltes Tränkungsverfahren behandelt wird. Die Tränkungsmatrix setzt sich aus Feinstzement, Mikrosilika-Suspension, Wasser und Fließmittel, bei einem Wasser-Bindemittel-Wert von 0,8 zusammen. Zur Stabilisierung der Bewehrungsform erfolgt eine Umwindung des frisch getränkten Materials mit Formgebungsgarn, bevor der Carbonstrang auf eine Spule aufgewickelt wird. Die Verarbeitungszeit eines derart hergestellten Faserstranges beträgt ca. 4 Stunden. Diese neue Art der nicht korrosiven Bewehrung weist hervorragende mechanische Eigenschaften, hohe Nachhaltigkeit und Dauerhaftigkeit auf. Entscheidend ist jedoch, dass MCF eine extrem hohe technologische Flexibilität bietet, da sie im frischen Zustand leicht geformt und vollautomatisch verarbeitet werden kann. Diese vollautomatische Integration von Bewehrungselementen in den 3D-Druck mit Beton ist eine Schlüsselfrage für die Technologie um eine entsprechende Marktdurchdringung zu ermöglichen. Bisherige Ansätze mit einer nachträglichen Applikation von herkömmlicher Stahlbewehrung oder moderner textiler Strukturen erscheint in Hinblick auf Aufwand und Kostenstruktur wenig zielführend. Daher lag der Fokus der Untersuchungen auf einer im Betonstrang integrierten Bewehrung was folgende Vorteile mit sich bringt:

- Druck- und Bewehrungsprozess sind vereint, was zu einer bautechnologischen Zeitersparnis führt;
- die Bewehrung wird vollständig umschlossen, es liegt ein ausgezeichneter Verbund vor;
- die Fuge/Interphase wird ausschließlich für den Verbund der Betonstränge genutzt und nicht durch die Bewehrungslage gestört.

Für die mineralisch getränkten Carbonfasergarne konnte eine Druckdüse entwickelt werden, welche bis zu 6 Faserstränge in einen Betonstrang integrieren kann. Aus dem Carbonbetonbereich bekannte Prüfverfahren wurden auf das neuartige Verfahren angepasst, um das Zug- und Biegeverhalten von

gedrucktem Carbonbeton sowie die Qualität des Verbunds zwischen Bewehrung und Beton zu beurteilen. Hierfür wurden neben 3-Punkt Biegeversuchen angepasste Dehnkörper mit jeweils 3 Carbonfasergarnen als auch Auszugskörper mit einem Faserstrang und verschiedenen Einbindelängen untersucht. Die Untersuchungen zum Biegetragverhalten wurden insbesondere als Vergleichsuntersuchungen zu innerhalb des Betonstrangs bewehrten Prüfkörpern gegenüber zwischen den Betonsträngen bewehrten Prüfkörpern durchgeführt. Neben der deutlich höheren übertragbaren Kraft bei inline bewehrten Proben wurde eine Veränderung des Versagensmechanismus vom Versagen im Bereich der Betonstrangverbundzone hin zu einem aus dem klassischen Stahlbeton bekannten Schubversagen beobachtet. Im Bereich der Dehnkörperuntersuchungen ergab sich ein gleichmäßiges Rissbild mit Rissabständen um die 30 mm und stabilen Einzelrissöffnungen. Faserstrangauszugsversuche ergaben einen mittleren Verbundfluss zwischen 75 und 80 N/mm, was in der Größenordnung aktueller textiler Strukturen mit vergleichbarer Filamentanzahl im Faserstrang liegt. Zusammenfassend ergaben die mechanischen Prüfungen eine mechanische Leistung des gedruckten Betons, die mit der von Textilbeton aus kunststoffgetränkten Carbonfasern vergleichbar ist. Die präsentierte Forschung hat die Machbarkeit und das sehr hohe Potenzial der neuen Technologie in Bezug auf die Digitalisierung und Automatisierung des Betonbaus nachgewiesen.

Tobias Neef ist wissenschaftlicher Mitarbeiter am Institut für Baustoffe an der Technischen Universität Dresden. Er schloss 2020 sein Studium des Bauingenieurwesens auf dem Gebiet des konstruktiven Ingenieurbaus mit der Spezialisierung Baustoffe ab.



Steffen Müller is a research assistant at the Institute of Building Materials at the TU Dresden since 2011. His field of research is alternative reinforcement materials for the construction industry, such as high-performance short fiber concretes (HP-FRC) or textile reinforced concrete (TRC).



CARBOCON

CARBOCON ist ein führender Dienstleister, wenn es rund um das Thema Carbonbeton geht. Durch unabhängige und neutrale Beratung erhalten Sie die beste Carbonbetonlösung. Seien es spezielle Fragen der Entwicklung und Zulassung innovativer und technischer Lösungen oder Patentanmeldungen.

Wir begleiten die Projekte von der ersten Analyse bis hin zur späteren Anwendung. Das Spektrum an Projekten reicht von der ganzheitlichen Beratung beim Einsatz von Carbonbeton bis hin zur „klassischen“ Planung bei der Verstärkung von Bestandsbauteilen, Neubauten und anderen Bauwerken mit Carbonbeton.

Wenn Sie einen Partner an Ihrer Seite suchen, der Ihnen mit über 10 Jahren Erfahrung im Bereich des Carbonbetons Ihre Projekte von der ersten Machbarkeitsstudie an, über die Entwicklung und Begleitung von Versuchsprogrammen bis hin zur sicheren Zulassung und späteren Überwachung der Produktanwendung unterstützt, dann sind wir der Richtige für Sie.

Kontaktieren Sie uns!

Ihr CARBOCON - Team



BESTENS BEWEHRT!



WILHELM KNEITZ
SOLUTIONS IN TEXTILE

Technische Textilien

Textile Beton-Bewehrungen der Marke **SiTgrid**® aus ein- oder zweilagigen Carbon- und Glas-Gittergelegen, die zur bautechnischen Sanierung und Verstärkung von marodem Stahlbeton und zur innovativen Herstellung von Beton-Fertigteilen dienen.

Gittergelege

- 2D und 3D Geometrien
- Bewehrungen und Armierungen
- Carbon, Glas und Basalt

CONSTRUCTION



SiTgrid®

Mehr Informationen:

www.solutions-in-textile.com

Die in diesem Tagungsband zugrundeliegenden Vorhaben des C³-Projekts wurden mit Mitteln des Bundesministeriums für Bildung und Forschung gefördert.

VORTRÄGE ✓

C³ | carbon
concrete
composite



Shear Strengthening of RC T-Beams with CRC



Sarah Bergmann, M.Sc.

Institute of Structural Concrete,
RWTH Aachen University, Aachen, Germany

✉ sbergmann@imb.rwth-aachen.de

Her main research area is the load-bearing behavior of reinforced concrete structures strengthened with carbon reinforced concrete.



Dipl.-Ing. Sebastian May

CARBOCON GmbH

Dresden, Germany

✉ may@carbocon-gmbh.de

His research interests include the material behavior of CRC in strengthening existing concrete structures and the development of new and thin large-scale structures made of CRC.

Contact: sbergmann@imb.rwth-aachen.de

1 Abstract

Many existing reinforced concrete (RC) structures, especially in bridge construction, have been planned for lower loads and have been dimensioned according to former design regulations. Therefore, deficits in shear capacity may exist. In order to achieve a cost and time saving extension of the design working life, strengthening with carbon reinforced concrete (CRC) can be an option. This study presents the results of large-scale tests using different strengthening configurations and gives a short outlook regarding the recalculation of the tests with an existing strut-and-tie model.

Keywords: carbon reinforced concrete (CRC); textile reinforced concrete (TRC); shear strengthening; shear capacity; large-scale tests; recalculation.

2 Introduction

The use of non-metallic, high-strength reinforcement materials minimizes the dimensions of the strengthening layers and contributes to a resource efficient and durable strengthening concept. Although carbon reinforcement is not necessarily anchored in the compression zone, high load increases can be achieved.

Previous studies have already proven the effectiveness of the strengthening with carbon reinforced concrete and calculation approaches for the shear capacity have already been derived [1, 3, 5, 6]. However, the load-bearing behavior and failure mechanisms of RC components strengthened with CRC have not yet been fully investigated.

At present, there is no generally valid or even approved calculation model for the design of RC components strengthened with CRC that accurately describes the shear capacity. This hinders the use of this innovative strengthening method in construction practice.

3 Experimental Investigation

3.1 Test Specimens and Materials

Experimental investigations were carried out to investigate the influence of the strengthening layer on the shear load-bearing behavior, the failure mechanisms and the load increase. This paper refers to experimental tests that have been described in detail in [7, 8].

Two RC cross-sections were investigated: a slim T-beam (sT) and a compact T-beam (cT). The dimensions of the cross-sections are shown in Figure 1. The RC T-beams were reinforced with grade B500B rebar steel and contained transverse reinforcement (stirrups). The concrete had a cylinder compressive strength of 30 to 40 MPa.

The strengthening layers consisted of an impregnated grid-like carbon reinforcement and a sprayable fine-grained concrete. The shotcrete Pagel TF10 is approved for the strengthening of RC components.

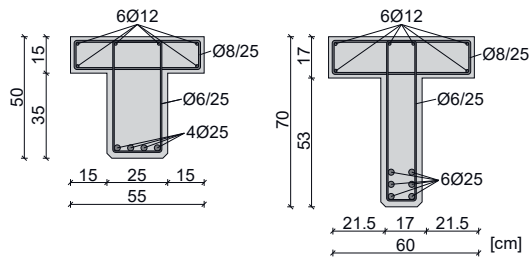


Figure 1: Cross-sections of RC T-beams: (a) compact; and (b) slim T-beam | graphic: Sarah Bergmann

In this study, SITgrid040, a polyacrylate (PA) based impregnated carbon reinforcement, and solidian GRID Q85/85-CCE-21, an epoxy (EP) resin impregnated carbon reinforcement, were used. The cross-sectional area of the PA-grid is 141 mm²/m in warp direction (0°) and 28 mm²/m in weft direction (90°). The biaxial EP-grid has a cross-sectional area of 85 mm²/m in both directions. The average tensile strength of the EP-grid was 3377 MPa (weft direction) and the average tensile strength of the PA-grid was 3160 MPa (warp direction). The given directions correspond to the orthogonal to the longitudinal axis of the specimens, if the grids have an alignment of 0°/90°.

The strengthening layers were applied between the support areas and applied in a laminating process using shotcrete. Every layer of shotcrete had a thickness of almost 5 mm. As a result, the strengthening layers had a thickness of 10 mm with one layer of carbon reinforcement and 15 mm with two layers.

3.2 Test Setup and Test Program

The test specimens were tested in four-point bending tests (Fig. 2). The shear slenderness λ was 3.3 in order to minimize the direct shear load transfer via the compression struts. Conventional measurement technology, such as inductive displacement transducers and ARAMIS, a measuring system based on digital image correlation, was used.

In total, 12 compact T-beams and 14 slim T-beams were tested. The test series included unreinforced specimens (reference/Ref), specimens strengthened with CRC and with unreinforced shotcrete (SC). Two test specimens with the same configuration were tested in each case. In addition to the RC T-beams (cT/sT), the type of carbon reinforcement grid (EP/PA), the number of reinforcing layers (1/2), the shape in cross-section (II/U), and the alignment of the grids in relation to the longitudinal axis of the specimen (90/45) were varied.

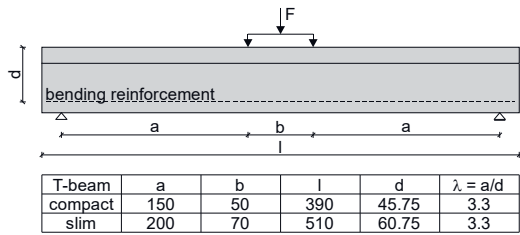


Figure 2: Schematic of test set-up | graphic: Sarah Bergmann

4 Experimental Results

4.1 Load-Deflection Behavior

Load increases of up to 40% were achieved in the tests. The test specimens were characterized by sufficient warning before ultimate failure, such as large deformation and wide cracks. Due to the steel reinforcement, the failure was much less brittle compared to components made entirely of CRC. As expected, the strengthened T-beams were stiffer than the reference T-beams and had a much finer crack pattern and smaller crack widths. Even an unreinforced shotcrete layer leads to a load increase (Fig. 3b, sT-II-SC-a/b). Not all test specimens failed due to shear forces (see section 4.2). The load deflection curves are presented in Figure 3.

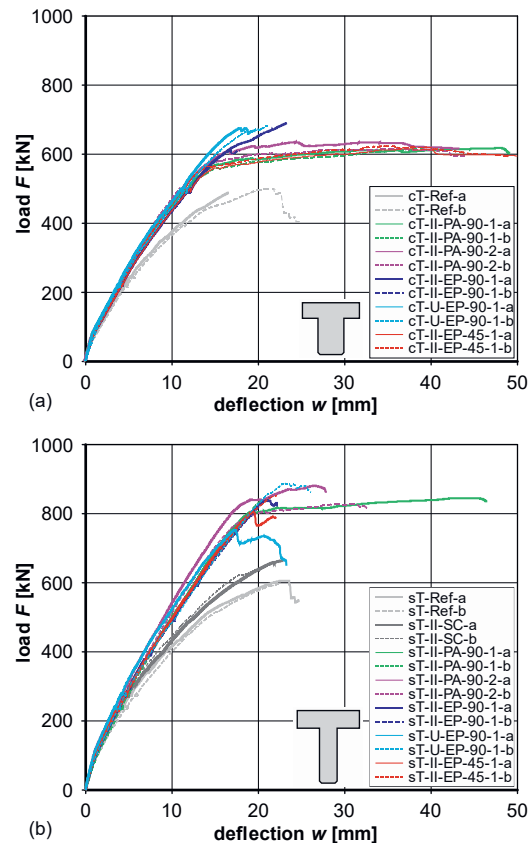


Figure 3: Load-deflection curves for (a) compact; and (b) slim T-beams | graphic: Sarah Bergmann

4.2 Failure Mechanisms

Different crack patterns and failure mechanisms were observed during the tests. Examples are given in Figure 4. Many test specimens failed as planned on shear by a failure of tension struts and crushing of concrete in the flexural compression zone. In a few cases the critical shear crack did not lead to failure, but the web cracked at the underside, starting from the support area, and the concrete thus failed on transversal tension. Starting from the critical shear crack, delamination often occurred, so that the concrete cover of the strengthening layer spalled. Delamination also occurred in some cases below the flange. In addition, some test specimens also failed unplanned due to bending. The main failure mechanism of each test is listed in [1].



Figure 4: Failure mechanisms observed in this study: (a) crushing of concrete in the flexural compression zone; (b) rupture of tension strut; (c) transversal tension failure of the web at the underside; (d) delamination | graphic: Sebastian May, Alexander Schumann

5 Recalculation

5.1 Strut-and-Tie Model

Brückner presented a strut-and-tie model for RC components strengthened with CRC under shear load in [1]. In this paper the recalculation of the experimental tests is done only for this model. The shear capacity of a strengthened RC element V_R is composed of the shear contribution of steel stirrup reinforcement $V_{R,s}$ according to Eurocode 2 and the contribution of the carbon reinforcement $V_{R,t}$. The shear contribution of the carbon reinforcement is indicated in eq. 1,

$$V_{R,t} = a_{w,t} \cdot f_t \cdot b_{w,t} \cdot \sin \alpha_t \quad 1$$

where $a_{w,t}$ is the cross-sectional area of the carbon reinforcement; f_t is the tensile strength; $b_{w,t}$ is the

width of the tension strut and α_t is the angle of the carbon reinforcement to the longitudinal axis of the component. The width of the tension strut depends on geometric parameters and bond properties of the textile reinforcement.

5.2 Results and Discussion

The recalculation is limited to the tests with shear failure. A few results are shown as an example in Figure 5. The shear capacity of the (unstrengthened) reference T-beams is clearly underestimated with the formula according to Eurocode 2. The total shear capacity of the strengthened T-beams is usually slightly underestimated by the model according to Brückner. The difference for the compact T-beams is greater than for the slim T-beams. An exception is the slim T-beam, which was strengthened with a single layer of PA-grid (sT-II-PA-90-1-b). In this case, the calculated shear capacity is greater than the shear capacity determined in the test. The reason for this is the much larger cross-sectional area per unit length compared to the EP-grid.

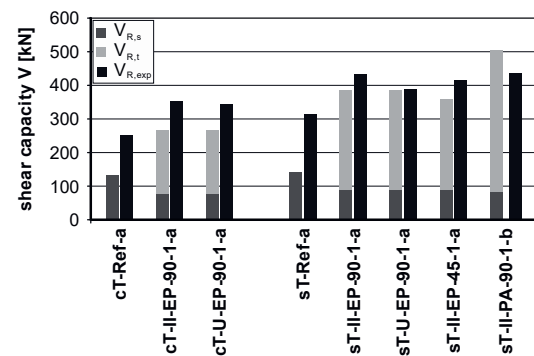


Figure 5: Shear capacity acc. to Brückner compared to the test results | graphic: Sarah Bergmann

Comparing the calculated contribution of steel stirrup reinforcement of the strengthened test specimens with the experimental shear capacity of the reference specimens, it is noticeable that the calculated contribution is clearly underestimated. The calculated contribution of steel reinforcement is therefore clearly overestimated.

Furthermore, the contribution of steel stirrup reinforcement is lower than the calculated shear capacity of the reference T-beams. This is due to the additional carbon reinforcement, which leads to steeper compression struts and a smaller width of the tension strut.

In order to capture the contribution of carbon reinforcement more realistically, a reduction factor for the tensile strength according to [9] could be added. The critical shear crack usually does not cross the fibre strands orthogonally. The fibre strands are therefore at an angle to the load direction and a lower tensile strength can be assumed. The angle between fibre strand and load direction is determined by the shear cracks, that cross the fibre strands, and the alignment of the grids in relation to the longitudinal axis of the specimen. If the formula in [9] can be transferred, the contribution of carbon reinforcement would be reduced by about 30%.

If either a tensile failure of the carbon reinforcement or a composite failure between the carbon reinforcement and the fine-grained concrete is decisive for the failure of the strengthening layer, either the tensile strength or the existing bond length of the fibre strands limits the capacity of the strengthening layer. With increasing stress in the fibre strands, the related anchoring length increases. This influences the strut-and-tie model of the carbon reinforcement. If the anchorage length is considered in relation to the tensile stress, an iterative calculation is necessary.

Since the project did not include extensive investigations on the tensile strength of the fibre strands at different load directions and bond properties of the used carbon reinforcements, the proposals cannot be verified at present.

6 Conclusion and Further Research

In this paper, experimental investigations on RC T-beams strengthened with carbon reinforced concrete were carried out. The main parameters of the RC-beams and the strengthening layers were varied. Due to the reinforced strengthening layers, fine crack patterns and smaller crack widths occurred. High load increases up to 40% could be achieved. Therefore, a high activation of the carbon reinforcement can be assumed. Both carbon reinforcements, the PA-grid and the EP-grid, are suitable for the strengthening of RC components.

The recalculation showed that the load increase cannot yet be described accurately. In particular, the model shows deficits in the shear contribution of steel stirrup and carbon reinforcement. The consideration of additional contributions to the shear capacity must be investigated. Moreover, the model does not consider a possible transverse

tension failure of the concrete at the bottom of the web. This failure mechanism must be appropriately considered.

Further investigations are necessary to derive a sufficiently accurate engineering model for the calculation of shear capacity of RC-components strengthened with CRC, which appropriately considers both the different failure modes and the shear contributions. In further tests the transverse reinforcement ratio and the dimensions of the RC beam as well as the slenderness should be varied, since these parameters have also a major influence on the main failure mechanism and the activation degree of the steel stirrups and the carbon reinforcement. Even if it is associated with a high effort, the use of a fibre optic strain measurement system would be very suitable for investigating the activation degree in order to carry out continuous strain measurements directly on the two reinforcements.

7 Acknowledgement

The authors thank the German Federal Ministry of Education and Research (BMBF) for funding the projects C³-V2.1 and C³-V2.7 within the research program C³ – Carbon Concrete Composite.

8 References

- [1] A. Brückner, "Querkraftverstärkung von Bauteilen mit textilbewehrtem Beton", dissertation, TU Dresden, 2011. <http://nbn-resolving.de/urn:nbn:de:bsz:14-qucosa-85729>.
- [2] C. Escrig, L. Gil, E. Bernat-Maso, and F. Puigvert, "Experimental and analytical study of reinforced concrete beams shear strengthened with different types of textile-reinforced mortar", *Construction and Building Materials* (83), pp. 248–260, 2015. doi: 10.1016/j.conbuildmat.2015.03.013
- [3] T. Blanksvärd, B. Täljsten, and A. Carolin, "Shear strengthening of concrete structures with the use of mineral-based composites", *Journal of Composites for Construction*, vol. 13, pp. 25–34, 2009. doi: 10.1061/(ASCE)1090-0268(2009)13:1(25)
- [4] M. Herbrand, V. Adam, M. Classen, D. Kueres, and J. Hegger, "Strengthening of Existing Bridge Structures for Shear and Bending with Carbon Textile-Reinforced Mortar", *Materials*, vol. 10, no. 9, 15 pages, 2017. doi: 10.3390/ma10091099
- [5] Z. C. Tetta, L. N. Koutas, and D. A. Bournas, "Shear strengthening of full-scale RC T-beams using textile-reinforced mortar and textile-based anchors", *Composites Part B Engineering*, vol. 95, pp. 225–239, 2016. doi: 10.1016/j.compositesb.2016.03.076
- [6] E. A. Tzoura, and T. C. Triantafyllou, "Shear Strengthening of Reinforced Concrete T-beams under cyclic loading with TRM or FRP jackets", *Materials and Structures* 49, pp. 17–28, 2016. doi: <https://doi.org/10.1617/s11527-014-0470-9>
- [7] S. Bergmann, S. May, J. Hegger, and M. Curbach, "Shear strengthening of reinforced concrete T-beams using carbon reinforced concrete", *ACI Spring 2020 Convention*, 2020. (submitted)
- [8] S. May, A. Schumann, S. Bergmann, M. Curbach, J. Hegger, "Versuche zur Querkraftverstärkung mit Carbonbeton", *Bauingenieur*, 2020. (submitted)
- [9] C. Kulas, "Zum Tragverhalten getränkter textiler Bewehrungselemente für Betonbauteile", dissertation, RWTH Aachen, 2013.

Serviceability limit state design for carbon reinforced concrete structures



Dipl.-Ing. Kai Schneider

TU Dresden, Dresden, Germany

✉ kai.schneider@tu-dresden.de

Mr. Kai Schneider focuses in his research mainly on the development of concrete composition and the bond behavior of carbon reinforcements.



Prof. Dr.-Ing. Viktor Mechtcherine

TU Dresden, Dresden, Germany

✉ mechtcherine@tu-dresden.de

Prof. Viktor Mechtcherine is Director of the Institute for Construction Materials at the TU Dresden, Germany. He is RILEM Fellow and member of the Science Academy of Saxony.

1 Abstract

The structural design in the serviceability limit state represents a major hurdle for a broader application of carbon reinforced concrete in the construction praxis. The bond between various carbon reinforcements and concrete was intensively investigated by means of pull-out tests. On this basis, an engineering design model for the serviceability limit state was developed. It enables a purposeful design of the end anchorage length and limitation of crack widths for the serviceability limit state.

Keywords: Carbon Reinforcement, Textile, Concrete, Crack Width, End Anchorage

2 Introduction

Crack widths in the concrete cover exhibit hardly any influence on the durability of carbon concrete due to an outstanding chemical resistance of carbon reinforcement against corrosive media [1]. However, both water tightness and optical requirements demand a limitation for crack widths in carbon concrete components with respect to the serviceability limit state [2]. In addition to the consideration of the crack widths, the end anchorage length must also be designed in such a way that no slippage occurs at the ends of reinforcing elements.

3 Materials and experimental program

The materials under investigation were two polymer-bonded and two mineral-bonded carbon reinforcements, see Figure 1 and Table 1. The two mineral-bonded reinforcements varied in the water-to-binder ratio of the fine cement-based impregnating suspension used, see also [3], [4]. All composite specimens were made with the high-

strength self-compacting fine-grained concrete BMK-30-200-2 developed in the framework of the project Carbon Concrete Composite – C³ [5].



Figure 1: Carbon reinforcements under investigation: a) Epoxy (EP), b) Acrylic based polymer (ACR) and c) two mineral-bonded carbon reinforcements (MIN-60 and MIN-80) | photos: Kai Schneider

The uniaxial tension tests were performed on the specimens had a width of 120 mm and a thickness of 12 mm. The strain of the composite was determined by means of displacement gauges and the crack development by photogrammetric measurements over a length of 270 mm. Five specimens were tested for each type of reinforcement.

Impregnation material of the carbon reinforcement	Acronym	Reinforcement content [tex]	Size [mm]	Reinforcement content in tension tests [tex]
Epoxy	EP	6500	5,5 x 1,9	5 x 6500
Acrylic based polymer	ACR	3200	3,2 x 1,5	9 x 3200
Ultra-fine cement suspension with W/B of 0.6	MIN-60	3450	Ø 3,75	9 x 3450
Ultra-fine cement suspension with W/B of 0.8	MIN-80		Ø 3,4	

Table 1: Overview of the carbon reinforcements under investigation

For the pull-out tests, an original setup developed by Schneider [4] was used, see Figure 2. The anchorage length x in the pull-out tests ranged between 10 mm and 40 mm. Nine specimens were tested per reinforcement and chosen embedment length.

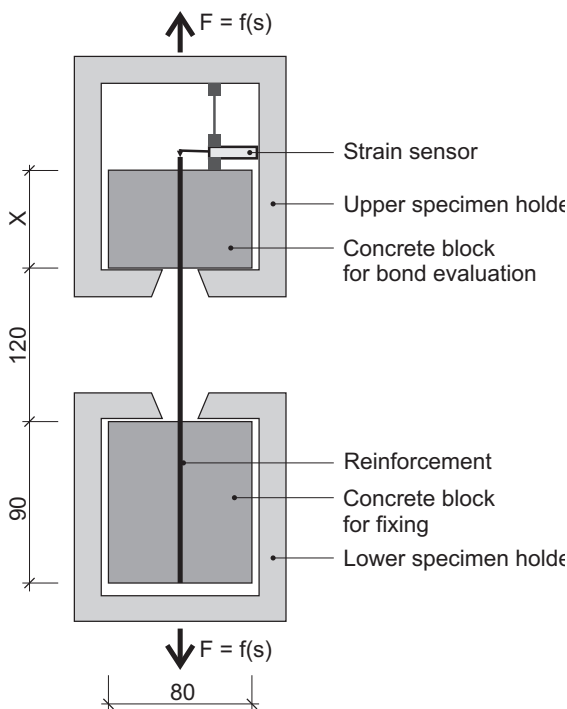


Figure 2: Used pull-out test | graphic: Kai Schneider

4 Tensile behavior and crack widths

The composite specimens were tested in uniaxial tension. The tensile force was related to the net carbon fiber cross-section. Figure 3 shows the typical fiber stress-strain relationships for various types of fiber. The composite behavior is characterized by a steep ascend of the stresses. This initial region before the formation of the first crack,

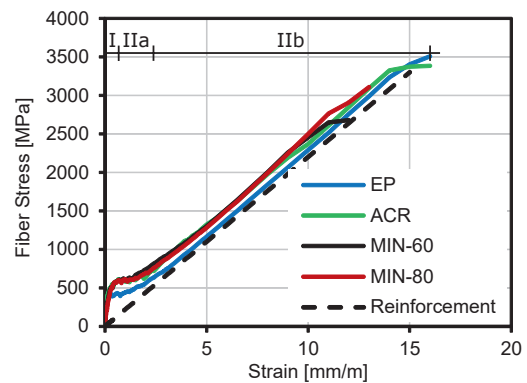


Figure 3: Fiber stress-strain relationship of the composite specimens in uniaxial tension tests and of a fictive reinforcement specimen with a modulus of elasticity of 220 GPa | graphic: Kai Schneider

the so-called state I, is determined by the stiffness and tensile strength of the concrete matrix. State I is followed by the crack formation stage, state IIa, and ends in a completed crack pattern, the state IIb. The state IIb is characterized by a linearly ascending curve which slope is defined by the stiffness of the reinforcement.

The surrounding concrete matrix contributes only little by tension stiffening. A straight line for a fictive carbon reinforcement with a modulus of elasticity of 220 GPa is added to the fiber stress-strain diagram as a reference indicating the stress-strain behavior of the carbon fiber reinforcement.

Figure 4 shows the mean crack width as a function of the crack density for the selected strain levels of 2, 4 and 8 mm/m. The mean crack width was calculated from the sum of all crack widths divided by the number of cracks.

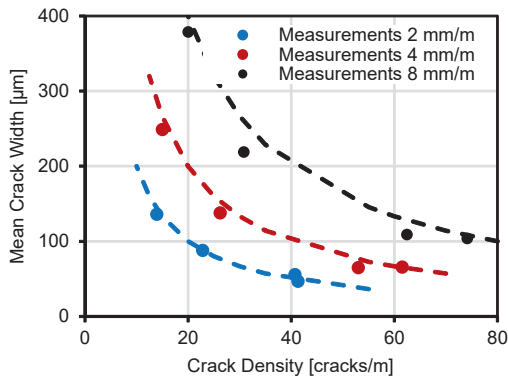


Figure 4: Mean crack width in the composite specimens as a function of the crack density for the strain levels of 2, 4 and 8 mm/m in the uniaxial tension tests | graphic: Kai Schneider

The crack width w_r can also be estimated from the average crack distance s_r , the strain of the reinforcement ϵ_b and the factor for the tension stiffening of the concrete matrix k_1 , using Eq.1:

$$w_r = s_r \times \epsilon_b \times k_1 \quad 1$$

Since the determined sum of the crack widths approximately corresponds to the measured deformation of the composite specimen, it can be concluded that the concrete strain tends to zero and thus can be neglected in the following considerations. Furthermore, it can be assumed that the deformation (strain) measured at the composite specimen approximately equals the deformation (strain) of the reinforcement. This considerations are also in line with the results by Büttner [6]. Consequently, the crack width can be expressed as the product of the crack distance and the strain of the reinforcing element or rather the strain of the composite material, see Eq.2:

$$w_r = s_r \times \epsilon_b \quad 2$$

Note that this is not a general statement on tension stiffening effects which should be considered separately in each specific case. Here, the very small strain stiffening of the concrete matrix allows for a conclusion that the bond behaviour has an almost negligible influence on the strain behaviour of the specimen and the sum of crack widths in the composite. Nevertheless, the bond behaviour is important with respect to the cracks patterns and the resulting individual/average crack widths.

The transfer of shear forces between the reinforcing element and the surrounding concrete matrix ensures that the strain states of the two components of the composite are equalized. In the

regions with equal strain states of the reinforcement and concrete, further cracks may develop when an increase tensile loading causes stresses exciding local tensile strength of concrete. For a completed crack pattern in state IIb, the theoretical crack distance s_r is in the range between the single and double load transfer length l_{ef} [2], [7], according to Eq. 3 with the theoretical minimum s_{rmin} and maximum s_{rmax} crack distance in the completed crack formation state:

$$s_{rmin} = l_{ef} \leq s_r \leq 2 \times l_{ef} = s_{rmax} \quad 3$$

Figure 5 schematically illustrates the two extreme values of the ideal crack spacing.

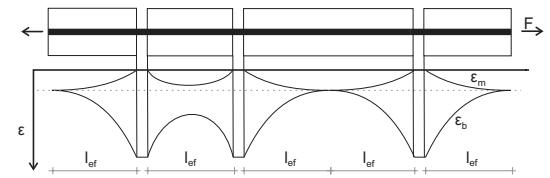


Figure 5: Schematic representation of the idealized crack distances (between the single and double load transfer length l_{ef}) in the closed crack pattern (with ϵ_m being the strain of concrete) | graphic: Kai Schneider

The load transfer length determining the crack spacing can be set equal to the anchorage length in the pull-out tests. By systematically changing the anchorage length and measuring the beginning of the pull-in, it is possible to predict the theoretical slip progress, see Figure 6.

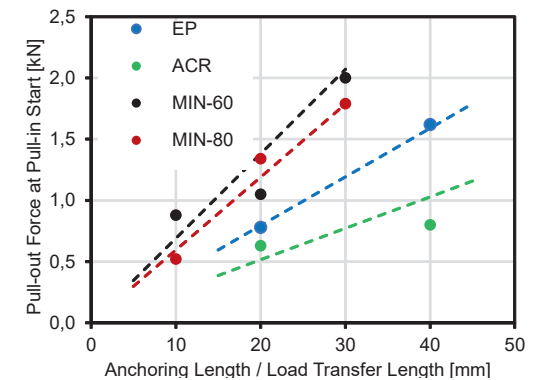


Figure 6: Slip progress flow estimated using Eq. (4) and the values obtained from the pull-out tests | graphic: Kai Schneider

The slip progress flow k_{lef} describes the bond condition when a continuous slippage begins over the entire bond length. The slip progress flow is determined from the mean values of the respective pull-out forces at the start of the pull-in $F_{s0=0}$ in relation to the anchoring length x of the pull-out test performed, see Eq. 4:

$$k_{l_{ef}} = \frac{1}{n} \sum_{k=1}^n \frac{F_{S_o=0}}{x} \tag{4}$$

The load transfer length depends directly on the initial cracking force F_{cr} of the enveloping concrete. By dividing the initial cracking force by the slip progress flow, a theoretical load transfer length is obtained, see Eq. 5:

$$l_{ef} = \frac{F_{cr}}{k_{l_{ef}}} \tag{5}$$

The first-crack force was read from the stress-strain relations obtained in the uniaxial tension tests on the composite specimens, see Figure 7. Table 2 shows the results of the evaluation. The reduction in the first crack force for the specimens with EP reinforcement when compared to the other reinforcement materials can be explained by the larger weft yarns acting as flow and predetermining failure cross-sections.

Under the assumption of a maximum crack distance of the double load transfer length, the maximum crack width $w_{r_{max}}$ is given by Eq. 6:

$$w_{r_{max}} = 2 \times l_{ef} \times \epsilon_b \times k_1 \tag{6}$$

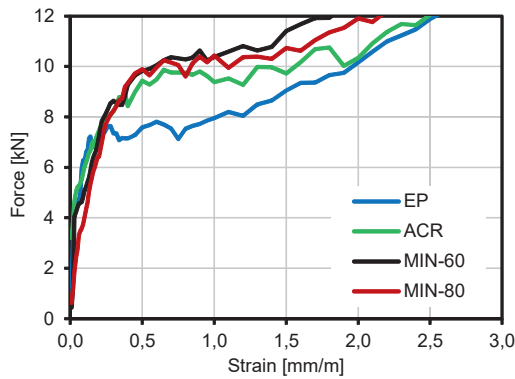


Figure 7: Force-strain curves in showing transition from the uncracked state to cracked state of composite specimens | graphic: Kai Schneider

Reinforcement	Slip progress flow [kN/mm]	First crack force composite specimen [kN]	First crack force per reinforcing element [kN]	Calculated load transfer length [mm]
EP	0,040	7,5	1,5	37,7
ACR	0,026	9	1	38,8
MIN-60	0,069	9	1	14,5
MIN-80	0,060	9	1	16,8

Table 2: Overview of the carbon reinforcements under investigation

Figure 8 shows both the measured maximum crack widths and the calculated maximum crack widths. The prediction accuracy by Eq. 6 is over 80%. The ratio of the measured mean crack widths to the maximum crack widths averaged over all tests is 0.63 and agrees well with the ratio of 0.6 determined by Füllsack [2].

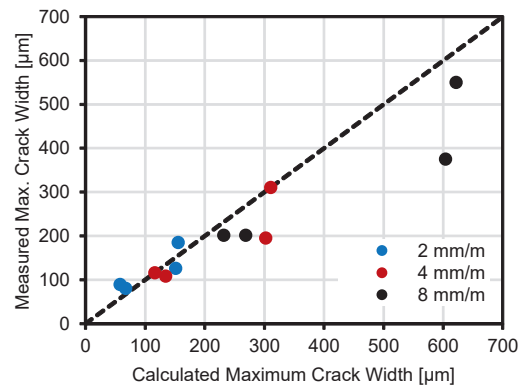


Figure 8: Comparison of maximum measured crack width and the calculated maximum crack width | graphic: Kai Schneider

Figure 9 shows the comparison of the measured mean crack widths and the calculated mean crack widths. The mean crack width w_r was calculated by multiplying the maximum crack width by the scaling factor k_2 of 0.63, see Eq. 7:

$$w_r = w_{r_{max}} \times k_2 \tag{7}$$

The formation of new cracks with increasing tensile load leads to a reduction of the load transfer length. While a tendency to overestimating the crack width was observed for a strain level of 2 mm/m by using above formulas, this trend reverses for a strain level of 8 mm/m. This can be traced back to the crack spacing decrease with increasing load and stress level. At the strain level of 4 mm/m, the prediction accuracy of the maximum crack width is the best, with nearly 87% reliability. This leads to a conclusion that the force

introduction length depends on the load level and thus should be considered as its function in order to increase the prediction accuracy.

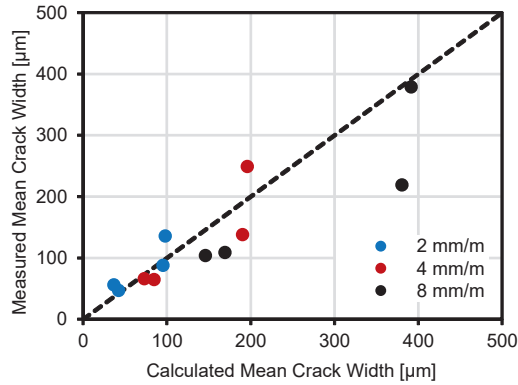


Figure 9: Comparison of mean measured crack width and the mean calculated crack width | graphic: Kai Schneider

5 End anchorage length

Lorenz [8] chose the ultimate limit state as a criterion for the design of the required end anchorage length and used the maximum bond flow as the design base. The deformations occurring prior to reaching the maximum force were not considered. In the serviceability limit state, the design of the end anchorage length is basically defined by the absence of slip at the end of the anchorage. By using the experimentally determined slip progress flow $k_{l_{ef}}$ the required minimum end anchorage length $l_{erf,GZG}$ for the service load F_{GZG} can be determined using Eq. 8:

$$l_{erf,GZG} = \frac{F_{GZG}}{k_{l_{ef}}} \quad 8$$

Figure 10 shows the schematically the design approach for the end anchorage length in the serviceability limit state by using slip progression measurements in comparison to the ultimate limit state according to Lorenz [8]. The maximum force is limited by the tensile load capacity of the reinforcing element.

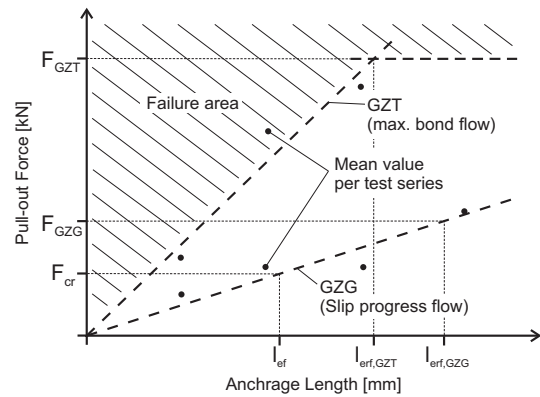


Figure 10: Suggested approach for the design of the end anchorage length in the serviceability limit state including the end anchorage length in the ultimate limit state and the initial crack force for the design of crack width | graphic: Kai Schneider

6 Summary

The slip progress flow describes the bond condition when a continuous slippage begins over the entire bond length. With the help of the experimentally determined slip progress flow, it is basically possible to carry out designs in the serviceability limit state, in particular, the design of crack widths in the structural element and the design of the end anchorage length of the reinforcement element in the serviceability limit state.

7 References

- [1] M. Curbach, R. Ortlepp, S. Scheerer and M. Frenzel, Verstärken mit Textilbeton–Weg von der Vision zur Anwendung. *Der Prüflingenieur*. 2011;39:32–44.
- [2] R. Füllsack-Köditz, Verbundverhalten von GFK-Bewehrungsstäben und Rissentwicklung in GFK-stabbewehrten Betonbauteilen. Dissertation Bauhaus-Uni Weimar. 2004
- [3] K. Schneider, A. Michel, M. Liebscher, L. Terreri, S. Hempel and V. Mechtcherine, Mineral-impregnated carbon fibre reinforcement for high temperature resistance of thin-walled concrete structures. *Cement and Concrete Composites*. 2019;97, 68-77.
- [4] K. Schneider, A. Michel, M. Liebscher and V. Mechtcherine, Verbundverhalten mineralisch gebundener und polymergebundener Bewehrungsstrukturen aus Carbonfasern bei Temperaturen bis 500° C. *Beton- und Stahlbetonbau*. 2018;113(12), 886–894.
- [5] K. Schneider, M. Butler and V. Mechtcherine, Carbon Concrete Composites C3–Nachhaltige Bindemittel und Betone für die Zukunft. *Beton- und Stahlbetonbau*. 2017;112(12):784–94.
- [6] T. Büttner, C. Morales Cruz and M. Raupach, Dauerhafte Schutzschichten aus Textilbeton für Bauwerksoberflächen im Wasserbau. *Bautechnik*. 2013;90(8):485–90.
- [7] J. Niewels, Zum tragverhalten von betonbauteilen mit faserverbundkunststoff-bewehrung. IMB, Eigenverl.; 2008.
- [8] E. Lorenz, Endverankerung und Übergreifung textiler Bewehrungen in Betonmatrices. Dissertation TU Dresden. 2014.

Mechanical model for the calculation of the splitting forces in textile-reinforced concrete



Philipp Preinstorfer

Dipl.-Ing. Dr. techn.
TU Wien, Vienna, Austria

✉ philipp.preinstorfer@tuwien.ac.at

Postdoctoral researcher at TU Wien. Finished his doctoral studies in 2019 on the splitting failure in textile-reinforced concrete.



Johann Kollegger

O.Univ.Prof. Dipl.-Ing. Dr.-Ing.
TU Wien, Vienna, Austria

✉ johann.kollegger@tuwien.ac.at

Professor and Head of the Research Unit Structural Concrete at TU Wien.

1 Abstract

The magnitude and distribution of the splitting forces in textile-reinforced concrete (TRC) strongly depend on the geometric characteristics of the fiber strand. Based on optical measurements of various types of textile reinforcement, researchers at TU Wien identified four parameters specifying their geometry. This allowed for a comparison of different fiber strands in experimental and numerical studies. Based on the results, a mechanical model for the calculation of the splitting forces in TRC is presented.

Keywords: Textile-reinforced concrete; splitting crack; bond; splitting tensile stress

2 Introduction

The bond between reinforcement and cementitious matrix is of utmost importance for the functionality of a reinforced structure. Due to the wide variety in terms of mechanical as well as geometrical properties of textile reinforcements, a direct transfer of the design rules for steel-reinforced concrete to textile-reinforced concrete (TRC) is not possible. The bond behavior of this novel material has therefore always been one of the main research topics since the beginning of textile reinforcement development.

In the past, investigations on the bond behavior of TRC usually dealt with the inner bond between the single filaments [1, 2] and the bond performance between the cementitious matrix and the fiber strand [3-5], where in the latter several possible influencing parameters could be identified (e.g. the surface roughness, knitting yarn...). The failure criteria for the pull-out of the fiber strand in this case is defined by the maximum value of the bond force transmitted between the two phases. The main bond mechanisms in this case were adhesive bond (before pull-out) and friction (after pull-out) [6].

With the development of fiber strands with a high yarn count (Heavy Tows) because of economic reasons [7], which are additionally impregnated with a stiff coating material (e.g. epoxy resin) in order to increase the effectiveness of the reinforcement, a new failure mechanism due to spalling of the concrete cover was observed [8-11]. The splitting failure is characterized by longitudinal cracking induced in the concrete once the maximum bond force is reached, leading to a progressive loss of the bond performance, which also affects the structural behavior [12, 13].

In contrast to steel-reinforced concrete, where longitudinal cracking is avoided by minimum values of concrete cover or a minimum amount of shear reinforcement overlapping the longitudinal reinforcement, such detailing would oppose the design philosophy of TRC of thin-walled filigree structural components. The focus therefore should be the consideration of possible longitudinal cracking by means of appropriate design models.

3 Geometric characterization of textile reinforcement

Longitudinal cracking is caused by high splitting tensile stresses occurring in the concrete. The magnitude and distribution of these stresses are mainly influenced by the geometric properties of the fiber strand, whereas the influence of the transverse fiber strand by knot resistance on splitting crack formation can be neglected [14]. This cracking behavior has often been observed in structural elements with textile reinforcement in which the fiber strands in weft and/or warp direction exhibit a pronounced regularly repeating variation in cross-sectional dimensions. In these cases a mechanical interlock is achieved in between the fiber strands and the cementitious matrix, leading to a high bond performance with simultaneous high stress concentrations [9, 14]. Additionally, a strong influence can be attributed to the cross-sectional shape of the fiber strands. Due to the manufacturing process, textile reinforcement often exhibits a flat elliptical shape amplifying the splitting tensile stresses in direction orthogonally to the reinforcement, resulting in the main occurrence of longitudinal cracking in the layer of the textile reinforcement [15]. This cracking behavior is further intensified by the fact, that the splitting tensile stresses in the layer of the textile reinforcement between adjacent fiber strands are inversely aligned and therefore are partly cancelling each other [5], whereas this is not the case for splitting tensile stresses orthogonally to the layer of the fabric (if there is only one layer of fabric).

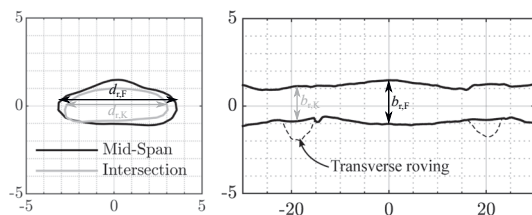


Figure 1: Cross section (left) and longitudinal section (right) of a typical fiber strand [14] | graphic: Philipp Preinstorfer

Based on optical measurements of various types of textile reinforcements the geometric characteristics of different fiber strands were depicted in the cross section as well as the longitudinal section (see exemplarily Figure 1). By comparing the different fiber strands, four geometric parameters – (a) the cross-section geometry, (b) the regularly repeating variation of cross-sectional dimensions, (c) the dominant direction of the regularly repeating variation of cross-sectional dimensions and

(d) the waviness of the fiber strand – were identified and first described by Preinstorfer [15], which predominantly influence the magnitude and distribution of splitting forces in TRC. These parameters are briefly summarized in this section, as they are of importance for the understanding of the mechanical model in Section 4.

3.1 Cross-section geometry

To describe the cross-sectional shape a parameter k_F is introduced. Starting off with k_F equaling 1.00 the fiber strand has a perfectly round cross-sectional shape. With an increasing k_F the fiber strand changes into an elliptical shape. Parameter k_F is calculated using Eq. (1):

$$k_F = \frac{U_r}{U_{kr}} \quad 1$$

with U_r being the circumference of the cross section of the fiber strand and U_{kr} being the circumference of a circle with an identical cross-sectional area as the fiber strand $A_r = A_{kr}$.

3.2 Regularly repeating variation of cross-sectional dimensions

The regularly repeating variation of the cross-sectional dimensions is described using parameter k_A , relating the cross-sectional area at midspan (typically maximum in size) to the cross-sectional area at the intersections with the transverse strands (typically minimum in size), see Eq. (2):

$$k_A = \frac{A_{r,F}}{A_{r,K}} \quad 2$$

If parameter k_A is 1.00 in size the fiber strand exhibits no variation in cross-sectional dimensions, while for bigger values the variation increases.

3.3 Dominant direction of repeating variation of cross-sectional dimensions

To describe in which direction the regularly repeating variation of cross-sectional dimensions is more pronounced (thickness or width), parameter k_p , which relates the change of thickness to the change of width per half mesh-width (midspan to the intersection), is introduced, see Eq. (3):

$$k_p = \frac{(d_{r,F} - d_{r,K}) - (b_{r,F} - b_{r,K})}{(d_{r,F} - d_{r,K}) + (b_{r,F} - b_{r,K})} \quad 3$$

If k_p is 0.00, the regularly repeating variation appears uniform, while for values $-1.00 < k_p < 0.00$ or $0.00 < k_p < 1.00$ the variation is dominant in direction of the width or thickness, respectively.

3.4 Waviness

A possible waviness of the fiber strand is described using the parameter k_w , which relates the deviation of the longitudinal axis of the fiber strand per mesh-width f (e.g. from midspan to the intersection) to the center-to-center distance of the transverse fiber strands e , see Eq. (4):

$$k_w = \frac{f}{e} \quad 4$$

If parameter k_w is 0.00 the fiber strand is straight in longitudinal direction, while for increasing values of k_w the waviness becomes more pronounced.

4 Splitting Force Model (SF-model)

4.1 Model approach

In the following section a mechanical model, which firstly was introduced by Preinstorfer in [15] is described, which allows for the calculation of the size and magnitude of the splitting forces in TRC, see Eq. (5) and (6). The model was established on the base of experimental and numerical studies, which were described in detail by the authors in a different publication [14]. The various terms in the equations can be directly linked to the geometric parameters introduced in Section 3. It is mentioned here, that this model is limited to fully impregnated fabrics with no porosity occurring between the single filaments. The fabric can therefore be considered as a homogeneous solid. This is often the case e.g. for epoxy impregnated textiles [2].

$$F_{sp,y} = \alpha_F \cdot \sin \varphi \cdot \tan \theta \cdot F_x \quad 5$$

$$F_{sp,z} = (1 - \alpha_F) \cdot \cos \varphi \cdot \tan \theta \cdot F_x \quad 6$$

with:

$$\alpha_F = \frac{a}{(a+b)} \quad 7$$

and a and b being ellipse axis (where $a > b$; see also section 4.1.1)

4.1.1 Influence of regularly repeating variation in cross-sectional dimensions

The presented research in this paper focuses on fiber strands exhibiting a pronounced regularly repeating variation in cross-sectional dimension. The variation acts as a flat rib consequently enabling a mechanical interlock between the fiber strand and the surrounding concrete. Similar to steel-reinforced concrete [16] a concrete compression strut originates where the thicker part of the fiber strand gets pulled out of the smaller concrete channel, see Figure 2.

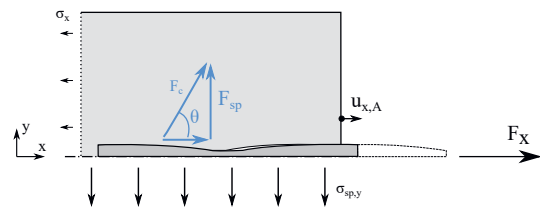


Figure 2: Resulting concrete compression strut and tensile splitting force thereof. | graphic: Philipp Preinstorfer

Due to the flat shape of the ribs, the concrete compression strut originating from the textile reinforcement is likely to have a steep angle. The splitting tensile stresses can be calculated according to Eq. (8).

$$F_{sp} = \tan \theta \cdot F \quad 8$$

Within the range of $1.20 < k_A < 1.80$, typical for standard textile reinforcement, the concrete compression strut was calibrated in numerical calculations to have an angle of 60° (see also subsection 4.2).

4.1.2 Influence of the cross-sectional dimensions

With increasing flatness of the fiber strand (elliptical shape), a decisive rise in the splitting stresses in direction of the smaller axis of the ellipse ($b < a$; see Figure 3) was noticed.

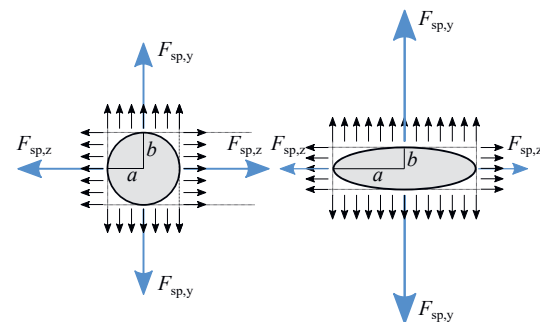


Figure 3: Simplified distribution of tensile splitting stresses for different cross-sectional geometries | graphic: Philipp Preinstorfer

By simplifying the concrete tensile stresses, as pictured in Figure 3, the non-uniform distribution of the splitting tensile stresses can be expressed by the factor α_F , see Eq. (9) and (10). This factor stands for the relation of the width of the fiber strand to the sum of its width and thickness (Eq. 6).

$$F_{sp,y} = \alpha_F \cdot F_{sp} \quad 9$$

$$F_{sp,z} = (1 - \alpha_F) \cdot F_{sp} \quad 10$$

α_F can be directly linked to parameter k_F by Eq. (11):

$$a = b \cdot \left(\frac{2}{9} \cdot \lambda^2 + \frac{2}{3} \cdot \lambda \sqrt{\frac{1}{9} \cdot \lambda^2 - 1} - 1 \right) \quad 11$$

with

$$\lambda = 2 \cdot k_F + 1 \quad 12$$

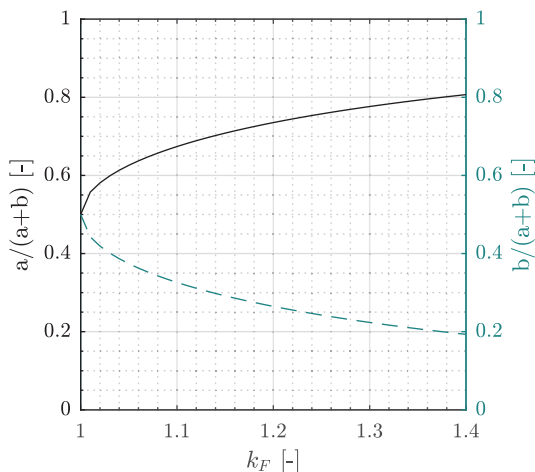


Figure 4: Influence of cross-section shape on the splitting tensile stresses [15] | graphic: Philipp Preinstorfer

In Figure 4 the non-uniform distribution of the tensile splitting stresses due to the elliptical shape of the strand is depicted for values $1.00 < k_F < 1.40$.

In Figure 4 it is clearly visible, that the tensile splitting stresses increase in direction of the smaller ellipse axis with the rising parameter k_F .

4.1.3 Influence of the dominant direction of the regularly repeating variation in cross-sectional dimensions

Additionally to the influence of the cross-sectional shape on the non-uniform distribution of the tensile splitting stresses, the dominant direction of the regularly repeating variation also plays a key role in this context. Figure 5 depicts this effect, with the area in light grey symbolizing a dominant

thickening (left) or a dominant widening (right) of the fiber strand respectively.

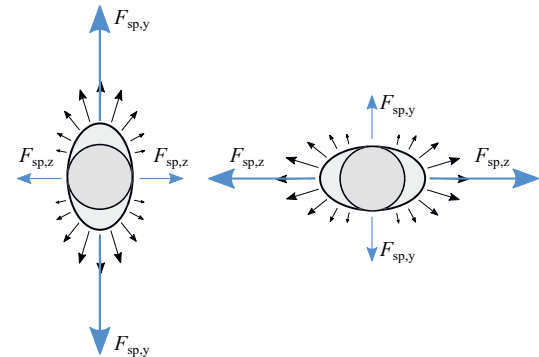


Figure 5: Distribution of splitting tensile stresses due to a thickening or widening of the fiber strand | graphic: Philipp Preinstorfer

In Figure 6 a segment of a fiber strand between π and $\pi/2$ is visualized. The area between function f (max. cross-sectional dimensions) and function g (min. cross-sectional dimensions) describes the widening between midspan and the intersection.

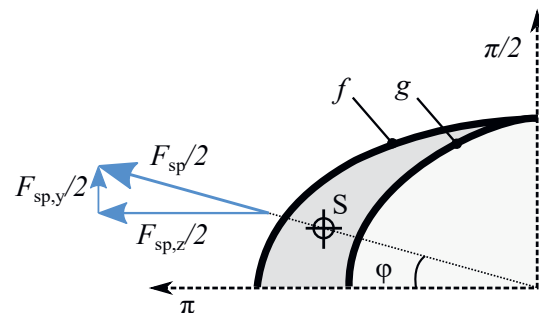


Figure 6: Inclination φ of splitting tensile force | graphic: Philipp Preinstorfer

In the following it is assumed that the resulting tensile splitting stress in this segment is orientated to the center of gravity of the widened part of the fiber strand (dark grey area between f and g). The inclination of the resulting splitting tensile force can therefore be calculated according to Eq. (13).

$$\varphi = \cot \frac{a_f^2 \cdot b_f - a_g^2 \cdot b_g}{a_f \cdot b_f^2 - a_g \cdot b_g^2} \quad 13$$

Thus the splitting tensile stresses are calculated by:

$$F_{sp,y} = F_{sp} \cdot \sin \varphi \quad 14$$

$$F_{sp,z} = F_{sp} \cdot \cos \varphi \quad 15$$

The inclination φ can be directly linked to parameter k_F , as this parameter is dependent upon the dimensions of the fiber strand at midspan as well as at the intersections. In Figure 7 the influence of

the dominant direction of the regularly repeating variation is depicted in terms of parameter k_p in the range of $-1.00 < k_p < 1.00$.

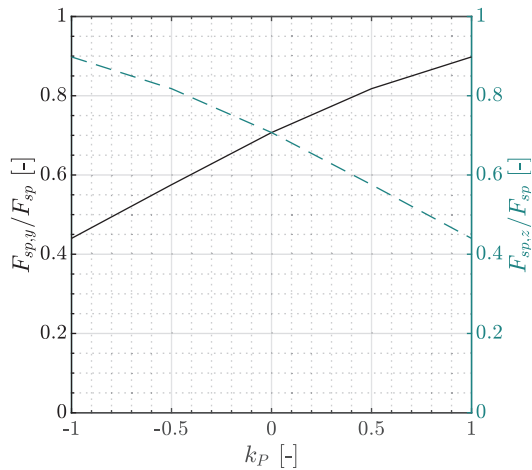


Figure 7: Influence of dominant direction on the splitting tensile stresses [15] | graphic: Philipp Preinstorfer

Even though it is not as decisive as the cross-sectional shape a clear influence of the dependency of the fiber strand dimensions is noticeable.

4.1.4 Influence of the waviness

The influence of the waviness of the fiber strand has been extensively investigated by Lorenz (e.g. [17]). Optical measurements of the different investigated fiber strands showed that all used samples of textile reinforcement were almost straight in longitudinal direction, therefore allowing for a disregard of the influence of the waviness. For higher values of the waviness the authors would refer to the calculation of the deviation forces by Lorenz [17] which can be taken into account additive to the splitting forces calculated using Eq. (5) and (6).

4.2 Comparison with numerical data

In this subsection the tensile splitting forces in y-direction calculated using Eq. (5) are compared with the results of a numerical study of fiber strands within the range $1.00 < k_p < 1.40$ (step size 0.1), $-1.00 < k_p < 1.00$ (step size 0.5) and $k_A = 1.50$. The numerical model was established and calibrated based on experimental data (for detailed information see [14]). By comparing the results according to the SF-model with the results of the numerical study a good correlation, as shown in Figure 8, can be stated.

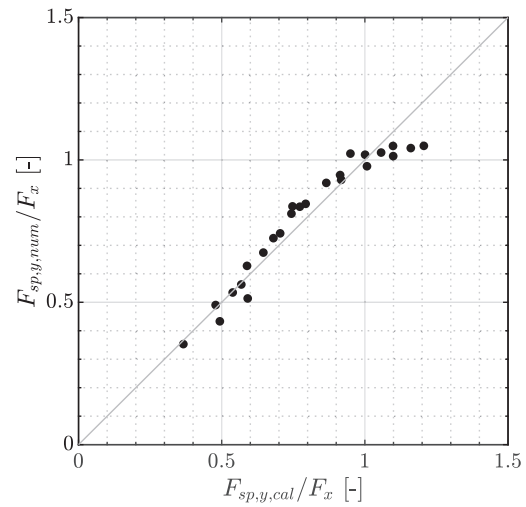


Figure 8: Calculated splitting forces according to SF-model in relation to the numerically calculated results [15] | graphic: Philipp Preinstorfer

The deviation of the results with increasing tensile splitting stresses in the y-direction can be addressed to uncertainties in the elliptical shape description of the fiber strand, as no exact values of the circumference of an ellipse exist. With increasing flatness of the ellipse the results of Eq. (11) became less accurate.

5 Conclusions

The bond behavior of TRC is still a major part of research due to the wide variety of mechanical and geometrical properties of the existing and newly launched textile reinforcements. For certain types of fiber strands a splitting failure due to high splitting tensile stresses could be observed. With regard to this effect following conclusions can be drawn from the research presented in this paper:

- Four geometric parameters – k_p , k_A , k_p , and k_w are introduced describing specific geometric properties of the fiber strands that were identified to play a key role in the magnitude and distribution of the tensile splitting stresses.
- A mechanical model is introduced, which allows for the calculation of the splitting tensile stresses in direction of the layer of the textile reinforcement as well as in direction orthogonally to the layer of the textile reinforcement.
- The parameters k_p , k_A , k_p are directly linked to the mechanical model taking into account the influence of those certain geometric properties on the tensile splitting stresses.

- In comparison to a broad numerical study, where the parameters k_p , k_A , k_p were varied in a wide range, the calculation of the tensile splitting stresses by the SF-model yields sufficient results.
- The calculation of the splitting tensile stresses occurring between the fabric and the cementitious matrix enables a way to account for a longitudinal cracking in TRC. By comparison with experimental data it is shown in [14] and [18], that the SF-model is capable of realistically estimating the magnitude and distribution of the splitting tensile forces.

6 Outlook

The SF-model described in Section 4 was established on the base of fiber strands impregnated with a stiff coating material. According to studies the stiffness of the coating material also plays a key role in the bond behavior. For this reason the influence of the stiffness of the coating material will be investigated in the near future in order to adopt the SF-model in terms of this parameter.

With the introduced SF-model it is possible to calculate the magnitude and distribution of the tensile splitting stresses. To assess the initiation of a longitudinal cracking due to high splitting tensile stresses it is necessary to investigate the concrete resistance. This topic will be the focus of further research in the future.

7 Acknowledgment

The authors want to express their sincere gratitude to solidian GmbH for their support during this research and to Prof. Benjamin Kromoser for the intensive scientific dialogue in the past years.

8 Data availability

The data will be made available by the authors on request.

9 References

[1] NADIV, R.; PELED, A.; MECHTCHERINE, V.; HEMPEL, S.; SCHROEFL, C.: Micro- and nanoparticle mineral coating for enhanced properties of carbon multifilament yarn cement-based composites. *Composites Part B: Engineering* 111 (2017), pp. 179-189. doi: 10.1016/j.compositesb.2016.12.005

[2] HAHN, L.; RITTNER, S.; NUSS, D.; ASHIR, M.; CHERIF, C.: Development of Methods to Improve the Mechanical Performance of Coated Grid-Like Non-Crimp Fabrics for Construction Applications. *Fibres and Textiles in Eastern Europe* 27 (2019), pp. 51-58. doi: 10.5604/01.3001.0012.7508

[3] BANHOLZER, B.: Bond behaviour of a multi-filament yarn embedded in a cementitious matrix. RWTH Aachen, doctoral thesis. 2004.

[4] JESSE, F.: Tragverhalten von Filamentgarnen in zementgebundener Matrix. TU Dresden, doctoral thesis. 2004.

[5] LORENZ, E.: Endverankerung und Übergreifung textiler Bewehrungen in Betonmatrices. TU Dresden, doctoral thesis. 2014.

[6] PREINSTORFER, P.; KROMOSER, B.; KOLLEGGER, J.: Categorisation of the bond behaviour of textile reinforced concrete. *Bauingenieur* 94 (2019), pp. 416-424.

[7] CURBACH, M.; JESSE, F.: Specifications and Application of Textile Reinforced Concrete (TRC). *Beton- und Stahlbetonbau* 104 (2009), pp. 9-16. doi: 10.1002/best.200800653

[8] PREINSTORFER, P.; KROMOSER, B.; KOLLEGGER, J.: Influencing parameters on longitudinal cracking in textile reinforced concrete. *Beton- und Stahlbetonbau* 113 (2018), pp. 877-885. doi: 10.1002/best.201800071

[9] BIELAK, J.; SPELTER, A.; WILL, N.; CLAßEN, M.: Anchorage behavior of textile reinforcement in thin concrete components. *Beton- und Stahlbetonbau* 113 (2018), pp. 515-524. doi: 10.1002/best.201800013

[10] SCHÜTZE, E.; CURBACH, M.: Experimental characterisation of the bond behaviour of carbon reinforced concrete with concrete splitting as significant failure mode. *Bauingenieur* 94 (2019), pp. 133-141.

[11] BEßLING, M.; ORLOWSKY, J.: Investigations on the bond behaviour of textiles with various coatings in TRC. *Proceedings of the fib Symposium 2019: Concrete - Innovations in Materials, Design and Structures*, Kraków, Poland, 2019, pp. 212-219.

[12] KROMOSER, B.; HUBER, P.; PREINSTORFER, P.: Experimental study of the shear load bearing behaviour of thin walled CFRP reinforced UHPC structures. *fib congress 2018 - better, smarter, stronger* (2018), pp. 364-365.

[13] PREINSTORFER, P.; KROMOSER, B.; KOLLEGGER, J.: Flexural behaviour of filigree slab elements made of carbon reinforced UHPC. *Construction and Building Materials* 199 (2019), pp. 416-423. doi: 10.1016/j.conbuildmat.2018.12.027

[14] PREINSTORFER, P.; KOLLEGGER, J.: New insights into the splitting failure of textile-reinforced concrete. *Composite Structures*, 243 (2020), pp. 1-10. doi: 10.1016/j.compstruct.2020.112203

[15] PREINSTORFER, P.: Zur Spaltrissbildung von textilbewehrtem Beton. TU Wien academic press, 2020. doi: 10.34727/2020/isbn.978-3-85448-034-1

[16] TEPFERS, R.: Cracking of concrete cover along anchored deformed reinforcing bars. *Magazine of Concrete Research* 31 (1979), pp. 3-12. doi: 10.1680/mac.1979.31.106.3

[17] LORENZ, E.; ORTLEPP, R.; HAUSDING, J.; CHERIF, C.: Efficiency Increase of Textile Reinforced Concrete by Use of Textile Reinforcements from the Extended Warp Knitting Process. *Beton- und Stahlbetonbau* 106 (2011), pp. 21-30. doi: 10.1002/best.201000072

[18] PREINSTORFER, P.; PINZEK, A.; KOLLEGGER, J.: Modellierung des Verankerungsverhaltens getränkter textiler Bewehrungen. *Beton- und Stahlbetonbau* 115. doi: 10.1002/best.202000011

Bearing behavior of Carbon-Textile-Reinforced Concrete Beams

Kissila Botelho Goliath

PhD Student

PUC-Rio, Brazil

✉ kissilagoliath@aluno.puc-rio.br

PhD Student in the area of structures with a focus on Textile Reinforced Concrete.

Daniel Carlos Taissum Cardoso

Adjunct Professor

PUC-Rio, Brazil

✉ dctcardodo@puc-rio.br

His interests include mechanics of composite materials and performance of composite structures.

Flávio de Andrade Silva

Associate Professor

PUC-Rio, Brazil

✉ fsilva@puc-rio.br

Prof. Silva research interests encompass the area of structures and materials with an emphasis in cement based composites.

1 Abstract

In the present work, the flexural behavior of carbon TRC I-beams is investigated. Four-point bending tests were performed in three beams, considering the following material conditions: i) regular cementitious matrix; ii) regular matrix and sand-coated textile; and iii) SHCC matrix. The main goal of the research was to correlate the improvements on interface and matrix properties with the crack pattern, failure mode and ductility. The carbon-TRC beams with plain concrete without and with the impregnation of sand-epoxy presented a less ductile behavior than beams with an SHCC matrix.

Keywords: Textile Reinforced Concrete (TRC), I-section beam, Carbon textile, SHCC.

2 Introduction

Textile reinforced concretes (TRCs) have been used for new constructions and load-bearing structural members [1-4]. The aforementioned advantages eliminate the need for large concrete covers, allowing the creation of thin, modular structures and slender concrete members [5,6].

Despite a significant number of works addressing the load-bearing behavior of full TRC beams under bending can be found in literature, [5-9], these have mainly focused on the calibration of design methods considering different types of textile, beam geometries and reinforcing ratio. In fact, the existing approaches are usually based on cross-section analysis (moment-curvature) adapted from design models available for RC, incorporating the influence of the different bond characteristics between matrix and reinforcement through the use of efficiency factors [7].

Some studies have found that the use of sand-epoxy impregnation can enhance mechanical

bond strength, frictional resistance and stiffness [10-18], thus improving member bearing. This is due to the increased surface roughness introduced by sand, reducing the slip between fibers and matrix [14] and making the forces between constituents to be transferred more effectively. Moreover, crack pattern is improved by reducing crack width and spacing. On the other hand, the strong bond strength may lead to a simultaneous abrupt fracture of all filaments comprising the textile, which characterizes a brittle failure [16].

Hybrid fiber reinforced composites consisting of strain-hardening based-cement composite (SHCC) matrices and continuous textile reinforcement yield a better crack control with a pronounced multiple cracking behavior [15-23]. Research papers [10, 17, 23] have reported an increase in composite strain capacity and mechanical properties when simultaneously applying textiles and short fibers as reinforcement in cementitious matrices in comparison to ordinary TRC. Conversely, other authors [11, 17, 24] have reported no gain in ultimate strain. In addition, the use of the SHCC

matrices results in high inelastic deformations, leading to a ductile behavior along with higher energy dissipation [18, 19].

The main goal of this research is to investigate the performance of Carbon-TRC beams considering different material conditions: plain TRC, sand-coated TRC and hybrid TRC-SHCC. An experimental investigation is carried out and the results such as failure modes, load-deflection curves and cracking patterns are reported.

2.1 Materials and Mechanical Characterization

2.1.1 Carbon Textile

A flexible carbon textile coated with styrene-butadiene rubber (SBR) resin supplied by the company V.FRASS denominated SITgrid017KB was used in the study. It is a bidirectional mesh with openings of 10 and 8.5 mm and widths of 4.2 and 2.7 mm in the warp and weft directions, respectively. Details of the warp yarns that form the textiles were observed using a Nikon stereo microscope model SMZ800N and a cross-sectional area of 3.32 mm² and a perimeter of 9.1 mm were measured. Santos [25] performed uniaxial tension test in the same carbon warp yarn. It was obtained an average tensile strength $f_f = 1140$ MPa and a modulus of elasticity $E_f = 189$ GPa, referred to the measured cross-section area.

For coated carbon textiles, the filament yarns are firstly coated to allow the fabric to be structured as well as for an improved force transfer between outer and inner filaments within the yarn. In the present work, the used textile consists in carbon filaments fully impregnated with SBR. Therefore, in order to improve the bond between textile and matrix, an extra impregnation with epoxy resin (Sikadur®-32) and sand with the same grain size as the sand used as fine aggregate in the matrix (1.18 mm) – hereafter referred as rigid impregnation – was applied over the yarns. The impregnation process was performed manually at least 24 hours before sample preparation. Epoxy resin was impregnated first, followed by sand pulverization. Throughout the work, the specimens made with textile with and without a rigid impregnation were denominated ST (sand-epoxy impregnation) and RT (plain SBR-coated reference textile), respectively.

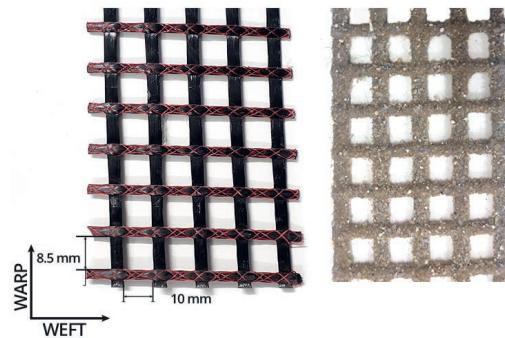


Figure 1: Carbon Textile: no coating (left) and sand-coated (right) | photos: Kissila Botelho Goliath

2.1.2 Matrix

Two different types of matrices were used in this study, the plain concrete and the strain-hardening cement-based composite (SHCC) with 2% in volume of PVA fibers (Polyvinyl Alcohol), designed M1 and M2 respectively. The Kuralon® REC15 fibers used, supplied by Kuraray™, had a length of 12 mm and an average diameter of 40 μm.

Properties	M1	M2
Compressive strength [MPa]	76.0 ± 2.6	37.8 ± 2.8
Compressive strain at peak [mm/mm]	0.0033	0.0038
Young's Modulus [GPa]	25.5 ± 0.8	23.1 ± 0.4

Table 1: Main compressive properties

The plain concrete was designed for a cement-based composite reinforced with textile, adapted from previous studies [11]. The SHCC matrix was chosen based on its ability to improve ductility of TRC [17-21]. For the composition of the mixture of the SHCC matrix, an adaptation of the dosage adopted by Curosu [22] was used. The main compressive properties are presented in Table 1 and mechanical response of the concrete matrices in compression test shown in Figure 2.

The normal strength SHCC is intended to improve the ductility and load-bearing capacity after first crack formation under uniaxial tensile loads. Although from the structural point of view it acts as the matrix, the SHCC is already a composite, being highly sensitive to its composition. The energy absorption and high strain-capacity are due to the occurrence of multiple cracking and the controlled crack opening [26]. To obtain this behavior and ensure the initiation of cracks, a restric-

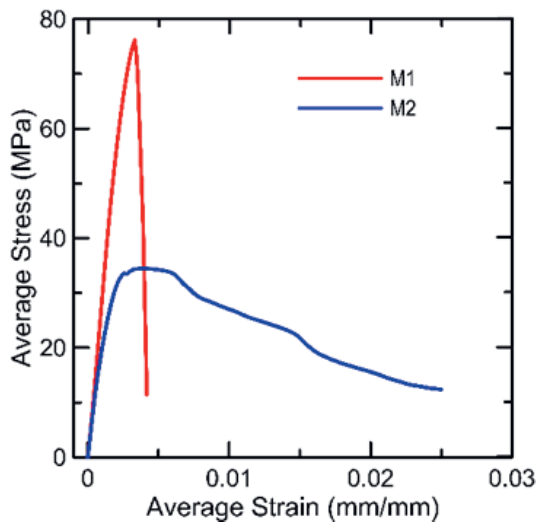


Figure 2: Mechanical response of the concrete matrices in compression test. | graphic: Kissila Botelho Goliath

ted particle size distribution is necessary, obtained with fine-grained material [22]. It is important to highlight the post-peak behavior of the M2 matrix (Figure 2). The SHCC shows a smooth drop after the maximum peak load which strongly contributes to ductility of the composite.

2.2 Four-Points Bending Test

Carbon-TRC beams were tested in four-points bending test to assess their flexural performance in three different conditions: with reference textile and plain matrix (RT-M1), with sand-epoxy impregnation and plain matrix (ST-M1) and with reference textile and SHCC (RT-M2). Three 2000 mm long beams having I-sections with 80 mm of flange width, 180 mm of depth and 12.5 mm of thickness for both web and flange were fabricated, one sample for each aforementioned condition.

The beams were cast using a steel formwork with the desired final dimensions. Care was taken to place the textile in the middle of the entire sample thickness, i. e. flanges and web. The warp direction was positioned longitudinally to the beam. The reinforcement assemble cage was put in the formwork before the concrete was cast horizontally. The beams were removed from the formwork after 48 hours and kept in a humid chamber until a day before testing. They were tested at 28 days of age at room temperature.

The beams were tested in a four-point bending configuration over an 1800 mm span and with a shear span of 750 mm. A hinge was placed over the load distribution beam to ensure equal forces to be applied at the loading points. Testing was conducted using a servo-controlled hydraulic actuator with load capacity of 500 kN under displacement control at a rate of 1 mm/min. The deflection was measured with a displacement transducer placed at the mid-span and a strain gage was installed at the top of the beam mid-span to capture the compressive strain evolution throughout the test. An overview of the test setup and a detailed scheme is presented in Figure 3.

3 Discussion, Conclusions and Acknowledgements

The bearing behavior of carbon-textile-reinforced concrete I-section beams was evaluated through four-point bending tests and compared to theoretical results. Table 2 summarizes the main results obtained experimentally. The tested beams presented different failure modes as seen in Tab-

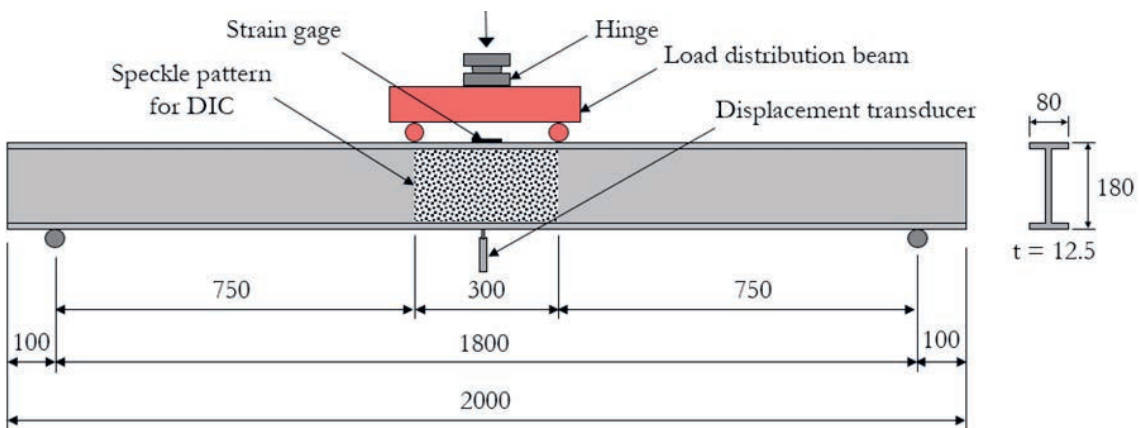


Figure 3: Four-point Bending Test: scheme and detailed dimensions (in mm) | graphic: Kissila Botelho Goliath

Samples	RT-M1	ST-M1	RT-M2
Failure mode	Shear	Flexural	Crushing of concrete
F _{max, exp} [kN]	13,5	16,1	12,7
F _{max, exp} / F _{max, theo}	0,83	0,85	-
δ _{max} [mm]	36,2	25,5	56,2

Table 2: Summary of results

le 2. Figure 4 shows the front and back beams at failure. RT-M1 exhibited three macro-cracks in the region between load application, i.e., the constant moment region. However, its failure was governed by shear between support and load application, causing the beam to fail prematurely before reaching its flexural capacity. The shear stress, characterized by the formation of critical diagonal crack and longitudinal tearing along web-to-flange junction, is shown in Figure 4a.

The yarns that connected the web to the flanges had low penetration into the matrix which could lead to failure. This is enhanced by the poor adherence of strands to the SBR coating, which does not occur in other cases. For the RT-M2 beam, the PVA fibers helped the load transferring between web and flange while the ST-M1 beam the weft yarns coated have better adherence and could provide a better transfer of load between web and flange.

In the case of the reinforced beam with surface treated textile, the failure mode was characterized by rupture of longitudinal yarn. The improvement in bonding between matrix and fabric modified the rupture shape, making ST-M1 failure by bending, as presented in Figure 4b. Finally, the beams with SHCC matrix (RT-M2) failed due to the crushing of concrete because of its lower compressive strength. RT-M2 rupture occurred near at the load application zone, forming a wedge mechanism (Figure 4c). It is also possible to observe in Figure 4c a network of micro-fibers formed in this beam.

The load-deflection curves of TRC beams, which were measured with displacement transducers, are shown in the Figure 5a. It can be noticed the ST-M1 presented the highest peak load, i.e. an increase of 19.5 % with respect to RT-M1. For both beams, an approximately linear elastic behavior was obtained for both beams, with a similar mid-span deflection at failure of 25 mm, followed by an abrupt failure (Table 2). The re-

sults therefore show there was an improvement in the flexural behavior in terms of strength and stiffness after sand-coating.

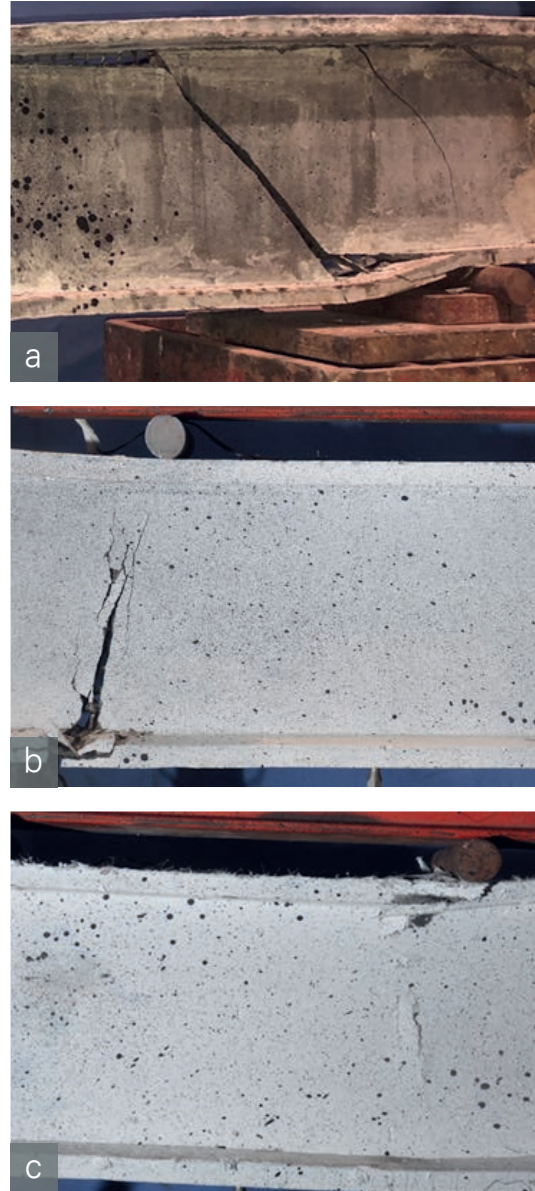
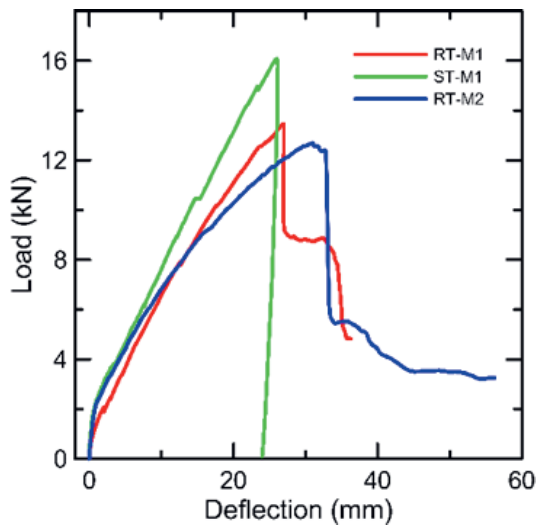
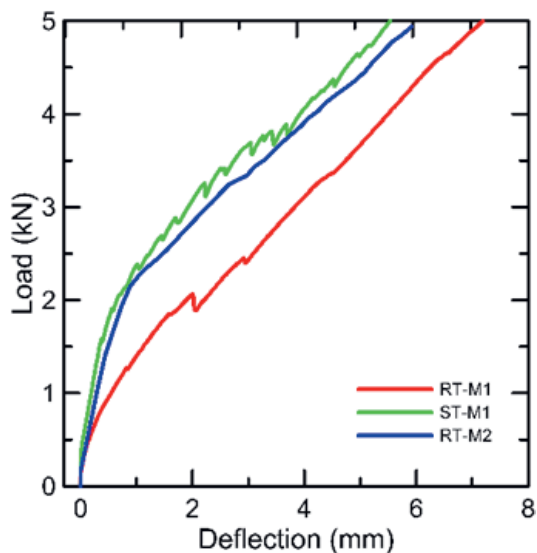


Figure 4: Failure mode of the (a) RT-M1, (b) ST-M1 and (c) RT-M2 beams | photos: Kissila Botelho Goliath



a



b

Figure 5: Load-deflection curve to four-point bending test (a) and initial loading stages (b) | graphic: Kissila Botelho Goliath

The RT-M2 presented behavior similar to ST-M1 at initial loading stages before the first crack and during the beginning of crack formation (Figure 5b). It is possible to observe better load transfer and greater deflection of the beam with short fiber in the matrix. For beam RT-M2, there is a loss of linearity after a deflection of approximately 20 mm and the final load was 5.6% smaller than RT-M1, but with a final deflection of 56.2 mm, i.e. % greater than RT-M1. The SHCC matrix has high tensile strength, enhanced crack control and improved stiffness in crack state compared to plain matrix beams; however, it has lower compressive strength. The ductility of RT-M2 in this case is associated to the

greater capacity of matrix to dissipate energy both in tension and compression. Differently from the other beams, RT-M2 did not fail abruptly after bending test.

A model based on plane section analyses was developed. The constitutive laws of concrete materials and textile reinforcement should be firstly known regardless of cross-section shape. These constitutive laws are experimentally determined in compression and yarn tensile tests [25]. Thus, diagrams can be converted into idealized models for a theoretical prediction as showed in Table 2. The difference between the experimental and theoretical results for RT-M1 may be due to their shear failure. The extra impregnation found in ST-M1 was not considered in this model. Other aspects, such as tension stiffening and adherence between materials was not taken into account. RT-M2 theoretical data also is still under analysis.

In the present work, the bending behavior of carbon-reinforced textile concrete I-beams for structural applications was studied. From the experimental results, the following conclusions can be drawn:

- 1) SBR-impregnated carbon fiber textiles were compared to those additionally treated with sand-coating. The effectiveness of the treatment was confirmed by the stiffer and stronger interface obtained after SBR impregnation.
- 2) the use of SHCC matrix did not affect significantly the bond performance between carbon-textile and concrete. The addition of fibers in matrix was able to improve ductility and crack pattern in carbon-TRC elements, yet it has not increased their load-bearing behavior. Slight changes during the uncracked stage was observed. However, after cracking, the use of fibers increased the stiffness of structural members and contributed to reduce crack spacings and openings.
- 3) the extra impregnation and the SHCC matrix changed the failure mode from shear to flexure-governed and crushing of concrete, respectively;
- 4) finally, the improved bonding resulted in increases in load-carrying capacity and stiffness of treated beam with respect to reference and the use of the hybrid reinforcement was efficient to improve ductility of the carbon-TRC beams.

4 References

- [1] Brameshuber, W. (2006) Report 36: textile reinforced concrete- state-of-the-art report of RILEM TC 201-TRC. RILEM Publications, Paris.
- [2] Scholzen, A., Chudoba, R. & Hegger, J. (2015) Thin-walled shell structures made of textile-reinforced concrete: Part I: Structural design and construction. *Struct Concr.* Vol. 16, 106–114.
- [3] Hegger J, Kulas C, Schneider HN, et al (2010) TRC pedestrian bridge-design, load-bearing behavior and production processes of a slender and light-weight construction. In: International RILEM conference on material science. RILEM Publications SARL, 353–364
- [4] Preinstorfer, P., Kromoser, B. & Kollegger, J. (2019) Flexural behaviour of filigree slab elements made of carbon reinforced UHPC. *Constr Build Mater* 199, 416–423.
- [5] Valeri, P., Ruiz, M. F. & Muttoni, A. (2020) Modelling of Textile Reinforced Concrete in bending and shear with Elastic-Cracked Stress Fields. *Engineering Structures* 215, 110664.
- [6] Molter, M. (2005) Zum Tragverhalten von Textilbewehrtem Beton. Ph.D. Thesis, RWTH Aachen University, Germany.
- [7] Hegger, J., Will, N., & Schneider, M. (2011) Textilbeton: Tragverhalten-Bemessung-Sicherheit. *Textilbeton in Theorie und Praxis*, 269-284.
- [8] Hegger, J. & Voss, S. (2008) Investigations on the bearing behaviour and application potential of textile reinforced concrete. *Engineering Structures*, Vol. 30, 2050–2056.
- [9] Kulas, C. (2013) Zum Tragverhalten getränkter textiler Bewehrungselemente für Betonbauteile. Ph.D. Thesis, RWTH Aachen University, Germany.
- [10] Hinzen, M. & Brameshuber, W. (2009) Improvement of Serviceability and Strength of Textile Reinforced Concrete by using Short Fibres. In: Curbach M, Jesse F (Eds) *Textile reinforced structures*. In: 4th colloquium on textile reinforced structures (CTRS4), Dresden, 261–272.
- [11] Yao, Y., Silva, F. A., Butler, M., Mechtcherine, V., & Mobasher, B. (2015) Tension stiffening in textile-reinforced concrete under high speed tensile loads. *Cement and Concrete Composites*, Vol. 64, 49-61.
- [12] Bielak, J., Li, Y., Hegger, J., & Chudoba, R. (2018) Characterization Procedure for Bond, Anchorage and Strain-Hardening Behavior of Textile-Reinforced Cementitious Composites. In: *Multidisciplinary Digital Publishing Institute Proceedings*. Vol. 2 (8), 395.
- [13] Donnini, J., Corinaldesi, V., & Nanni, A. (2016) Mechanical properties of FRCM using carbon fabrics with different coating treatments. *Composites Part B: Engineering*, Vol. 88, 220-228.
- [14] Xu S, Krüger M, Reinhardt H-W, Ozbolt J (2004) Bond Characteristics of carbon, alkali resistant glass, and aramid textiles in mortar. *J Mater Civil Eng*, Vol. 16, 356–364.
- [15] Silva, R. M. de C., de Andrade Silva, F. (2020) Carbon textile reinforced concrete: materials and structural analysis. *Materials Structures*, Vol. 53, 1-17.
- [16] Yin, S., Xu, S. & Li, H. (2013) Improved mechanical properties of textile reinforced concrete thin plate. *Journal of Wuhan University of Technology, Mater. Sci. Ed.*, Vol. 28 (1), 92-98.
- [17] Li, Q. & Xu, S. (2011) Experimental Research on Mechanical Performance of Hybrid Fiber Reinforced Cementitious Composites with Polyvinyl Alcohol Short Fiber and Carbon Textile. *Journal of COMPOSITE MATERIALS*, Vol. 45 (1), 5-27.
- [18] Gong, T.; Hamza, A.A.; Curosu, I. (2019) On the synergetic action between strain-hardening cement-based composites (SHCC) and carbon textile reinforcement. In: 10th International Conference on Fracture Mechanics of Concrete and Concrete Structures FraMCoS-X, Bayonne, France, 23–26.
- [19] Gong, T., Heravi, A. A., Alsous, G., Curosu, I. & Mechtcherine, V. (2019) The Impact-Tensile Behavior of Cementitious Composites Reinforced with Carbon Textile and Short Polymer Fibers. *Applied Science*, Vol. 9, Iss. 19.
- [20] Barhum, R. & Mechtcherine, V. (2012) Effect of short, dispersed glass and carbon fibres on the behaviour of textile-reinforced concrete under tensile loading. *Eng Fract Mech* Vol. 92, 56–71.
- [21] Barhum, R. & Mechtcherine, V. (2013) Influence of short dispersed and short integral glass fibres on the mechanical behaviour of textile-reinforced concrete. *Materials and Structures*, Vol. 46 (4), 557–572.
- [22] Curosu, I. (2017) Influence of Fiber Type and Matrix Composition on the Tensile Behavior of Strain-Hardening Cement-Based Composites (SHCC) under Impact Loading. Ph.D. Thesis, Technische Universität Dresden, Dresden, Germany.
- [23] Zhu, D. et al. (2019) Effects of short fiber and pre-tension on the tensile behavior of basalt textile reinforced concrete. *Cement and Concrete Composites*, Vol. 96, 33–45.
- [24] Silva, F. de A., Butler, M., Mechtcherine, V., Zhu, D. & Mobasher, B. (2011) Strain rate effect on the tensile behaviour of textile-reinforced concrete under static and dynamic loading. *Mater Sci Eng A*, Vol. 528, 1727–1734.
- [25] Santos, F. C. A. dos (2018) Behavior of Textile Reinforced Concrete (TRC) Slender Columns Subject to Compression. Master thesis. Pontifical Catholic University of Rio de Janeiro. Rio de Janeiro, Brazil.
- [26] Mechtcherine, V., Millon, O., Butler, M. & Thoma, K. (2011) Mechanical behaviour of strain hardening cement-based composites under impact loading. *Cement Concrete Composite*, Vol. 33, 1–11.

Corrosion tests for hybrid construction with concrete, metal and carbon

Dr. rer. nat. Jürgen Triebert

Institut für Korrosionsschutz, Dresden, Germany

✉ juergen.triebert@iks-dresden.de

1987–1992 Chemistry studies at Technische Hochschule Merseburg

1992–1997 Promotion at Martin-Luther-Universität Halle-Wittenberg

Since 2003 Institut für Korrosionsschutz Dresden (IKS), Head of the Department Coatings and Analytics

Dipl.-Ing. Maximilian May

Technische Universität Dresden, Faculty of Civil Engineering, Institute of Concrete Structures, Dresden, Germany

✉ maximilian.may@tu-dresden.de

2011–2016 Mechanical Engineering studies at Technische Universität Dresden

Since 2017 Research assistant at the Institute of Concrete Structures, Technische Universität Dresden

Univ.-Prof. Dr.-Ing. Dr.-Ing. E.h. Manfred Curbach

Technische Universität Dresden, Faculty of Civil Engineering, Institute of Concrete Structures, Dresden, Germany

✉ manfred.curbach@tu-dresden.de

1977–1982 Studies of Civil Engineering at Universität Dortmund

1987 Promotion at Universität Karlsruhe

Since 1994 Chair of Institute of Concrete Structures, Technische Universität Dresden

Contact: juergen.triebert@iks-dresden.de

1 Abstract

Despite the high corrosion resistance of carbon reinforced concrete, the use of carbon resp. CFRP can lead to completely new corrosion problems. Carbon is electrically conductive and forms an electrochemical potential in aqueous media (and thus also in damp concrete). This potential is very high in common media compared to unalloyed and also stainless steels. When contacting carbon fibres with such steels, e.g. with built-in parts, anchors and dowels, there is – at least in theory – the risk of bimetal corrosion. This was examined in the project C3-V3.4 in the frame of the research initiative „Carbon Concrete Composite – C3“; the findings of which are to be presented here.

Keywords: Carbon reinforced concrete, metal built-in parts, corrosion, bimetallic corrosion, renovation

2 Introduction

Amongst other aspects, carbon reinforced concrete (or short ‘carbon concrete’) is used due to its high corrosion resistance. Nevertheless, the use of carbon in concrete can also lead to completely new corrosion problems. Carbon fibres are electrically conductive and form an electrochemical potential in aqueous media (and thus also in damp concrete). In conventional aqueous electrolytes, this is very high compared to the potential of unalloyed steels up to that of stainless steels. In the case of direct contacting of carbon fibres with such steels, there is – at least in theory – the risk of contact corrosion resp. bimetal corrosion. Such contacts are often unavoidable and can often be expected, e.g. in the following cases:

A) New structures/components made of carbon concrete or hybrid constructions made of concrete, metal and carbon:

- Use of built-in parts or fixings made of higher alloyed stainless steels, e.g. anchors, dowels, connecting or prestressing elements,

B) Repair or strengthening of steel reinforced concrete (RC) structures (e.g. due to carbonation, contamination with chloride, change in use ...) using carbon reinforced concrete:

- Introduction of stainless steel built-in parts into the renovated system, e.g. anchoring of the reinforcing layer,
- Unintended contact of reinforcing steel and carbon fibre when applying a rehabilitation system to the exposed and derusted reinforcing steel of the old concrete.

The danger of bimetallic corrosion on metallic components in contact with the electrochemically much nobler carbon fibre is already well known from machine, aircraft and automobile construction ([1]–[6]). The carbon fibre always acts as the cathode and the base metal acts as the anode, on which the metal dissolution takes place. The corrosion damage always occurs on the base metal, in the case of hybrid design on the built-in parts made of stainless steel or in the case of the repair on the reinforcing steel in (carbonated) old concrete. In contrast to the known corrosion phenomena in the areas mentioned, only a few investigations into the risk of bimetal corrosion on built-in parts in carbon concrete or in renovation solutions.

For bimetallic corrosion to occur at all in carbon concrete, the following requirements must be met:

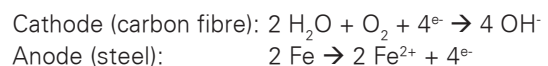
- A sufficient potential difference between the carbon fibre and the steel of >50 mV in the medium in question, i.e. in damp (alkaline, carbonated and/or chloride-contaminated) concrete,
- An electrically conductive contact for electron transfer between the materials,
- An aqueous medium (electrolyte) connecting the two materials with a sufficiently high conductivity for ion transport, and
- A sufficiently large ratio of the surface areas from cathode to anode.

In practice, the actually flowing corrosion current or the resulting corrosion current density are more important than the potential difference between the materials in the corresponding medium. However, this depends crucially on the surface area between the cathode (carbon fibre) and the anode (stainless steel components or unalloyed reinforcing steel). Bimetal corrosion only occurs if the active surface of the cathode is significantly larger than that of the anode. Since the carbon reinforcement used are always impregnated, they generally do not have as large an effective surface as one might expect from their spatial expansion in carbon concrete.

Nevertheless, there are pores and micro cracks in the impregnation layer, and further cracks can form due to mechanical stress when installing the reinforcement in the concrete or mechanical stress during use. In addition, the carbon fibre fabrics can be cut during subsequent drilling of holes for installing of stainless steel built-in or add-on parts such as e.g. dowels or anchors in the carbon

concrete structure, thus exposing numerous carbon fibres for bimetal corrosion processes. In [7], [8] it was recently shown that an epoxy resin impregnated carbon fibre fabric as an intermediate layer in conventional reinforced concrete can even be used as an external current anode for the preventive cathodic corrosion protection of the steel reinforcement. Sufficient protective current densities were thus achieved for the reinforcing steel at standard supply voltages. The active surface of the carbon fibre fabrics in the carbon reinforced concrete does not seem to be so small that bimetal corrosion processes can a priori be excluded.

In principle, the following reactions take place in the case of bimetal corrosion between the carbon fibre and the steel:



It can be seen that for the cathodic partial reaction (oxygen reduction) there must be a sufficiently large supply of oxygen and moisture (electrolyte) in the concrete. When using high-strength and very dense concretes, which are mainly used for carbon reinforced concrete, this is probably only the case near the surface. However, cracks in the concrete and holes for built-in parts represent relevant weaknesses. The corresponding relationships are very complex and the actual situation in real, media-stressed carbon concrete elements is difficult or impossible to predict. For this reason, the problem of possible bimetallic corrosion between carbon fibre and stainless steels and unalloyed reinforcing steel in repair applications (old concrete) was examined in detail in the joint research project C3-V3.4. In addition to exemplary electrochemical tests in aqueous concrete eluates, a large number of test specimens made of carbon reinforced concrete were produced and subjected to different exposures.

3 Experimental concept

3.1 Selection of materials and electro-chemistry

The C3 reference textile SITgrid 040 [9], Figure 1, was selected as textile reinforcement for all tests. In the main bearing direction, the yarns have a fineness of 3200 tex and therefore a reinforcement cross-section of 141.02 mm²/m; the centre distance between the yarns is 12.7 mm. In the

cross direction, the centre distance is 16 mm, the yarn fineness 800 tex and the reinforcement cross-section 28.02 mm²/m. The carbon grid is penetrated and impregnated with an aqueous film-forming polymer dispersion based on polyacrylate. The polymer mass proportion of the consolidated textile was approx. 30%.

In addition to the investigations on whole grids, for the potential difference measurement with metallic components, three carbon rovings with a fineness of 3200 tex and different polymer mass fractions of 0%, 15% and 30% were used.

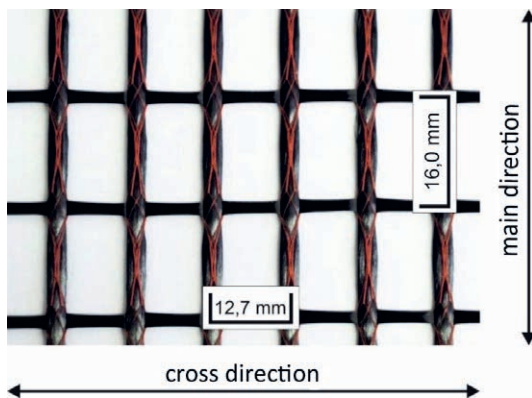


Figure 1: C3 reference textile SITgrid 040 | graphic: Institut für Massivbau, TU Dresden

For the electrochemical investigations, high-alloy, stainless steels from the A4 area were selected, which are usually used for anchors and fastening elements in conventional RC and are therefore also interesting for carbon concrete components. Table 1 shows the corresponding steels and their composition.

Material	Composition
1.4571	X6CrNiMoTi17-12-2
1.4462	X2CrNiMoN22-5-3
1.4404	X2CrNiMo17-12-2
1.4529	X1NiCrMoCuN25-20-7
Reinforcing steel B500	St52

Table 2: Stainless steels and unalloyed reinforcing steel B500 for electrochemical investigations

Extensive electrochemical tests in aqueous eluates of the Pagel TF 10 [10] mortar were carried out on these materials. These eluates were adjusted to pH 13 on the one hand with sodium hydroxide solution (original concrete), and on the other

hand brought to approx. pH 7 by introducing CO₂ (carbonated concrete). Both variants were used as media for the electrochemical experiments both without additional chloride and after adding 3 g/l NaCl. In these media, the comparative determination of the resting potentials of the individual materials was first carried out (potential difference for possible bimetal corrosion processes). In a second step, actions from the three differently impregnated carbon rovings were each electrically conductively contacted with another material and the short-circuit currents in the four eluates were measured. The surface ratio of carbon fibre (cathode) to steel (anode) was always 1:1. The size of this short-circuit current allows conclusions to be drawn about the possibility of bimetal corrosion occurring in a real structural element. The greater the measured corrosion current, the more likely is bimetal corrosion between the corresponding material pairing.

The core of the project were tests on the corrosive stressing of test specimens (prisms and plates) made of carbon reinforced concrete with focus on special repair measures or in combination with old (carbonated) reinforced concrete. Rods and anchors made of stainless steels were introduced into the test specimens during production or by subsequent inserting anchors in holes, which resulted in cut carbon fibre inside the samples. The following stainless steels were selected for this:

- 1.4404, 1.4462 und 1.4571.

The following concretes were used for the test specimens (the mechanical properties acc. to [11], [12] were determined on prisms after 28 days storage (7 days wet followed by 21 days in standard climate)):

For all new build variants:

- High-performance concrete C3-B2-HF-2-145-5 [8], compressive strength: 136 MPa, porosity: 8.38 vol.%, pore media diameter D50: 0.026 µm,
- High-performance concrete C3-B2-HF-2-145-5, modified via significantly increased water/binder value and additives*: compressive strength: 65 MPa, porosity: 17.1 vol.%, pore median diameter D50: 0.036 µm;

For all repair variants:

- Normal-strength concrete C20/25 as old concrete, produced in the Otto Mohr laboratory, Technische Universität Dresden
- Fine-grained concrete Pagel TF 10 [9], compressive strength: 90,5 MPa, bending tensile strength: 8,25 MPa
- Fine-grained concrete Pagel TF 10, modified via significantly increased water/binder value and additives*, compressive strength: 40,2 MPa, bending tensile strength: 4,45 MPa,

* Simulation of the worst case, significantly increased water, chloride and CO₂ uptake (carbonatisation).

As common steel reinforcement, steel rods with 6 mm diameter were used.

3.2 Specimen variants and production

The experimental tests were carried out with two different test specimen geometries. For the corrosion tests in the climatic chamber, 50 prisms with a length of 160 mm, a width of 40 mm and a height of 40 resp. 50 mm were produced in five different variants, which are shown schematically in Figure 2. Variants A to D represent different scenarios of strengthening of an existing RC element with carbon concrete with two embedded layers of carbon textile. Variant N reflects the new construction situation.

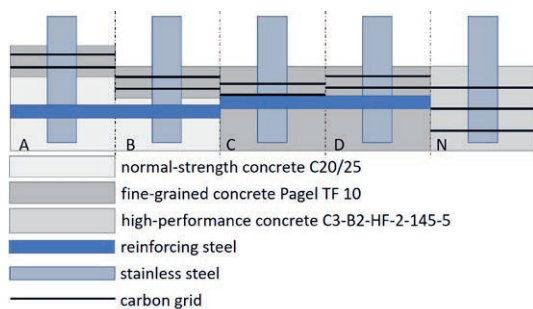


Figure 2: Different test specimen variants of the corrosion tests in the climate chamber | graphic: Maximilian May

In variants A and B, the influence of different concrete covers was investigated. The different concrete covers of the steel reinforcement should reflect the influence of different degrees of pretreatment and exposure of the aggregates in the old concrete. The old concrete surface on the strengthening side was produced as exposed aggregate concrete (Figure 3). Prior to the application of the strengthening layer, one half of the base bodies were subjected to a 17-day rapid car-

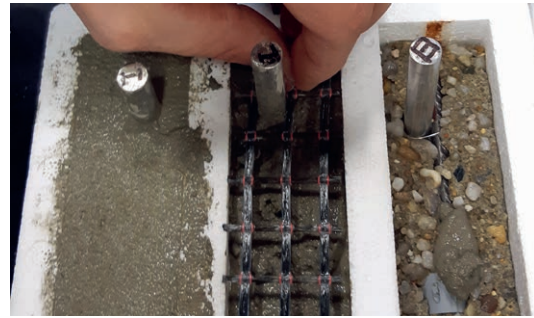


Figure 3: Concreting of the strengthening layer, variants A and B | photo: Maximilian May

bonation process. The other basic bodies were subjected to chloride stress during the same period.

Variants C and D represent the situation of repairing an exposed and oxidized steel reinforcement. The reinforcement steel was blasted bright before concreting. Variant C represents the case that the carbon grid was pressed into the concrete up to the existing reinforcement when the reinforcement layer was applied. In variant D, however, there is a separating concrete layer.

Specimens for variant N were produced with three layers of carbon fabric and the high-strength concrete using the casting method.

For the corrosion tests under open-air conditions (Figure 4), 19 plates in four different variants were produced. The 13 rectangular test specimens for the variants B – strengthening (number of samples n = 4), C – rehabilitation (n = 4) and N – new construction (n = 5) were 40 cm long, 20 cm wide and 6 cm thick.

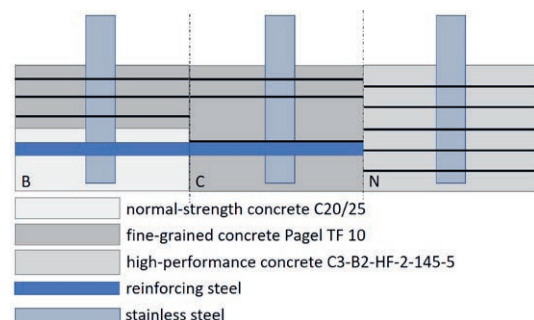


Figure 4: Schematic of the outdoor weathering samples | graphic: Maximilian May

In addition to the stainless steels already embedded in concrete, standard A4 stainless steel sleeve anchors were subsequently inserted into the panels. The holes for the anchors were drilled

in such a way that a contact was created between the anchors and the existing textile and steel reinforcements.

In addition to the 13 plates, 6 square test specimens with an edge length of 30 cm and a height of 3 cm were produced for a variant of a façade panel. Here, commercial facade anchors and their auxiliary reinforcement were cast with 3 layers of the carbon fabric in contact with the high-strength concrete variants. As can be seen in Figure 5, there was direct contact between the exposed carbon fibres and the anchor elements in the areas where the grids for the stainless steel components had to be cut through.

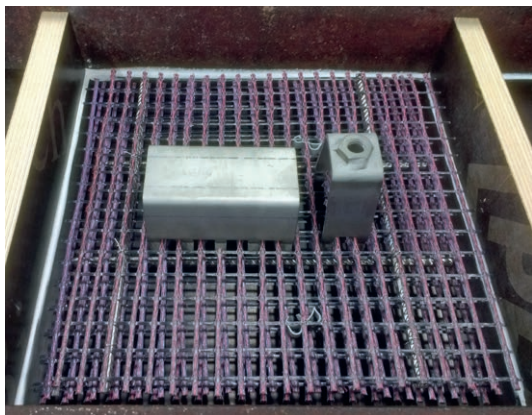


Figure 5: Arrangement of the facade anchors with the carbon grids | photo: Maximilian May

To ensure permanent contact between the individual reinforcing and connecting elements, they were fixed with stainless steel wire before concreting. The carbon grids were grinded at individual contact points in order to investigate the influence of the polymer impregnation and to illustrate the case of a subsequent installation of the stainless steel elements. In comparison, stainless steel elements were also placed in the test specimens without any contact and at a certain distance from the carbon reinforcement. Furthermore, all test specimen variants for the investigations were manufactured and tested with the normal concrete/mortar compositions as well as in the modified variants.

3.3 Corrosive stress on the carbon concrete test specimens

The test specimens were exposed to different stresses. In a modified pollutant gas climatic chamber, a part of the test specimens was subjected to rapid carbonation by exposure to CO_2 -

and cyclical humidity. In other samples, chloride exposure was carried out by cyclical outsourcing attempts in 2 molar NaCl solution. The target value was approx. 1.0% Cl by mass of cement at a depth of approx. 1 cm. The test specimens thus prestressed were then exposed to either outdoor weathering or a defined climatic chamber stress.

The 50 concrete prism variants were exposed to corrosion in a climate chamber with a specially developed climate program for 7 months, see Figure 6. They were then exposed to outdoor weathering in Dresden for 3 months in the winter.

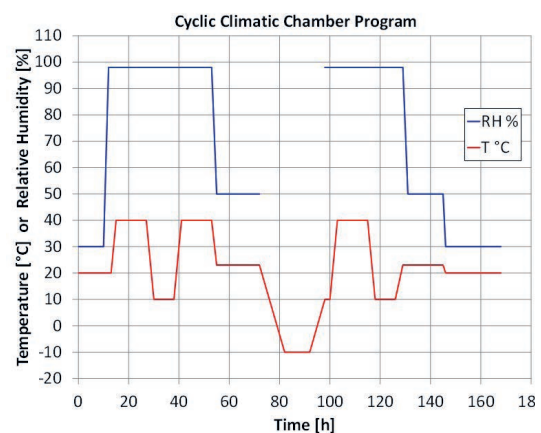


Figure 6: Cyclic climatic chamber program for stressing the carbon concrete prisms over a period of 7 months | graphic: Jürgen Triebert

The 19 concrete plate variants were subjected to corrosive exposure in the outdoor weathering facility at the Dresden Institute for Corrosion Protection (see Figure 7). So far, 8 plates have been obtained and examined after an exposure period of 14 months. The exposure of the remaining 11 plates is to be extended to 2 years beyond the end of the project.



Figure 7: Carbon concrete slabs with built-in parts on the free weathering stand of the Institute for Corrosion Protection in Dresden | photo: Jürgen Triebert

4 Results

4.1 Electrochemical investigations

The electrochemical tests in various aqueous concrete eluates showed a potential difference, which is in principle sufficient for bimetal corrosion between carbon fibres and different stainless steels as well as in particular to the unalloyed reinforcing steel B500 (see Table 2).

Material	Quiescent potential in [mV] against Saturated Calomel Electrode (SCE) in concrete eluates	
	pH 13,0 3 g/l NaCl	pH 7,0 without Cl-addition
Carbon fibre*	-147	+15
1.4571	-250	-65
1.4462	-240	-75
1.4404	-305	-10
1.4529	-355	-70
Reinforcing steel B500	-350	-695

* Carbon fibre roughened, with 30% impregnation

Table 2: Determined rest potential for the investigated materials in selected concrete eluates

Furthermore, in the event of short-circuit contacting of these material pairs in the various concrete eluates, contact currents (corrosion currents) were measured, see Figure 8.

It can be seen from Table 2 that a combination in particular seems to be very critical: the contact between carbon fibre and unalloyed reinforcing steel B500 in carbonated concrete (eluate with pH 7.0). The potential difference is over 700 mV. This would affect possible repair solutions for steel reinforced concrete with carbon concrete.

From Figure 8 it can be seen that the contact pair carbon fibre–reinforcing steel B500 shows very high corrosion currents, particularly in the neutral eluates. This is related to the lack of passivation of the reinforcing steel at pH 7 and illustrates the problem with the repair of reinforced concrete with carbon concrete. In contrast, the stainless steels in electrical contact with the carbon fibre show only very small, hardly measurable corrosion currents. These pairings are obviously rather uncritical.

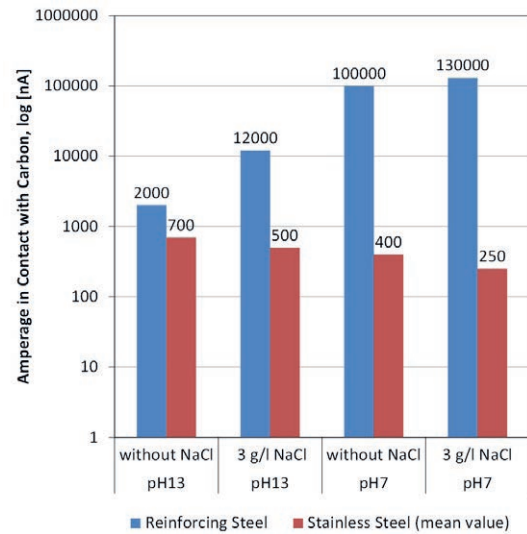


Figure 8: Measured corrosion currents for contact pairs made of carbon fibres and various steels (see Tab. 1, averages) in concrete eluates | graphic: Jürgen Triebert

4.2 Carbon concrete prisms in climatic chambers

None of the new construction variants **N** with concrete B2 original or modified with CO₂- and/or chloride exposure showed even rudimentary bimetal corrosion between carbon fibres and the different stainless steels, not even in the variants with extra-ground abraded carbon fibres, see Figure 9.



Figure 9: Opened test specimen of one variant **N** (B2 Hf modified and CO₂) after exposure in the climatic chamber: no corrosion between carbon fibre grid and stainless steel insert | photo: Jürgen Triebert

For the repair variants **A** and **B**, which are based on a limited removal of the damaged concrete surface, the remaining of the reinforcing steel in the carbonated (realkalization) or moderately chloride-contaminated old concrete and the subsequent application of a carbon concrete

layer for reprofiling and/or strengthening, the following results were obtained:

- All test specimens showed very strong corrosion on the unalloyed reinforcing steel B500 over the entire circumference and the entire length. This reinforcing steel was in contact with the coated (partially grinded) carbon fibre fabrics via stainless steel rods. These results are supported by the electrochemical tests, which had shown a high contact current between carbon fibres and the unalloyed reinforcing steel, especially in carbonated concrete, for these renovation variants in the aqueous concrete eluate. Figure 10 illustrates this finding.



Figure 10: Refurbishment variant B after breaking the test specimen; the carbonated normal strength RC can be seen after removing of Pagel TF 10 layer; typical picture with very strong corrosion on the unalloyed reinforcing steel B500, mostly over the entire circumference and the entire length | photo: Jürgen Triebert

- The bars made of the three stainless steel grades 1.4404, 1.4462 and 1.4571 contacted with the B500 often showed locally limited, rather low and extensive corrosion, no (pronounced) pitting corrosion directly at the contact point with the unalloyed reinforcing steel. On the one hand, it could be caused by the corrosion products of the B500 in that extraneous rust on the surface interferes with the passive layer formation on the stainless steel. On the other hand, this could also partly be crevice corrosion (see Figure 11).



Figure 11: Typical contact point between stainless steel rod and corroded B500 reinforcing steel, low local, only surface corrosion on stainless steel | photo: Jürgen Triebert

- The depth of the corrosive attack at the contact points of the stainless steel bars is only small and amounts to a maximum of a few μm . Pitting corrosion was only found using SEM in two cases. There was very limited local presence. The pitting corrosion is illustrated in Figure 12.

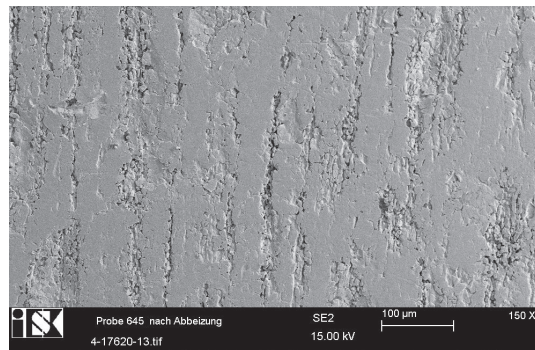


Figure 11: Typical SEM image of a pickled contact point with corrosion on a stainless steel insert towards the rebar B500; the attack depth is very low | graphic: Jürgen Triebert

- In no single repair variant A or B, corrosion was found at the contact points between the carbon fibre grids and the three different stainless steels.

The following results were obtained for the renovation variants C and D, which simulate a complete exposure and rust removal of the corroded reinforcement steel and the subsequent application of a strengthening layer made of carbon concrete:

- When using the original Pagel TF 10 mortar, the steel concrete blasted to Sa 2½ (standard degree of purity) [13] showed only very little, locally limited corrosion, which could

be attributed to cracking conditions in addition to bimetal corrosion. The stainless steel rods used here showed no corrosion.

When using a modified Pagel mortar TF 10 with significantly lower strength and greater porosity, the reinforcing steel B500 blasted to Sa 2½ showed very strong corrosion over the entire circumference and the entire length. This was particularly strong at the direct contact points between the carbon fabric and the B500 (variant C).

- The stainless steel built-in parts showed, as with the renovation variants A and B, only at the direct contact points to the B500 a locally limited, only near-surface, flat corrosion and no pitting corrosion.
- In no variant corrosion was found at the contact points between the carbon fibre and the three stainless steels.

4.3 Carbon concrete plates after outdoor weathering

In the new construction variants N with modified, less solid and more porous concrete B2 Hf and CO₂ or chloride effect, all inserts made of three stainless steels 1.4404, 1.4462 and 1.4571 as well as the subsequently installed A4 heavy-duty sleeve anchors were completely free of corrosion. This is also confirmed by the results of tests with concrete prisms in climate chambers, which also showed the principle feasibility of this combination, Figure 13.



Figure 13: Carbon concrete slab, variant new construction with concrete B2 Hf modified and carbonated, after 14 months free weathering after cutting; the shown A4 heavy duty anchor and all other stainless steel components in contact with carbon are not corroded | photo: Jürgen Triebert

In the case of modified concrete B2 Hf and relatively high chloride contents of approx. 1.6–2.4 wt% Cl-/cement, pitting corrosion of the stainless steel near the concrete surface (there is sufficient O₂ and water available) was observed in the simulated façade panels with A4 façade panel anchor systems. However, even in these cases no bimetallic corrosion between the carbon fibre and the stainless steel was detected. The internal concrete components and the A4 auxiliary reinforcement were completely free of corrosion.

In the case of the renovation variants B and C, as with the concrete prisms in the climate chambers, the unalloyed concrete steels B500 corroded very strongly in all the variants investigated (see Figure 9). The stainless steel bars did not show any corrosion at the contact points to the carbon grid in any single place. At the points of contact with the B500 reinforcing steel, as with the concrete prisms in the climatic chamber, slight corrosion occurred on the stainless steel rods (extraneous rust, disturbed formation of the passive layer, splitting conditions).

Figure 14. Carbon concrete plate after 14 months of chloride exposure after cutting, renovation variant C, fine concrete Pagel TF 10 modified; view from below (reinforcing steel): 0–1 cm: 3.1 wt% Cl-/cement, 1–2 cm: 1.4 wt% Cl-/cement

The following was also found for renovation variant C (old concrete removed, corroded reinforcing steel exposed and derusted, carbon fibre fine concrete Pagel TF 10 applied) with modified fine concrete and chloride application:

- Near the surface of individual plates, some of which were cracked, some stainless steel components showed corrosion which was relatively far away from the carbon fibre layers and the reinforcing steel B500 (see e.g. Figure 14). This was not bimetallic corrosion, but chlorine-induced pitting corrosion.

5 Discussion and Conclusions

Electrochemical tests with contact pairs of coated carbon fibres and various stainless steels of the A4 range in aqueous concrete eluates already showed very low corrosion currents both at pH 13 and pH 7 (carbonated), with and without chloride exposure. This already indicated that this pairing in carbon reinforced concrete could be rather un-critical.

Completely different results were obtained with contact pairs of coated carbon fibres and unalloyed reinforcing steel B500. Very high corrosion currents were measured especially in concrete eluates which were brought to pH 7 by introducing CO₂ (carbonated concrete) and those which additionally contained chloride. This rather pointed to corrosion problems to be expected in such pairings, for example in the renovation of reinforced concrete with carbonated concrete.

These results of the electrochemical tests were confirmed by real tests with 50 different variants of carbon concrete prisms and 19 concrete slabs, which on the one hand were exposed to corrosive attack in climate chambers and on the other hand in outdoor weathering at the Dresden site. In both cases, not a single test specimen showed bimetallic corrosion between the carbon fibre layers and the stainless steels 1.4404, 1.4462 and 1.4571.

In contrast, intense corrosion was found on the unalloyed reinforcing steel B500 in all rehabilitation variants. This was either directly in contact with the carbon fibre layers or indirectly connected to them via the stainless steel rods. This was predominantly bimetallic corrosion, in some cases intensified by crevice and chloride-induced corrosion. The distance to the concrete surface was at least 2.0 cm in all cases for the B500 reinforcing steel, which is considered realistic in the tests carried out.

In some chloride-contaminated variants, corrosion began to appear on individual stainless steel components near the concrete surface. Both the bimetallic corrosion and the chloride-induced pitting corrosion require oxygen and moisture for the cathodic partial reaction, which is more likely to be present near the surface than inside the concrete. The literature ([14]–[16]) does not contain clear values for chloride limit concentrations that cause pitting corrosion, since these depend on a number of parameters in each individual case. Nevertheless,

the following ranges are given for non-cracked reinforced concrete with sufficient concrete cover:

- unalloyed reinforcing steel: approx. 0.4–1.0 (2.0) wt% Cl-/cement [14]–[16],
- stainless, austenitic Cr-Ni-Mo steels: approx. 1.5 wt% Cl-/cement, depending on certain conditions even up to 4–5 wt% Cl-/cement [16].

With reference to the carbon concrete prisms and plates of the presented study, this means that some test specimens, especially those with cracked concrete, with approx. 1.7–3.5 wt% Cl-/cement were already in the range of the critical chloride content which causes pitting corrosion. In the project, values of around 1.0 wt% Cl-/cement were targeted as planned. In these cases, it can therefore be assumed that the corrosion phenomena described on the stainless steel near the surface are mainly or exclusively due to the influence of the chlorides and not to bimetallic corrosion.

The following summarizing findings result from the previous project status after 14 months of outdoor weathering or 7 months of exposure in a climatic chamber including another 3 months of outdoor weathering:

- From a corrosion point of view, fasteners, built-in and add-on parts made of austenitic, stainless steels comparable to the qualities 1.4404, 1.4462 and 1.4571 or higher tested here can be used with a high degree of safety in newly erected carbon-concrete structures. The prerequisite for this, however, is the use of a very dense, pressure-resistant and low-pore special concrete such as B2 Hf developed in the C3 project and, in the case of built-in parts close to or penetrating the surface (see façade panel anchor), the avoidance of high chloride contents in the concrete (< 1.0 wt% Cl-/cement).

In the case of repair solutions for reinforced concrete, great importance should generally be attached to avoiding contact of the unalloyed reinforcing steel with the carbon reinforcement and also with built-in parts made of stainless steel. Indirect contact between carbon fibres and reinforcing steel, e.g. through subsequent insertion of stainless steel anchors/plugs into the structure, will also lead to corrosion problems sooner or later. This applies particularly to carbonated and/or chloride-contaminated old concrete or fine concrete. This problem can only be counteracted with insulating measures on the installed parts.

The authors point out that the conclusions are based only on the results obtained from the material combinations examined. A transfer, for example, to normal samples cannot be made. The influence of a combined stress from environmental conditions and acting mechanical loads was not investigated.

The project on which this report is based was funded by the Federal Ministry of Education and Research (BMBF) under the funding code 03ZZ0334. The authors are responsible for the content of this publication. The project partners thank the BMBF and the Project Management Organisation Jülich (PTJ) for funding the project.

6 References

- [1] A. Zockoll, P. Plagemann, "Kontaktkorrosion mit CFK verhindern," *Magazin für Oberflächentechnik* mo, Jahrg. 68 (2014) 9, S. 34–37
- [2] H. Schreckenberger, "Risiko der Kontaktkorrosion bei CFK-Bauteilen," *WOMag* (2013) 04, S. 6–7.
- [3] W. C. Tucker, R. Brown, L. Russell, „Corrosion Between a Graphite/ Polymer Composite and Metals," *Journal of Composite Materials* 24 (1990), pp. 92–102.
- [4] B. Reinhold, D. Blücher, M. Korte, „Herausforderungen an Füge- und Oberflächentechnik für zukünftige Leichtbaukonstruktionen im Automobilbau," *Materialwissenschaft und Werkstofftechnik* 44 (2013), pp. 58–69.
- [5] M. Tavakkolizadeh, H. Saadatmanesh, "Galvanic Corrosion of Carbon and Steel in Aggressive Environments," *Journal of Composites for Construction* (2001), pp. 200–210.
- [6] A. Bauer, "Korrosionsanalytische Untersuchungen von CFK basierten Hybridwerkstoffen," *Dissertation, Universität Paderborn*, 2016
- [7] C. Driessen-Ohlenforst, A. Faulhaber, M. Raupach, „SMART-DECK: Monitoring des Feuchtegehaltes und kathodischer Korrosionsschutz des Bewehrungsstahles in Brückenfahrbahnen durch Zwischenschicht aus Textilbeton," *Bauingenieur* 95 (2020) 3, pp. 96–104.
- [8] D. Koch, M. Mahjoori, "Kathodischer Korrosionsschutz mit Textilbeton: Anspruch, Entwicklung, Performance und Langzeiterfahrung," *Ostfildern*, 2016
- [9] Homepage Projekt C³ – Carbon Concrete Composite: <https://www.bauen-neu-denken.de /c3-vorhaben/> [Zugriff am 17.06.2020].
- [10] TUDAG: Allgemeine bauaufsichtliche Zulassung Z-31.10.-182: Verfahren zur Verstärkung mit von Stahlbetonbauteilen mit TUDALIT® (Textilbewehrter Beton). Ausgabe: November 2016.
- [11] DIN EN 196-1:2016: Prüfverfahren für Zement – Teil 1: Bestimmung der Festigkeit. Deutsche Fassung, Ausgabe November 2016.
- [12] DIN ISO 15901-1:2016: Bewertung der Porengrößenverteilung und Porosität von Feststoffen mittels Quecksilberporosimetrie und Gasadsorption – Teil 1: Quecksilberporosimetrie. Deutsche Fassung, Ausgabe März 2019.
- [13] DIN 55928-1:1991: Korrosionsschutz von Stahlbauten durch Beschichtungen und Überzüge; Allgemeines, Begriffe, Korrosionsbelastungen. Deutsche Fassung, Ausgabe Mai 1991.
- [14] W. Breit, „Kritischer korrosionsauslösender Chloridgehalt – Sachstand und neuere Untersuchungen," *Düsseldorf*, 2000
- [15] Deutscher Ausschuss für Stahlbeton, J. Schnell, M. Raupach, "Positionspapier Kritischer korrosionsauslösender Chloridgehalt," *Berlin*, 10/2015.
- [16] Y. Schlegg, F. Hunkeler (Schweizerische Gesellschaft für Korrosionsschutz), „Korrosionsbeständigkeit von nichtrostenden Betonstählen," *Zürich*, 2012.

Durability of FRP rebars in concrete structures – current test methods and approaches

Nora Susanne Bies, M.Sc.

TU Kaiserslautern, Kaiserslautern, Germany

✉ nora.bies@bauing.uni-kl.de

Since 2019 research assistant at the TU Kaiserslautern and researches the durability and degradation behaviour of FRP rebars.

Dipl.-Ing. Mona Lisa Keller

TU Kaiserslautern, Kaiserslautern, Germany

✉ mona.keller@bauing.uni-kl.de

Research assistant at the TU Kaiserslautern since 2015 in the field of developing a new durability test concept for FRP rebars.

Prof. Dr.-Ing. Matthias Pahn

TU Kaiserslautern, Kaiserslautern, Germany

✉ matthias.pahn@bauing.uni-kl.de

Head of Department “Baukonstruktion und Fertigteilbau” at the TU Kaiserslautern, main focus on FRP reinforcement, Member of standardisation committees.

1 Abstract

Currently, the lack of data on the long-term performance of FRP rebars, the international variation in approaches and the FRP product diversity result in the absence of an international agreement in the methods of FRP durability testing. This paper aims to compare the current state of the art with the state of research, and to identify essential differences between the common test methods. In addition, a test method combining an alkali resistance test and a creep rupture test is presented.

Keywords: Fibre-reinforced polymer (FRP), FRP reinforcing bars, Durability, Long-term behaviour, Specifications and guidelines, Tensile strength, Sustained stress, Alkali resistance, Alkaline solution, Accelerated aging

2 Introduction

Reinforcing bars made of fibre-reinforced polymers (FRP) represent an alternative to conventional reinforcing steel, as corrosion issues can be excluded and the application limits extended. Products range of FRP rebars available on the market includes a variety of fibres (especially carbon, aramid and glass) and type of resin used as well as surface textures. To ensure the safety of an FRP reinforced load-bearing structure, extensive investigations of the durability of FRP rebars are required. Yet limited research seems to have been carried out and there exists a lack of experimental long-term studies owing to the high effort and the long duration of the testing [1, 2]. The lack of real-time performance data, the international variations in approach and the product diversity of FRP rebars result in the absence of an international agreement on the methods and appropriateness of FRP durability tests. Although national guidelines and design codes exist for instance in Norway, Canada, Japan and the USA, they relate to different approaches to the experimental deter-

mination of long-term properties of FRP rebars [3]. Current guidelines generally suggest immersing the FRP rebar in an alkaline solution and the subsequent testing of the residual tensile strength to investigate the durability behaviour. However, this approach does not consider the synergetic effect of simultaneous attack due to mechanical, physical and chemical exposure of the rebar, as would typically occur in the real installation situation in concrete [4]. Thus, a test method combining an alkali resistance test and a creep rupture test was developed, in which the FRP rebar is subjected to a constant uniaxial tensile load until failure occurs. At the same time, the rebar is embedded in water-saturated, highly alkaline concrete. The ambient temperature can be controlled e.g. room temperature (23 °C), 40 °C or 60 °C to analyse the effect of temperature on the degradation mechanism of the FRP rebar [5].

This paper aims to compare the current state of the art with the state of research and to identify essential differences between the known test methods.

3 International approaches

In international comparisons, the Canadian and American standards have the most important significance.

In the United States of America, the standards published by Committee 440 of the American Concrete Institute (ACI) specify the manufacture, design and dimensioning of FRP reinforced concrete structures. ACI 440.1R-15 "Guide for the design and construction of structural concrete reinforced with fiber-reinforced polymer (FRP) bars" defines standards for design and construction [6]. ACI 440.3R-12 „Guide Test Methods for Fiber-Reinforced Polymer (FRP) Composites for Reinforcing or Strengthening Concrete and Masonry Structures“ describes test methods for investigating the mechanical and thermomechanical short- and long-term properties as well as durability issues [7].

The Canadian Standards Association Group (CSA Group) develops standards in several areas, including construction materials. The relevant documents for the manufacture, design and construction of building structures with fibre-reinforced polymers are CSA S806-12 (reaffirmed 2017) and CSA S807:19 [8, 9]. CSA S807:19 "Specification for fibre-reinforced polymers" is intended to ensure product quality by setting requirements for the manufacturing process and provides methods for

classification as well as for determining mechanical, physical and durability properties [8]. CSA S806-12 (R2017) „Design and construction of building structures with fibre-reinforced polymers“ defines rules for design, execution and testing of FRP reinforced concrete components [9]. In the following chapters, the methods of ACI 440.3R-12 and CSA S806-12 (R2017) for determining alkali resistance and creep behaviour of FRP rebars are compared and the main contents are summarised. In particular, differences in approaches are highlighted.

3.1 Test method for alkali resistance of FRP rebars

The test methods for alkali resistance of FRP rebars are defined by ACI 440.3R-12 Chapter B.6 "Accelerated test method for alkali resistance of FRP bars" and CSA S806-12 (R2017) Annex M "Test method for alkali resistance of FRP rods".

The test method of ACI 440.3R-12 and CSA S806-12 (R2017) specifies the test requirements for evaluating the alkali resistance of FRP reinforcing bars by subjecting to an alkaline environment at 60 °C, with or without stress, and then measuring tensile capacity retention and the mass change. The alkaline environment can be provided by a concrete cylinder in which the rebar is locally embedded or by an aqueous alkaline solution. The

Document	ACI 440.3R-12	CSA S806-12 (R2017)
Test method for alkali resistance of FRP rebars		
Structure	Specification of three procedures A to C A) Immersion without load B) Immersion under sustained tensile load C) Embedding in moist concrete under sustained tensile load	No specification
Length of the test section	Length > 40x the (effective[10]) diameter of the FRP rebar	100 mm ≤ Length ≤ 40x the nominal diameter of the FRP rebar
Level of sustained tensile stress	Load-induced tensile strain in glass FRP rebars of 2000 microstrain (or higher)	Load-induced tensile strain in glass FRP rebars of 3000 microstrain (or higher)
Concrete cylinder	Curing for 28 days in water before testing	Curing for 28 days before testing
pH value	Between 12.6 and 13	No specification
Measuring of the pH value	At the beginning and after the test; during testing at least every 5 days and adjusted if necessary	Before and after the test
Exposure times	1, 2, 3, 4, and 6 months (or longer)	1, 3, and 6 months
Test method for weight change of FRP rebars		
Drying	Drying according to Procedure D of ASTM D5229/D5229M	Drying at 105 ± 1 °C
Masses	W_0, W_1	W_0, W_1, W_2

Table 1: Differences in approaches of the American and Canadian standard for alkali resistance of FRP rebars

concrete cylinder shall have a diameter of 150 mm and a length of 200 mm (according to Fig. B.6.6.3 [7], and Fig. M.1 [9]). The recommended composition of alkaline solution is 118.5 g of $\text{Ca}(\text{OH})_2$, 0.9 g of NaOH, and 4.2 g of KOH in 1 L of deionized water [7, 9]. The alkaline solution is representing the alkaline milieu of the pore water in concrete environment. During immersion, evaporation of water and absorption of atmospheric CO_2 must be prevented. In order to avoid the infiltration of solution via the ends of the rebars, both ends should be coated with epoxy resin. The specified temperature for conditioning should be 60 ± 3 °C [7, 9]. The level of sustained tensile stress should be based on the expected stresses caused by the dead loads, and any part of the live loads that is sustained. If service live conditions are unknown, the stress level should be set to induce a tensile strain equal to 2000 [7] or 3000 [9] microstrain (see Table 1). Higher levels of sustained stress can be used as an accelerating condition. After conditioning, the rebar is tested in residual tensile strength to failure.

The weight-change test is carried out on specimens which are immersed in aqueous alkaline solution without sustained tensile stress. Before immersion, the rebars are dried and weighed until the mass remains constant (W_0). After immersion in the alkaline solution, the specimens are washed with water [9] or deionized water [7], dried with tissue paper, and then immediately weighed (W_1). According to the Canadian standard the specimens are then dried and weighed a second time until the mass remains unchanged (W_2).

The calculation of the mass change separately for an increase respectively decrease is performed according to the equations (1) to (3).

According to American and Canadian standards:

$$\text{Mass gain (\%)} = \frac{W_1 - W_0}{W_0} \cdot 100 \quad [7, 9] \quad \mathbf{1}$$

According to the American standard ACI 440.3R-12:

$$\text{Mass loss (\%)} = \frac{W_0 - W_1}{W_0} \cdot 100 \quad [7] \quad \mathbf{2}$$

According to the Canadian standard CSA S806-12:

$$\text{Mass loss (\%)} = \frac{W_0 - W_2}{W_0} \cdot 100 \quad [9] \quad \mathbf{3}$$

3.2 Test method for creep of FRP rebars

Annex H of CSA S806-12 (R2017) defines the test method for determining the creep properties of FRP rebars [9], whereas the ACI 440.3R-12 refers to ASTM D7337/D7337M "Standard Test Method for Tensile Creep Rupture of Fiber Reinforced Polymer Matrix Composite Bars" by ASTM International (American Society for Testing and Materials) [7, 11].

This test method is used to measure the load-induced, time-dependent tensile strain under controlled environmental conditions and load rates. By testing different stress levels, a correlation between the applied load and time-to-failure can be derived. The specimen has to be anchored at both ends for testing. The level of sustained load is based on the short-term tensile strength of the FRP rebar. According to CSA S806-12 (R2017), the load ratio is specified as 20-80% [9], and ASTM D7337/D7337M refers to the fibre architecture and fibre volume fraction, which is why the load ratios have to be determined specifically for each rebar [11]. The tests should include multiple (four [11] or five [9]) load ratios with at least 5 specimens per load ratio. The ASTM specifies the stress limits based on the time-to-failure, whereby four out of five specimens' ruptures at a time of greater than 1 h at the highest stress level, and the lowest stress level should be determined so that one of the five specimens subjected to this load ratio ruptures at a time of greater than 8000 h [11]. The CSA specifies that the test results should span three decades of time (such as 1 h, 10 h, 100 h, and 1000 h) [9]. The axial deformation of the FRP rebar should be recorded over the whole test duration.

4 Simultaneous testing of alkali resistance and creep rupture

4.1 Motivation

Civil engineering structures have to resist not only mechanical loads but also chemical and biological attacks as well as environmental influences throughout the intended service life. Therefore, the durability of an FRP-reinforced structure should be guaranteed considering the simultaneous stresses present in the load-bearing structure [12]. The test method should be designed so that on the one hand the real installation situation of the FRP rebar is simulated in the laboratory and on the other hand an aggressive test environment is generated with regard to the endurance-limiting

influencing parameters. Four parameters have been identified: the mechanical tensile stress, the alkaline environment of the concrete, moisture, and the ambient temperature (see Figure 1).

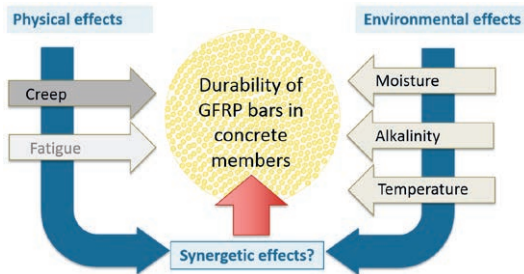


Figure 1: "Effects on durability of GFRP bars" [4] | graphic: TU Kaiserslautern

The failure values of the investigated FRP rebars provide important information regarding the use of FRP as internal reinforcement in concrete structures.

4.2 Design of the test set-up

The test stand is used to investigate the long-term performance of straight FRP rebars. The rebars are tested in tensile stress until failure occurs. In order to simulate the installation situation of a FRP reinforcing bar in the laboratory, the tensile and bond stresses should be represented as realistically as possible. The investigated rebar is thus embedded locally in a concrete cylinder (see Figure 2). The cylinder is 220 mm long and measures 75 mm in diameter. The concrete provides the alkaline milieu for the rebar with pH above 13 by using a CEM I with a Na₂O content of 1%. Fine aggregates of 0-2 mm are used and the water/cement ratio ranges between 0.56 and 0.6. In order to transmit the mechanical stress into the reinforcing bar, the FRP rebar is anchored at both ends in concrete abutments with the dimensions 600 x 400 x 250 mm. The size of the concrete abutments has to be adapted in accordance with the geometry of the examined rebar in order to ensure the anchoring of the bar.

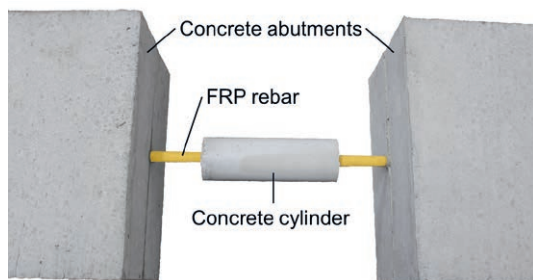


Figure 2: "FRP rebar embedded in concrete abutments with cylinder" | graphic: TU Kaiserslautern

The sustained tensile stress is applied by two hydraulic cylinders (see Figure 3). Both are aligned vertically and horizontally so as to subject the rebar to axial stress. Since the cylinders are hydraulically coupled to each other, the load can be controlled and pressure-related imbalance can be avoided. The level of sustained load depends on the hydraulic cylinders used and can therefore be adjusted as required by the choice of the cylinders. In addition, the residual tensile strength of a specimen can be determined in a test stand if no failure occurs even after a long test duration.

During the whole test duration, the elongation of the FRP rebar due to the applied sustained load is measured by a displacement transducer (LVDT), which is installed between the concrete abutments above the rebar. To ensure that the initial elastic elongation and the creep elongation of the rebar under load can occur unhindered, one of the two abutments has to be supported with low adhesion to the substrate.

A water basin placed below the concrete cylinder is used to ensure permanent contact of the lower third of the cylinder with water. At regular intervals, a control unit measures the water level within the basin and adjusts if necessary, so that the level is kept at a consistent level throughout the test duration. Immediately after the application of the sustained stress, the concrete cylinder cracks perpendicular to the direction of loading as a result of the initial elastic elongation of the rebar.

Due to the capillary action of these cracks, the water gets to the rebar, creating a moist environment. By tempering the water (e.g. room temperature, 40°C, 60°C or higher) in the basin by the temperature device, the deterioration can be accelerated.

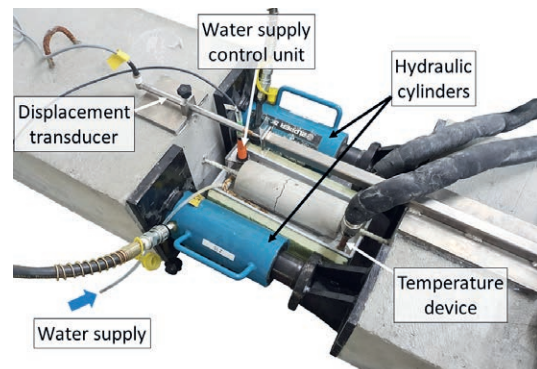


Figure 3: Test setup | photo: TU Kaiserslautern

5 Comparison of the approaches

Comparing the presented test methods and approaches, the following can be stated:

Previous studies have already shown that immersing the bare FRP rebar directly in an aqueous alkaline solution at elevated temperatures to accelerate aging leads to a conservative prediction of service life as the test conditions are excessively harsh and cause premature deterioration of the rebar [1, 3]. This is because in the real load-bearing structure, mechanical stresses, environmental conditions, as well as chemical and biological attacks, lead to a decrease of the alkaline milieu of the concrete.

The tensile stress required to cause an axial elongation of 2000 [7] or 3000 [9] microstrain when testing alkali resistance under sustained load varies depending on the properties of the rebar, but is generally rather low because of the high Young's modulus of FRP compared to reinforcing steel. Therefore, the long-term tensile strengths determined cannot be directly transferred to higher load levels and lead to an overestimation of the load capacity.

While multiple steps are required to determine the alkali resistance of a rebar according to Canadian or American standards, whereby influences due to the handling of the specimen cannot be excluded, the combined test stand allows to evaluate the residual tensile strength without changing the position of the rebar.

Regular measurement of the pH value according to the American standard ensures that the reservoir has to be accessible during testing. It should be considered whether the air changes associated with the checks require readjustment of the pH value for long test durations.

In relation to the glass transition temperature, drying of the FRP rebar for the determination of the weight change at 105 ± 1 °C according to the Canadian standard [9] is to be evaluated critically.

When investigating creep behaviour, the number of specimens and time-to-failure depending on the level of sustained load are important, as statistical analysis of the test data demands a certain amount of valid tests. The examination of several decades was found to be a reasonable approach to predict the long-term properties of FRP rebars.

The simultaneous testing of alkali resistance and creep rupture provides a more realistic representation of the in-service conditions of the reinforcement in concrete structures. In addition, the test method takes up the main specifications of the international standards, including creating a moist, highly alkaline environment, the consideration of temperature effects, the testing under sustained tensile load etc.

6 Conclusion

In this study, the current test methods for determining alkali resistance and creep behaviour of FRP rebars of the American (ACI 440.3R-12) and Canadian standard (CSA S806-12 (R2017)) were discussed and compared. In addition, an approach combining an alkali resistance test and a creep rupture test was presented.

The American and Canadian test methods are very similar and offer e.g. several procedures to determine the alkali resistance of FRP rebars: with or without permanent load, embedded in concrete or immersed in an aqueous alkaline solution. In the combined test, the rebar is embedded locally in water-saturated concrete and simultaneously subjected to long-term tensile stress.

The quantitative evaluation of the test methods is complicated due to the limited number of experimental endurance studies, the wide range of products available on the market, and the diversity and variety of raw materials (fibres, matrix systems), and surfaces.

Currently, comparative tests are being carried out at the TU Kaiserslautern to evaluate the influence of the test procedure in relation to the bar environment generated in the laboratory on the residual tensile strength.

7 References

- [1] H. Fergani, M. Di Benedetti, C. Miäs Oller, C. Lynsdale und M. Guadagnini, „Durability and degradation mechanisms of GFRP reinforcement subjected to severe environments and sustained stress“, *Construction and Building Materials*, Jg. 170, S. 637–648, 2018, doi: 10.1016/j.conbuildmat.2018.03.092.
- [2] G. Nakurunziza, B. Benmokrane, A. S. Debaiky und R. Masmoudi, „Effect of Sustained Load and Environment on Long-Term Tensile Properties of Glass Fiber-Reinforced Polymer Reinforcing Bars“, *Structural Journal*, Jg. 102, S. 615–621, 2005.
- [3] E. A. Byars, P. Waldron, V. Dejke, S. Demis und S. Heddadin, „Durability of FRP in concrete - deterioration mechanisms“, *IJMPT*, Jg. 19, 1/2, S. 28, 2003, Art. no. 3554, doi: 10.1504/IJMPT.2003.003554.
- [4] M. L. Keller und M. Pahn, „Durability of GFRP Bars with Different Bar Diameters“ in *International Association for Bridge and Structural Engineering Symposium I (ABSE)*, Guimarães, 2019, S. 603–610.
- [5] N. S. Bies, M. L. Keller und M. Pahn, „Degradation Behaviour of GFRP Bars in Highly Alkaline Water-saturated Concrete under Sustained Load“ in *9th Biennial Conference on Advanced Composites In Construction (ACIC 2019)*, Birmingham, 2019, S. 39–44.
- [6] *Guide for the design and construction of structural concrete reinforced with fiber-reinforced polymer (FRP) bars*, ACI 440.1R-15, 2015.
- [7] *Guide test methods for fiber-reinforced polymers (FRPs) for reinforcing or strengthening concrete and masonry structures*, ACI 440.3R-12, 2012.
- [8] *Specification for fibre-reinforced polymers*, CAN CSA S807:19, 2019.
- [9] *Design and construction of building structures with fibre-reinforced polymers*, CAN CSA S806-12 (reaffirmed 2017), 2012.
- [10] *Standard Test Method for Tensile Properties of Fiber Reinforced Polymer Matrix Composite Bars*, ASTM D7205D7205M - 06, 2006.
- [11] *Standard Test Method for Tensile Creep Rupture of Fiber Reinforced Polymer Matrix Composite Bars*, ASTM D7337 / D7337M - 12, 2012.
- [12] F. Knab, A. Weber und J. Schweinfurth, „Sicherer Einsatz von Glasfaserbewehrung im Bauwesen“, *Beton- und Stahlbetonbau*, Jg. 110, Nr. 12, S. 822–831, 2015, doi: 10.1002/best.201500060.

Effect of Tension Forces on Shear Capacity of Thin Slab Segments

Jan Bielak, M.Sc.

Institute of Structural Concrete, RWTH Aachen University, Aachen, Germany

✉ jbielak@imb.rwth-aachen.de

Research Assistant since 2016 in the field of non-metallic reinforcement with focus on characterization methods, standardization and shear capacity.

Henrik Becks, M.Sc.

Institute of Structural Concrete, RWTH Aachen University, Aachen, Germany

✉ hbecks@imb.rwth-aachen.de

Research Assistant since 2020, working on non-metallic reinforced structures and fatigue of concrete.

Univ.-Prof. Dr.-Ing. Josef Hegger

Institute of Structural Concrete, RWTH Aachen University, Aachen, Germany

✉ jhegger@imb.rwth-aachen.de

Full professor and head of the institute since 1993. Major research areas are non-metallic reinforcement, shear, punching, and prestressed concrete.

Contact: jbielak@imb.rwth-aachen.de

1 Abstract

Thin TRC slabs show high application potential in high-rise construction as well as for secondary structural systems in bridges. In both cases, combinations of moment and shear with normal forces might occur, e.g. through external bracing loads, temperature gradients, and shrinkage. The effect of separation cracks and tension forces on shear capacity has been investigated with a newly developed setup. Shear capacity decreases with increasing axial tension, but vertical pre-cracking did not diminish ultimate load.

Keywords: Textile reinforced concrete; shear; tension; interaction; slabs

2 Introduction

The resistance to corrosion and the superior mechanical characteristics of non-metallic reinforcement are perfectly suited for applications with severe combined exposition to moisture, frost and de-icing salt. Constructions for infrastructure, such as bridges [1–3], and structural applications for hydraulic engineering, e.g. pipes, channels, piers etc. are typical examples for such expositions [4, 5]. Shear resistance may govern the design in those applications if cross-sections with small effective depth are subjected to high concentrated loads.

When slabs are cast in-situ, e.g. for replacement of defective steel-reinforced elements, normal forces and cracks due to restrained shrinkage or temperature gradients might occur. Other typical examples for tension in slabs are bracing loads or loads through activation of subordinate slabs in the tension zone of continuous beams. Those situations call for appropriate design models covering the interaction between normal force, shear force and moment. For combinations of com-

pressive normal forces and shear, investigations for textile reinforced concrete (TRC) exist [6, 7]. This is the typical case for prestressed systems. Interaction of normal load and bending moment is investigated in [8]. However, for tension forces and full separation cracks, systematic studies for TRC with shear failure are amiss. Investigations for steel-reinforced concrete [9–12] and current discussions for new Eurocode 2 design provisions show that this topic is still relevant also for conventional reinforced concrete. This study presents a test setup to investigate interaction of shear, normal force and moment as well as the influence of separation cracks. A series of slab segments was tested with different configurations of tension force and crack states.

3 Materials and Methods

3.1 Test setup

The test setup (Figure 1) is suitable for testing thin slab segments with various combinations of normal and shear loading and corresponding

moment. Vertical and axial loads are controlled by two different hydraulic circuits. The normal load is transferred over the full width of the specimen by two steel bolts which pass through steel pipes in mid-depth of the specimen. Longitudinal reinforcement passes over the pipes and is fully anchored in the projecting cantilever sections of the slab segment. Thus, transfer of normal force to the reinforcement is achieved solely by bond to surrounding concrete without clamping stress.

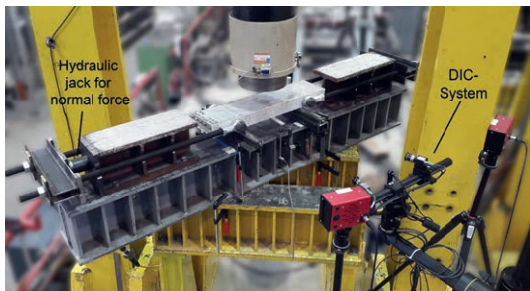
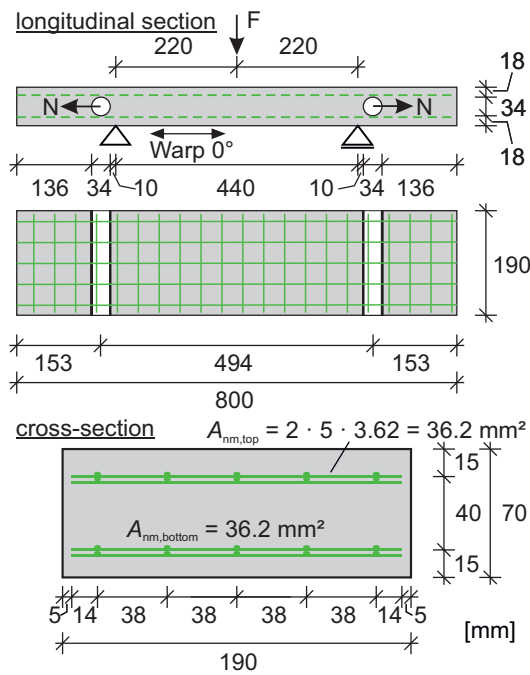


Figure 1: Test setup for interaction of moment, shear and normal load in slab segments | graphic/photo: Jan Bielak

From the offset between the axis of the normal force and the two reinforcement layers result splitting forces which need to be covered either by additional vertical reinforcement in the cantilever section or, as in the test series presented here, solely by concrete tensile stress. The chain of hinges formed by rod ends, crossbeams and hydraulic jack prevents unintended eccentricities in load introduction. A shear span of $a = 220 \text{ mm}$ ($a/d = 4$) was chosen to avoid direct shear strutting to the supports.

3.2 Instrumentation and test procedure

The deflection at mid-span was measured with two linear-variable displacement transducers. To trace crack width and crack propagation throughout the test, a 3D digital image correlation (DIC) system with two cameras was utilized. Two different loading scenarios were applied: For series V1–V3, in part A of the test the normal load N was increased with 5 to 15 kN/min until the specimen showed a saturated vertical crack pattern at a load level of $\approx 75 \text{ kN}$, approximately 30% of the tensile capacity of the reinforcement. After complete unloading, part B of the test was started. There, the axial load was increased up to the target level (0, 15 or 30 kN) and subsequently the vertical load was increased with 1 mm/min up to failure. Series V4–V6 were tested directly according to part B of the test procedure, as shown in Table 1.

No.	N part A	N part B	N_{cr}	d
	[kN]	[kN]	[kN]	[mm]
V1-1	76,4	0	54	57,6
V1-2	71,8	0	38	57,3
V1-3	75,7	0	45	57,9
V2-1	77,1	15,6	52	58,9
V2-2	75,6	14,8	42	55,2
V3-1	76,8	30,7	51	58,6
V3-2	76,1	30,3	43	57,0
V4-1	0	0	-	56,4
V4-2	0	0	-	57,8
V5-1	0	14,9	-	57,0
V5-2	0	14,9	-	56,6
V6-1	0	30,0	-	56,6
V6-2	0	30,1	-	57,2

Table 1: Test specimen matrix

3.3 Reinforcement

The carbon fibre-reinforced polymer (CFRP) reinforcement utilized for all tests was a bi-directional warp-knitted grid (Figure 2) with a filament cross-sectional area of 95 mm²/m per layer and per direction. The modulus of elasticity and ultimate tensile strength in test direction (0°, warp) are 244,835 MPa and 3,221 MPa, respectively. Further material properties are given in [13].

To secure the positioning in mid-span, the reinforcement projected beyond the formwork and was slightly prestressed before concreting. Thus, spacers affecting first-cracking load in the shear span could be avoided. A low variation of effective depth d of the bottom reinforcement layers was determined on saw cuts in the critical section (Table 1).

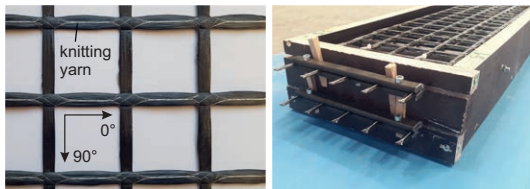


Figure 2: CFRP reinforcement | photo/graphic: Henrik Becks

3.4 Concrete

A self-compacting concrete ($d_{\max} = 4$ mm) specifically designed for the requirements of TRC was employed. The mix design is given in [13]. The mean modulus of elasticity (of cylinders, $d/h = 150/300$ mm) was 41,750 MPa, while mean compressive strength reached 123 MPa for 150 mm cubes and 107 MPa for cylinders at the same day of testing the slab segments. A database evaluation of all batches cast at IMB of this concrete mix revealed a mean conversion factor of 1.19 between cubes and cylinders of age 7 to 60 days. Splitting tensile strength determined on cylinders was 4.8 MPa. The mean stress at first full vertical cracking in the span of V1–V3 was $N_{cr} / (b \cdot h) = 3.4$ MPa (Table 1). It corresponds well with the lower 5% quantile of the uniaxial tensile strength of the concrete ($\approx f_{ctk;0.05} = 0.7 \cdot 0.9 \cdot 4.8 = 3.0$ MPa, calculated according to Eurocode 2).

4 Results

4.1 Failure mechanisms and failure load

All specimens failed in shear through reduction of the compression zone by the critical shear crack

and subsequent concrete compression failure (shear compression failure). In series V2, V3 and specimen V1-3, a typical S-shaped shear crack formed from one of the pre-loading cracks, as shown exemplarily for specimen V2-1 in Figure 3. In those specimens, at least one part of the vertical separation crack was incorporated in the critical shear crack.

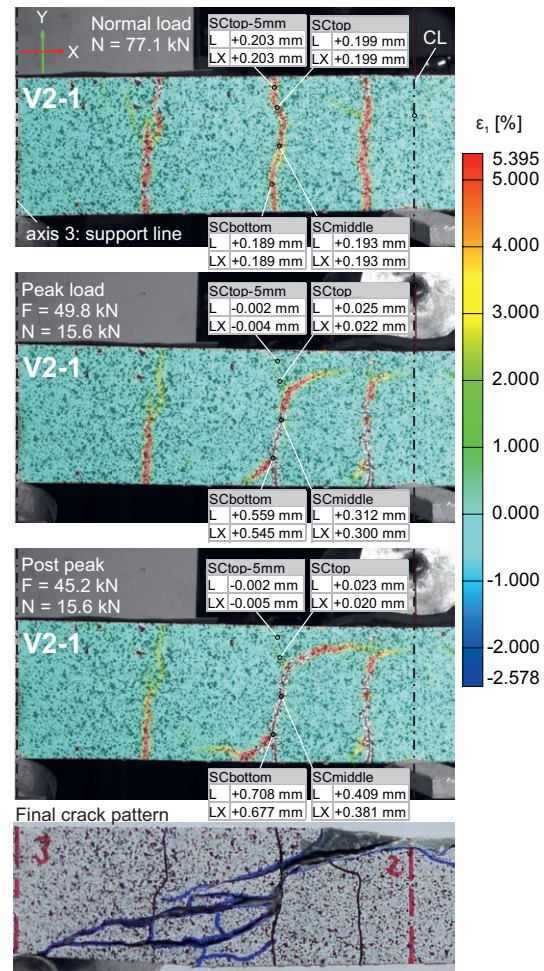


Figure 3: DIC analysis of principal strain and crack width of critical shear crack for specimen V2-1 at preloading, peak- and post-peak load and final crack pattern | graphic: Jan Bielak

For specimens V1-1 and V1-2, linear shear cracks led to failure, which ran between two vertical separation cracks (Figure 4) and were not influenced in their shape by part A of the test.

In Series V4–V6, shear cracks formed from bending cracks, which led as well to shear compression failure. Those shear cracks were either S-shaped or linear, but the middle part of the S was typically more inclined and less straight than for pre-cracked specimens. Figure 4 (center and bottom) compares the crack shape of two speci-

mens which differ only in pre-loading. The shear crack in V2-1 is edgy and supports a higher load without failure, as the critical shear crack formed on the other side, as shown in Figure 3. For V5-1, the shear crack it is rounder, and the vertical part is slightly inclined towards the center of the specimen. This crack was critical and led to failure at a comparatively lower load. It is comparable in its shape to that of V1-2, which might explain the similar ultimate resistances of those specimen. For some specimen, shear crack shape differs from one surface to the other, indicating a 3D-crack topology in between.

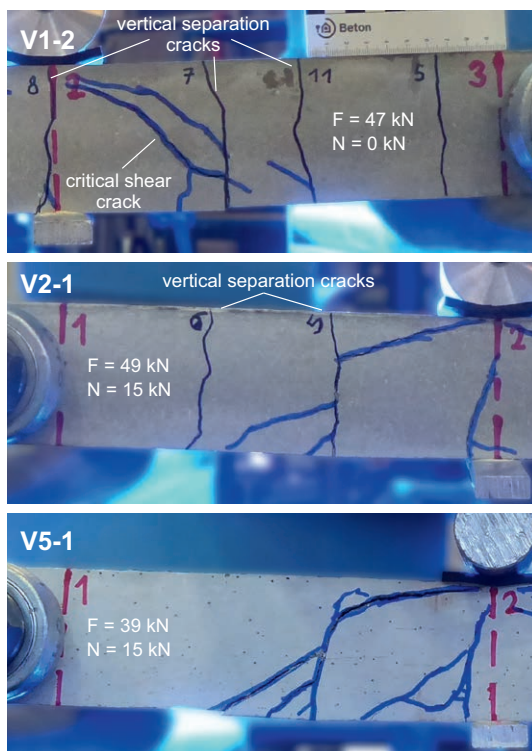


Figure 4: Crack shape and corresponding crack load for specimen with and without separation cracks | graphic: Jan Bielak

The ultimate shear resistances $V_{exp,u}$ shown in Figure 5 include self-weight. The vertical component resulting from deviation of normal loading in mid-span was subtracted from test load, as it does not contribute to shear load in the shear crack. Calculation of this reduction was performed with measured mid-span deflection assuming a polygonal deflection figure. Shear failure occurred at the first significant drop of load (see black circles in Figure 6). In some instances, secondary reallocation allowed load increase after initial shear failure, which led to formation of secondary shear cracks and new load paths, for example in V2-1 (Figure 3, bottom). This mechanism depends on local interlocking effects, e.g. of the concrete wedge in the

compressive zone which is constricted in its rotation by the vertical load introduction, and occurs randomly. As it would not necessarily persist after unloading (path dependency), it was not taken into account in evaluation of ultimate resistance.

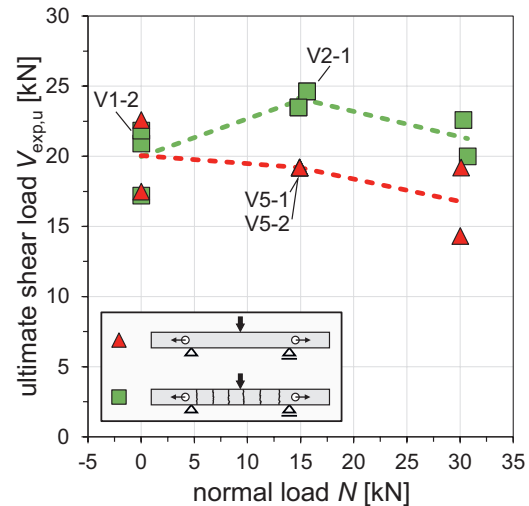


Figure 5: Ultimate shear resistance of specimens with different tension load | graphic: Jan Bielak and Henrik Becks

4.2 Shear load-deflection behavior

Specimens without separation cracks show distinctive drops of load at formation of bending cracks. Their stiffness, however, is similar to pre-cracked specimens (Figure 6). Both ultimate load and corresponding deflection are higher for pre-cracked series for specimens with normal loads of 15 and 30 kN.

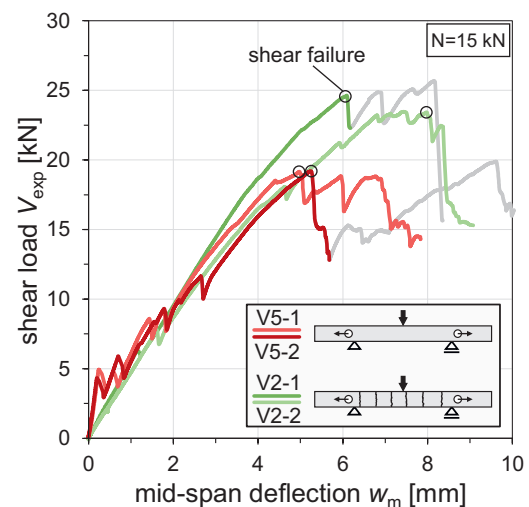


Figure 6: Load-Deflection behavior of slab segment series V2 with and V5 without separation cracks | graphic: Jan Bielak and Henrik Becks

5 Discussion and Conclusions

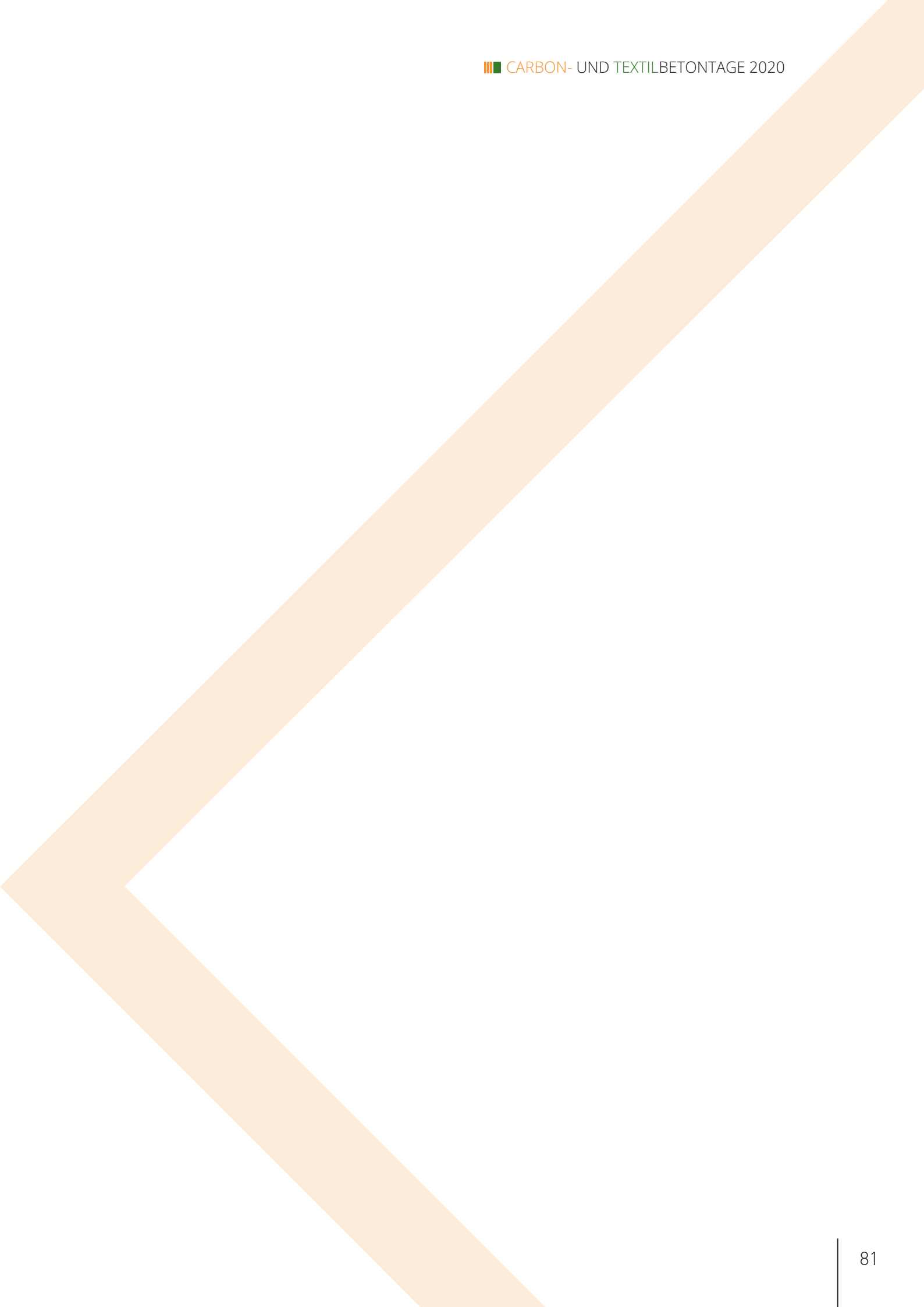
The initial assumption that axial normal forces reduce shear resistance of textile-reinforced slab segments seems justified, as a decreasing trend with increasing normal load in Figure 5 indicates. This effect should be incorporated in design models, just as for conventional steel-reinforced concrete.

Vertical separation cracks in this test program did not reduce shear resistance. The corresponding moment present in the tests closed the cracks in the compression zone completely (Figure 3) and allowed to transmit inclined compressive forces. Interestingly, pre-loading up to saturated vertical crack pattern increased resistance, as seen for Series V2 and V3 with normal loads of 15 and 30 kN. This effect might be attributed to different shear crack shapes. The form of the critical shear crack has major influence on shear resistance, especially for small slabs with high-strength concrete where cracks run through the aggregates and thus aggregate interlock is limited. Here, mechanical interlock of crack interfaces allows for transfer of shear stress. As vertical cracks induce more edgy S-shaped shear crack forms and an inner 3D topology of the shear crack, global rotation of specimen halves along the shear crack, which is necessary for further reduction of compression zone and subsequent failure, is more effectively hindered. One alternative explanation for increase of shear resistance might be the early activation of dowel action also in the top reinforcement layers, which could also influence shear crack evolution. A significant contribution of dowel action to shear resistance of thin slabs has been identified in previous studies on TRC at IMB of RWTH Aachen [14].

Vertical cracks in constrained elements occur randomly (or not at all, depending on the evolution of tensile strength during hardening), and their position does not necessarily coincide with the section critical for shear. Thus, potential positive effects should not be taken into account in design. However, no negative effect on shear resistance for slab segments with shear and corresponding moment could be observed, either. Future studies should clarify if this is also valid at points of contraflexure where no moment is active, and if the finding can be generalized to different member depth. With a larger database, calculation approaches considering the effect of tension loads on shear resistance of thin TRC slab segments could be developed.

6 References

- [1] Bielak, J.; Bergmann, S.; Hegger, J.: Querkrafttragfähigkeit von Carbonbeton-Plattenbrücken mit C-förmiger Querkraftbewehrung. In: *Beton- und Stahlbetonbau* 114 (2019), Heft 5, S. 465-475 – DOI: 10.1002/best.201900001.
- [2] Bielak, J.; Will, N.; Hegger, J.: Zwei Praxisbeispiele zur Querkrafttragfähigkeit von Brückenplatten aus Textilbeton. In: *Bautechnik* 97 (2020), Heft 7, S. 499-507 – DOI: 10.1002/bate.202000037.
- [3] Sydow, A.; Kurath, J.; Steiner, P.: Extrem leichte Brücke aus vorgepanntem Carbonbeton. In: *Beton- und Stahlbetonbau* 114 (2019), Heft 11, S. 869-876 – DOI: 10.1002/best.201800108.
- [4] Quadflieg, T.; Goldfeld, Y.; Dittel, G. et al.: New Age Advanced Smart Water Pipe Systems Using Textile Reinforced Concrete. In: *Procedia Manufacturing*, Vol. 21 (2018), pp. 376-383 – DOI: 10.1016/j.promfg.2018.02.134.
- [5] Rahimi, A.; Westendarp, A.; Morales Cruz, C. et al.: Merkblatt für die Instandsetzung von gerissenen Betonflächen mit textilbewehrten Mörteln/Betonen. In: *Beton* 69 (2019), Heft 3, S. 68-71.
- [6] Kueres, S.; Hegger, J.: Variable strut inclination model for shear design of FRP reinforced concrete members with shear reinforcement. In: *Engineering Structures*, Vol. 206 (2020) – DOI: 10.1016/j.engstruct.2019.110154.
- [7] Kromoser, B.; Huber, P.; Preinstorfer, P.: Experimental study of the shear behaviour of thin walled CFRP reinforced UHPC structures. In: Foster, S.; Gilbert, I.R.; Mendis, P. et al. (eds.): *Better, Smarter, Stronger. Proceedings for the 2018 fib Congress held in Melbourne, Melbourne, Australia, 2018*, pp. 1744-1750.
- [8] Rempel, S.; Ricker, M.; Hegger, J.: Biegebemessungsmodell mit einer geschlossenen und iterativen Lösung für Textilbetonbauteile. In: *Beton- und Stahlbetonbau* 115 (2020), Heft 3, S. 218-230 – DOI: 10.1002/best.201900086.
- [9] Adam, V.; Claßen, M.; Hegger, J.: Versuche zum Querkrafttragverhalten bei gleichzeitiger Zugnormalkraft. In: *Beton- und Stahlbetonbau* 115 (2020) – DOI: 10.1002/best.202000003.
- [10] Ehmman, J.: Querkrafttragfähigkeit zugbeanspruchter Stahlbetonplatten in Verbundbrücken. Stuttgart, Dissertation, 2003 – DOI: 10.18419/opus-183.
- [11] Zararis, P.D.; Zararis, I.P.: Shear Strength of Reinforced Concrete Slender Beams with or without Axial Forces—A Generalized Theory. In: *ACI Structural Journal*, Vol. 106 (2009), Iss. 6, pp. 782-789 – DOI: 10.14359/51663179.
- [12] Yamada, M.; Kiyomiya, O.: Shear Capacity Of Reinforced Concrete Beams With Initial Cracks. In: *Transactions of the Japan Concrete Institute* 17 (1995), S. 297-304.
- [13] Bielak, J.; Adam, V.; Hegger, J. et al.: Shear Capacity of Textile-Reinforced Concrete Slabs without Shear Reinforcement. In: *Applied Sciences*, Vol. 9 (2019), Iss. 7, 1382 – DOI: 10.3390/app9071382.
- [14] Kulas, C.: Zum Tragverhalten getränkter textiler Bewehrungselemente für Betonbauteile. Aachen, RWTH Aachen University, Dissertation, 2013.



Carbon Textile Reinforced Concrete at ambient and high temperatures

Panagiotis Kapsalis

PhD candidate, Department Mechanics of Materials and Constructions, Vrije Universiteit Brussel (VUB) Brussels, Belgium and Department of Civil Engineering, Structural Materials Laboratory, University of Patras (UPatras) Patras, Greece

✉ Panagiotis.Kapsalis@vub.be

Panagiotis Kapsalis is a MSc civil engineer and currently a PhD candidate on a joint program between UPatras and VUB.

Thanasis Triantafillou

Professor, Department of Civil Engineering, Structural Materials Laboratory, University of Patras, Patras, Greece

✉ ttriant@upatras.gr

Thanasis Triantafillou specializes in the area of advanced structural materials, with a focus on strengthening and seismic retrofitting with textile-based and FRP composites.

Tine Tysmans

Professor, Department Mechanics of Materials and Constructions, Vrije Universiteit Brussel (VUB), Brussels, Belgium

✉ ttysmans@vub.be

Tine Tysmans graduated as a Civil Engineer in 2006 and received her PhD degree in 2010. Her research is driven by the search for material-efficient lightweight structures using textile reinforced cement (TRC) composites.

Contact: Panagiotis.Kapsalis@vub.be

1 Abstract

The mechanical behavior of Textile Reinforced Concrete after exposure to fire is poorly investigated so far. This study investigates the tensile and flexural capacity of carbon TRC at ambient conditions and after fire exposure, focusing on the influence of the surface treatment of the textiles and the thickness of the concrete cover. The results show that polymer coatings negatively influence the fire resistance while uncoated fibers maintain their stiffness for temperatures up to 500 °C. Also, increasing the cover by 4 mm can keep the specimen unaffected for temperatures up to 300 °C.

Keywords: Carbon Textiles, Concrete Cover, Fire Testing, High temperature, Textile Coating, Textile Reinforced Concrete, Textile Reinforced Mortars.

2 Introduction

In the past decades, Textile Reinforced Concrete (TRC) has become increasingly popular in scientific studies and in practice, because it offers the potential to create lightweight, strong, durable and easily tailored structural elements. The most commonly used textiles are made of AR-glass, basalt or carbon fibers. One of the main advantages of carbon fibers with respect to glass is their resistance to high temperatures.

This temperature resistance at the level of the fiber however does not directly imply the good performance of a carbon-TRC (CTRC) element in case of a fire. Firstly, the damage of thin CTRC elements under fire might be severe due to spalling. Additionally, the carbon fibers' heat resistance is hindered when they are exposed to oxygen: carbon fibers' strength degrades significantly after

exposure to 500 °C or higher in an oxidizing environment [1, 2]. However, when heated at inert atmospheric conditions the carbon fibers do not degrade and might even present a strength increase at 1000-1600 °C [3]. Nevertheless, in the case of a heated and cracked TRC element, part of the reinforcement might be exposed to oxygen, thus, the element degrades severely [2,4]. Finally, the performance of the composite can be hindered by the degradation of the matrix-to-reinforcement bond, especially in the case of textiles with coating which might be burnt off and, thus, deteriorate the bond. Consequently, early failure of CTRC specimens has been observed for temperatures below 500 °C [2], [4-7]. However, studies in this area are limited, and available experimental data is not adequate to quantify the effect of each parameter that affects this behavior. To obtain general degradation laws and design guidelines, more research is required.

This paper discusses an experimental campaign investigating the effect of fire exposure on the residual capacity of CTFC. The effect of temperature is quantified by exposing the specimens to three fire tests with varying duration and, thus, varying target temperatures (approximately 200 °C, 300 °C and 500 °C). Tensile tests on fully fire exposed specimens reinforced with coated or uncoated textiles, showed the effect of the coating. The effect of the concrete cover is studied by bending tests on specimens with uncoated textiles only. In this case the specimens are exposed only from one side, leading to non-uniform heating.

3 Materials and methods

3.1 Matrix and reinforcement

The textiles that were used for this study are the following:

- (i) Uncoated (dry) carbon textile with a weight of 170 g/m² and 12 mm axial distance of the rovings.
- (ii) Epoxy coated carbon textile with the same geometry as the uncoated, manually impregnated with epoxy resin in the laboratory. The average resin content was 34% of the uncoated weight (standard deviation 6%).
- (iii) Styrene-Butadiene-Rubber (SBR) coated carbon textile with a weight of 516 g/m² (before coating) and 12.5 mm axial distance of the rovings.

All textiles have equal distribution of their fibers in two perpendicular directions and a square mesh. Tensile tests on textile samples gave the following results of tensile strength and elastic modulus:

- (i) Uncoated: $\sigma_{max} = 2231$ MPa, $E = 212.5$ GPa
- (ii) Epoxy coated: $\sigma_{max} = 4062$ MPa, $E = 203.5$ GPa
- (iii) SBR coated: $\sigma_{max} = 1444$ MPa, $E = 235.0$ GPa

A commercial cementitious mortar with short polymer fibers, quartz sand and other additives has been used in this study. The compressive and flexural strength are equal to 68.2 MPa and 7.1 MPa respectively, as obtained from tests on prisms of 40x40x160 mm, according to EN12190 and EN196-1.

3.2 Layups definition: geometrical details and nomenclature

The following figure summarizes the geometry of specimens (Figure 1a) as well as the cross-sectional details of the tension specimens (Figure

1b) and of the flexure specimens (Figure 1c). The nomenclature of the layups is also shown in this figure.

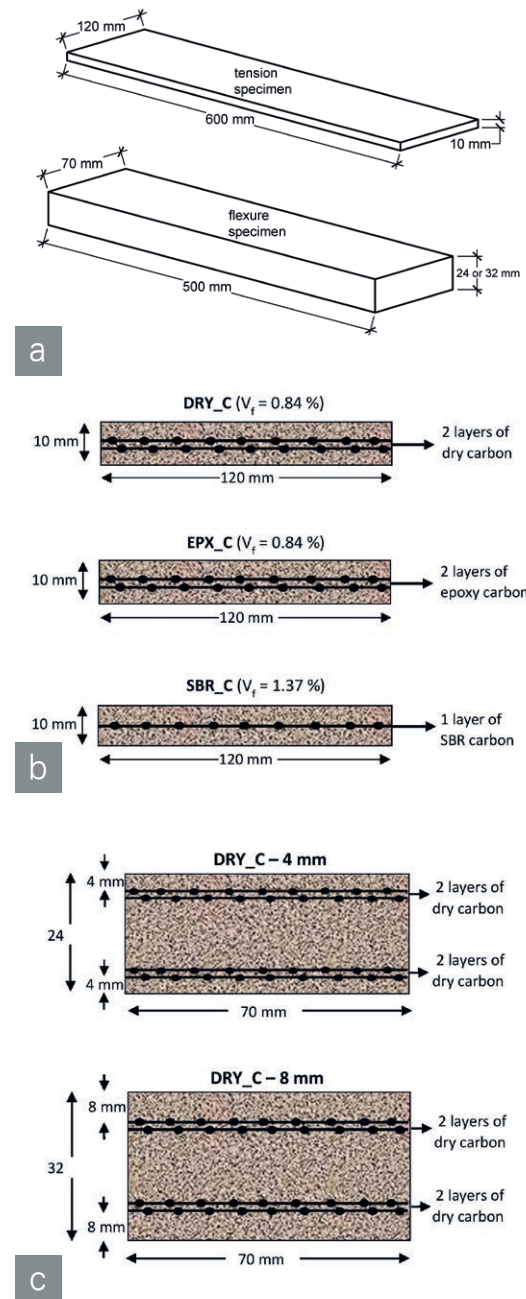


Figure 1: Geometrical properties and nomenclature of layups; (a) dimensions of specimens; (b) cross-sections of tension specimens; (c) cross-sections of flexure specimens | graphic: Panagiotis Kapsalis

3.3 Specimens manufacturing and testing

All specimens were manufactured by hand layup and the curing was done by wrapping the specimens with wet fabrics and plastic foil for 28 days. After the 28 days and before the fire test, all specimens were dried in an electric furnace for 4 days.

The fire tests were conducted following the ISO834 standard fire curve, using the Fire Testing Facility at the University of Patras (see Figure 2). As seen in Figure 2c, since the flexure specimens were exposed only to one side, the other sides were insulated with mineral wool. The exposed side was the same that was subjected to tension during bending. Therefore, the fibers that were closer to the exposed surface were the ones at the effective depth of the specimens during bending.

The temperature was monitored by thermocouples that were embedded in the specimens during casting. Three thermocouples per specimen were placed: for the tension specimens one at each surface and one in the middle; and for the bend-

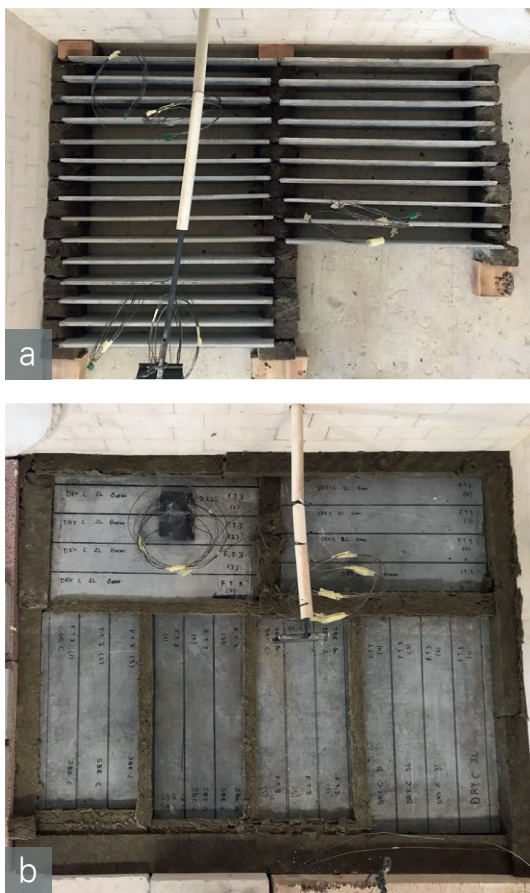


Figure 2: (a) positioning of tension specimens in the furnace; (b) positioning of flexure specimens in the furnace | photos: Panagiotis Kapsalis

ing specimens one at the exposed surface, one at the level of the effective depth and one at the unexposed surface. However, as insufficient sensors were available to monitor all specimens, the temperatures of some specimens are estimated based on the temperatures of their neighboring specimens.

The tension specimens were tested with the “clevis type” set up (see Figure 3a) which has been well described in [8]. The deformation was measured by video-extensometers monitoring the two borders of the specimen’s free length. Thus, the stress-strain curves were obtained.

The flexure specimens were tested in 4-point bending as shown in Figure 3b. From the bending tests the load vs. mid-span displacement curves were obtained.

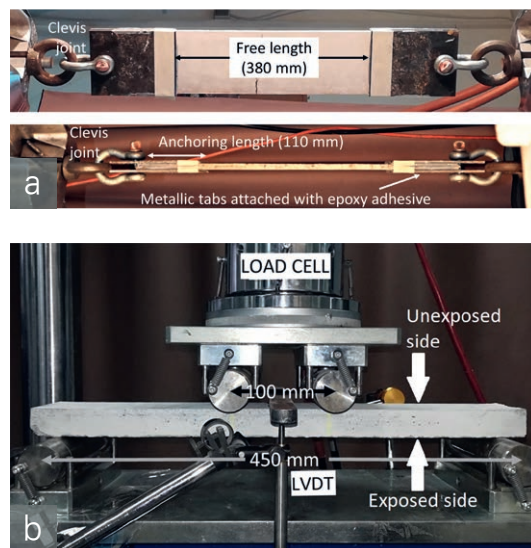


Figure 3: Mechanical tests set-ups: (a) “clevis-type” set-up for tension; (b) 4-point bending set-up | photos: Panagiotis Kapsalis

4 Results and Discussion

4.1 Fire tests results

Three fire tests have been conducted with durations of 7, 19 and 28 minutes. The times were not predefined; the fire tests stopped when the target temperature at the tension specimens were achieved. The temperature evolution during fire exposure is indicatively given in Figure 4 for a tension coupon and a flexure specimen of DRY_C layup during fire test 3. As observed in Figure 4a, the temperature of the coupon was practically uniform through its thickness. This was observed for all specimens (to be tested in tension), in all

fire tests. The maximum temperature in the specimens (to be tested in bending), however, not only differs at each measuring position, but it is also reached at different time (Figure 4b). However, in this study the maximum temperatures are of interest since the residual properties of the specimens are investigated (the degradation of the materials' properties is assumed to be irreversible).

The temperatures of the tension specimens and the maximum temperatures of the flexure specimens are given in Table 1, where it can be observed that due to the non-uniform distribution of the temperature in the furnace, the temperatures have sometimes significant differences in the same fire test.

Note that the EPX_C specimens for tension were not tested in fire test 3 (28 minutes) since previous experience showed that severe damage is expected even at low temperature. The reason is that severe spalling occurs, caused by the evaporation of the heated resin. The other specimens did not suffer any spalling in any test. Only minor cracks were formed at the exposed surfaces, which are attributed to the thermal stresses.

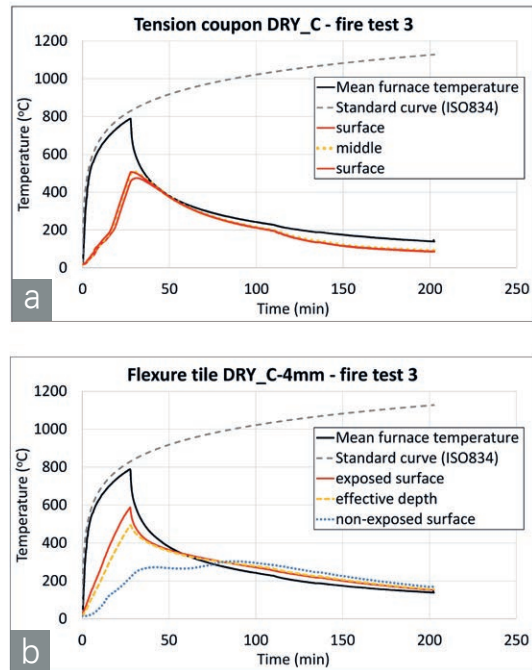


Figure 4: Temperature evolution during fire test 3 (28min.) of an indicative: (a) tension specimen; (b) flexure specimen | graphic: Panagiotis Kapsalis

	Tension specimens (°C)			Flexure specimens (°C)		
	DRY_C	EPX_C	SBR_C		DRY_C-4mm	DRY_C-8mm
Fire test 1 (7 min)	238	179	179	exposed surface	264	226
				effective depth	168	151
				unexposed surface	137	96
Fire test 2 (19 min)	302	314	305	exposed surface	291*	291
				effective depth	-	-
				unexposed surface	-	134
Fire test 3 (28 min)	496	-	514	exposed surface	587	587
				effective depth	494	444
				unexposed surface	303	313

Table 1: Measured and estimated(*) maximum exposure temperatures of all specimens during the fire tests

4.2 Tensile tests results: influence of textile surface treatment

As comparison of the tensile stress strain curves for DRY_C, EPX_C and SBR_C in Figure 5 shows, the different textile surface treatments, as well as the different amount and distribution of fibers have a significant influence on the residual mechanical behavior after exposure to fire. It is noteworthy that in all cases failure occurred due to pull out as there was no fiber rupture observed. It is also reminded that the SBR_C layup did not only differ on the surface treatment with respect to the other layups but

also to the amount and distribution of the fibers. Hence, a direct comparison with the other layups should be done cautiously.

The uncoated carbon layup presents a typical 3-stage behavior as defined from the ACK theory [9] for TRC. The fibers have suffered almost no degradation at all, for temperatures up to 300 °C, thus, the post-cracking stiffness of the composite is the same as for ambient temperatures. The ultimate

stress has a minor decay, caused by the drop of the first cracking stress, thus, it is attributed to the degradation of the mortar. It is also observed that the transition between the three stages becomes smoother with increasing temperature. This is the result of the pre-cracked mortar due to fire exposure before the tensile testing. The crack pattern was the same in all cases, with the number of cracks varying between 9-12. A significant loss of ultimate stress ($\approx 43\%$) was observed for exposure at 500 °C while the stiffness was still intact. This is mainly attributed at the oxidation reaction of the carbon fibers which initiates at this temperature. However, it could also be attributed to the degradation of the textile-to-matrix bond, caused by the mortar degradation and the developed cracks due to the fire exposure (see Figure 6a).

The epoxy coated carbon layup presents a similar tensile behavior to the DRY_C layup up to 300 °C. At ambient conditions, the load-bearing and deformation capacity of this layup was superior to the DRY_C, since the epoxy resin enforces the activation of more filaments. The degradation due to exposure at 179 °C seems to be minor and the drop of the tensile strength is mainly caused by the drop of the first cracking stress. The specimens exposed at 314 °C present a small decay in the post cracking stiffness, which is attributed not only to the resin burn off but also to the development of cracks that resembled a form of delamination at the level of the reinforcement layers (see Figure 6b). This was the result of the epoxy resin burn off, which as a thermoset material, evaporates without going through a melting phase, which, causes severe spalling. This effect was less pronounced near the edges of the specimens which were partially protected between mineral wool that was used to keep the specimens in a vertical position (see Figure 2a). Thus, it was possible to clamp the specimens and perform the tensile tests.

The SBR_C layup presented a much weaker behavior with respect to the other layups, even though the fiber volume fraction was higher. These specimens hardly showed a 3-stage behavior. They failed at much lower stresses and higher strains and they had only 2-3, very wide cracks (see Figure 6c). This means that the bond between the reinforcement and the matrix was weak and the rovings were being pulled out, thus, the inner filaments were less activated. As a result, the shape of the SBR_C curves at 20 °C, indicates a short "stage 2" behavior and then a "stage 3" which is mainly controlled by the pull-out properties.

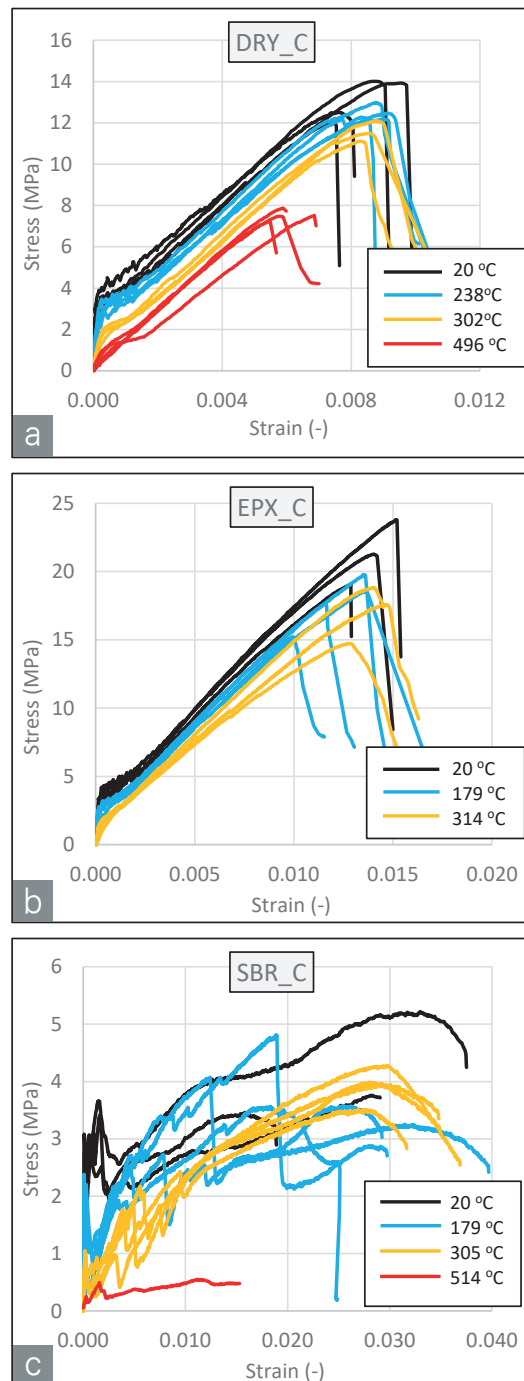


Figure 5: Stress-strain curves of ambient and fire exposed TRC layups: (a) DRY_C; (b) EPX_C; (c) SBR_C | graphic: Panagiotis Kapsalis

However, the curves at 179 °C and 300 °C, apart from the earlier cracking of the mortar and more severe load drops, also indicate a "Stage 3" which is characterized by continuous load drops without forming more cracks, meaning that the pull-out properties are different. The difference probably lies on (i) the partial evaporation of the coating, which weakens the bond even more, and (ii) the



Figure 6: (a) Specimen of DRY_C layup after tensile testing with visibly cracked mortar due to tension and due to fire exposure at 496°C; (b) Specimen of EPX_C layup after exposure to 314°C, before tensile testing, with visible longitudinal delamination at the level of the reinforcement; (c) Specimen of SBR_C layup, not exposed to fire, with visible wide cracks while tested in tension | photos: Panagiotis Kapsalis

partial melting of the coating and absorption by the inner filaments or the surrounding mortar. The second phenomenon enhances the tensile behavior which might explain why the maximum stress level did not drop significantly and might also be a reason why spalling due to evaporation was not observed to this layup. Finally, the specimens exposed to 514 °C were severely damaged and they had practically no residual strength. As observed by visual inspection after the tensile tests, the coating was completely burnt off and the bond between the textile and the mortar was practically lost (the rovings could be pulled out by hand).

It is noted that the total mass of the SBR polymer in a specimen was almost half than the total mass of epoxy resin at the EPX_C specimens. This fact, as well as the melting of the SBR polymer (in contradiction to the epoxy resin) before evaporation, pose a possible explanation why there was no spalling in this layup.

4.3 Bending tests results: influence of concrete cover

The DRY_C layups were also tested in flexure with 4 mm or 8 mm of concrete cover (see Figure 7). The flexural behavior is similar to the tensile behavior since they both present three stages, while the transition between them becomes smoother with increasing temperature. Both cases suffered increasing decay of maximum force and stiffness with increasing exposure time. In the 7-minute exposure (fire test 1), no degradation was noticed since the achieved temperatures were rather low. The temperature at the most stressed fibers (effective depth) is less than 170 °C and as it can be

deduced from the tensile stress-strain behavior at that temperature in Figure 5a, their degradation is minimal. At the same time, the temperature at the non-exposed surface (mortar in the compressive area during bending) is less than 140 °C. For common cementitious mortars no severe degradation is yet observed at such temperatures.

Fire exposure for 19 minutes (fire test 2) degraded only the DRY_C-4mm layup (maximum load decayed by 13% and post-cracking stiffness decayed by 17%) while the DRY_C-8mm did not suffer any load or stiffness loss, indicating the protection that a thicker concrete cover can offer, by reducing the temperature at the effective depth. Both layups degraded considerably after the 28-minute fire exposure (fire test 3). Specifically, the maximum load dropped by 28% for both layups while the post-cracking stiffness of DRY_C-4mm dropped by 30% and the stiffness of DRY_C-8mm dropped by 25%.

5 Conclusions

In this study, the results of an experimental campaign investigating the effect of the textile coating (by tensile tests) and the concrete cover (by bending tests) of fire exposed CTCRC layups have been presented and discussed. The tests were conducted on layups with uncoated (dry) or coated (epoxy or SBR) carbon textiles and the target temperatures were approximately 200 °C, 300 °C and 500 °C.

The conclusions are summarized here:

- (i) The uncoated carbon fiber layups maintained their stiffness for temperatures up to 500 °C. They suffered minimal decay of strength for temperatures up to 300 °C while at 500 °C the strength dropped by 43%.
- (ii) The epoxy impregnation of the fibers significantly improves the performance of the specimens in ambient conditions but causes additional degradation of the properties of the heated specimens due to spalling caused by the resin's evaporation.
- (iii) The SBR coating does not lead to severe degradation for temperatures up to 300 °C when exposed to fast heating rates (as in this study). However, the residual performance is almost negligible when exposed to 500 °C.

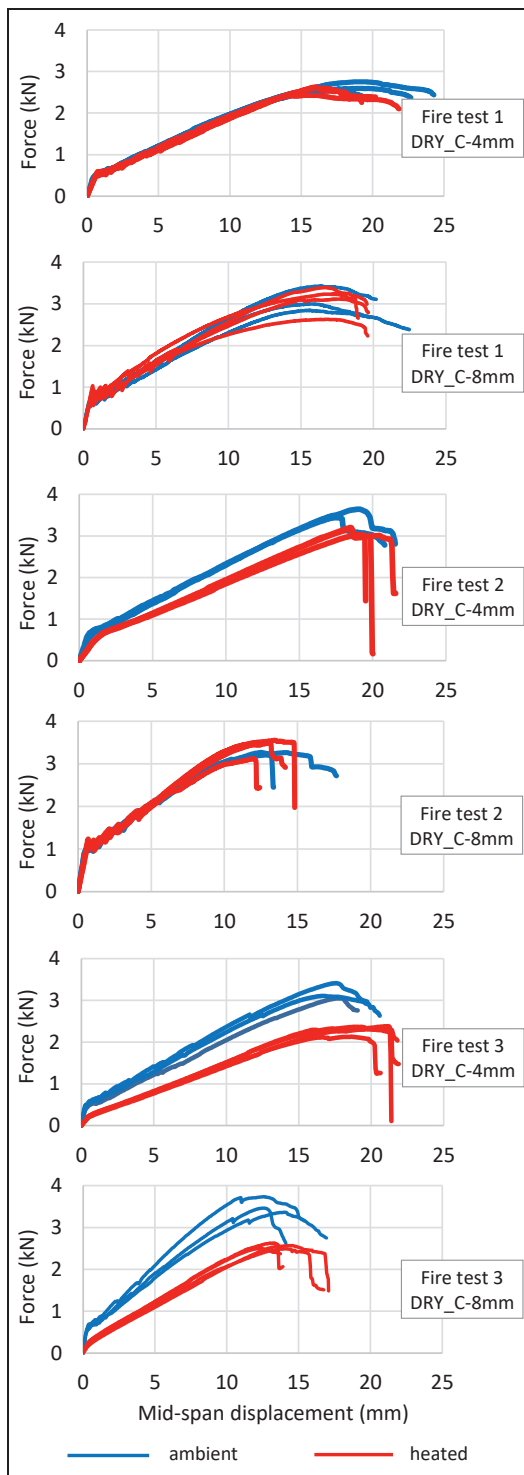


Figure 7: Residual flexural behavior of ambient and fire exposed DRY_C layouts | graphic: Panagiotis Kapsalis

- (iv) The flexural behavior of uncoated carbon TRC after fire exposure can be related to its 3-stage tensile performance, remaining unaffected for surface temperatures of the exposed side up to 260 °C. For exposed surface temperatures up to 590 °C, degradation in the order of 25-30% is expected for the load bearing capacity and the stiffness.
- (v) Increasing the concrete cover by 4 mm delays the temperature increase at the reinforcement by 50 °C after 28 minutes of fire exposure.

6 Acknowledgements

This research is co-financed by Greece and the European Union (European Social Fund- ESF) through the Operational Programme «Human Resources Development, Education and Lifelong Learning» in the context of the project “Strengthening Human Resources Research Potential via Doctorate Research” (MIS-5000432), implemented by the State Scholarships Foundation (IKY).



Operational Programme
Human Resources Development,
Education and Lifelong Learning
Co-financed by Greece and the European Union



7 References

- [1] L. G. Tang, „Influence of boron treatment on oxidation of carbon fibre in air.“ *Journal of Applied Polymer Science*, vol. 59, pp. 915-921, 1996.
- [2] M. T. Tran, X. H. Vu, E. Ferrier, “Mesoscale experimental investigation of thermomechanical behaviour of the carbon textile reinforced refractory concrete under simultaneous mechanical loading and elevated temperature,” *Construction and Building Materials*, vol. 217, pp. 156-171, 2019.
- [3] C. Sauder, J. Lamon, R. Pailler, “Thermomechanical properties of carbon fibres at high temperatures (up to 2000 C),” *Composites Science and Technology*, vol. 62(4), pp. 499-504, 2002.
- [4] A. Younes, A. Seidel, T. Engler, C. Cherif, D. Ehlig, “Mechanical behaviour of carbon and glass filament yarns under high temperatures for composite applications,” *Journal of The Textile Institute*, vol. 104(3), pp. 251-259, 2013.
- [5] D. Ehlig, F. Jesse, M. Curbach, „High temperature tests on textile reinforced concrete (TRC) strain specimens.“ *International RILEM Conference on Material Science*. RILEM Publications SARL, 2010.
- [6] F. A. Silva, M. Butler, S. Hempel, R. D. F. Toledo, V. Mechtcherine, “Effects of elevated temperatures on the interface properties of carbon textile-reinforced concrete,” *Cement and Concrete Composites*, vol. 48, pp. 26-34, 2014.
- [7] P. Kapsalis, M. El Kadi, J. Vervloet, M. De Munck, J. Wastiels, T. Triantafillou, T. Tysmans, “Thermomechanical behavior of textile reinforced cementitious composites subjected to fire,” *Applied Sciences*, vol. 9(4), 747, 2019.
- [8] J. Donnini, V. Cordinalesi, “Mechanical characterization of different FRCC systems for structural reinforcement,” *Construction and Building Materials*, vol. 145, pp. 565-575, 2017.
- [9] J. Aveston, G. A. Cooper, A. Kelly, “Single and Multiple Fracture. The Properties of Fiber Composites,” *Proceedings of the National Physical Laboratories, IPC Science & Technology Press Ltd. Conference*, London, 1971.

Positioning aids for textile reinforcements

Dr.-Ing. Kristin Mandel

Chemnitz University of Technology,

Department of Lightweight Structures and Polymer Technology, Chemnitz, Germany

✉ kristin.mandel@mb.tu-chemnitz.de

Dr. K. Mandel works as a research associate on the material and component development for building applications.

Dipl.-Ing. Marco Lindner

Chemnitz University of Technology,

Department of Lightweight Structures and Polymer Technology, Chemnitz, Germany

✉ marco.lindner@mb.tu-chemnitz.de

Current developments of research associate M. Lindner are focused on alternative reinforcements for lightweight concrete elements.

Prof. Dr.-Ing. habil. Sandra Gelbrich

Chemnitz University of Technology,

Department of Lightweight Structures and Polymer Technology, Chemnitz, Germany

✉ sandra.gelbrich@mb.tu-chemnitz.de

Prof. S. Gelbrich is head of the research group "Lightweight Constructions in Civil Engineering".

Contact: kristin.mandel@mb.tu-chemnitz.de

1 Abstract

The establishment of textile concrete depends on the provision of useful methods for the integration of reinforcements. In this study, mineral-based positioning aids with concrete-like properties were developed and their integration behaviour in textile concrete was examined. As a result, two appropriate variants are presented. They both show no negative effect on the load-bearing capacity of textile concrete, are easy to handle, use inexpensive raw materials and are suitable for series production.

Keywords: textile concrete, reinforcement integration, positioning aids, mineral-based materials

2 Introduction

Due to its resource-saving properties, textile concrete is a promising alternative to conventional reinforced concrete [1-4]. However, the practical use is currently still associated with many obstacles [5-7]. One difficulty, for example, is the exact positioning of the textile reinforcement grid, which can be facilitated by special positioning aids. The user-specific requirements for such elements are:

- Functionality, especially for different grid types,
- Availability in large quantities,
- Low price,
- Easy handling even for "builders' hands",
- No creation of weak points and no negative impact on the load-bearing capacity of the concrete component, and
- Low rigidity gap as well as good interface connection between element and concrete matrix.

Currently, there is no all-encompassing solution for all these requirements, but several approaches are available [8]. The practical and economic demands can be met by using series production processes such as injection moulding and a suitable structural design. For the implementation of these substantial requirements, mineral-based materials offer promising properties [9].

In this study, wollastonite phosphate cements (Wo-PC) and mineral filled plastic (MFP) composites with a high degree of filling were selected as mineral-based materials for the positioning aids and corresponding designs as well as production methods were developed in order to meet the above-mentioned challenges. These two materials were chosen because of their concrete-like properties and favourable raw material prices.

3 Materials and Methods

3.1 Wo-PC

The Wo-PC was made from a mixture of 60% phosphoric acid with aluminium and zinc additives as well as the partially calcined powder *Wollastonit F* (Mineralmühle Leun, Rau GmbH & Co.KG) with an acid/powder ratio of a/p=1.2. Injection moulding, transfer moulding and powder infiltration were tested as suitable forming processes for the Wo-PC.

The temperature-dependent pot life t_{SG} (sol-gel transition) was determined with the help of a HAAKE MARS III rheometer with a 20 mm diameter parallel plate setup and a gap of 1.5 mm in oscillation mode with a frequency of 1 Hz.

The true density of the Wo-PC was determined with a helium pycnometer. Three-point bending strength tests were carried out in accordance with DIN EN 843-1 on a ZMART.PRO with a 100 N load cell, a preload of 0.5 N and a test speed of 0.2 mm/min. The span was 30 mm, the radius of the supports 2 mm and the radius of the bending punch 3 mm. The samples were produced with a specially manufactured injection moulding tool. 37 samples were tested for the statistical evaluation using Weibull statistics according to DIN 843-5.

3.2 MFP

Different MFP composites were produced and investigated. The matrix material used was PP Moplen HP 500 V Natural with 2% TPPP 8012 GA as coupling agent. The coupling agent is a PP, functionalised with maleic anhydride, which acts as an adhesion promoter and improves the mechanical properties. Marble powders from sh minerals GmbH with different grain sizes and barytes from Sachtleben Minerals GmbH & Co. KG were used as fillers. The filler content was varied in the range from 50 to 62% mass. The compounds are listed in Table 1. The compounding was carried out with the help of a twin-screw compounder ZSC 25 / 44D (Noris Plastic). For the determination of the characteristic values, test specimens of type A were manufactured according to DIN EN ISO 32167 with an ARBURG All Drive 370 injection moulding machine with an appropriate mould (Axxicon). Tensile tests according to DIN EN ISO 527 were performed with a Zwick / Roell Z010 universal testing machine and impact tests according to DIN EN ISO 179 with an instrumented Zwick

HIT25P pendulum. Furthermore, the melt index MFR (Melt Flow Rate) was examined according to DIN EN ISO 1133-1 with a MeltFlow@on plus.

	Filler	Proportion in %	
		by mass	by volume
PP/T-S50	Saxolith S 2 HE (up to 13 µm)	50	24.7
PP/T-SE50	Saxolith extra 70 (up to 200 µm)	50	24.7
PP/T-SC50	Saxocarb 200 (up to 200 µm)	50	24.7
PP/T-Bx50	Baryt CH1013 (up to 34 µm)	50	17
PP/T-Bx62	Baryt CH1013 (up to 34 µm)	62	24.7

Table 1: MFP compounds

3.3 Design and production studies

Based on the material and user-related design requirements as well as the test results obtained, various designs for the two types of positioning aids were created and iteratively adapted. The positioning aids for basic testing were initially produced on a laboratory scale using specially manufactured tools (Wo-PC) or 3D printing (MFP). In this way, knowledge of material and application properties was obtained and the design was successively improved.

3.4 Integration into textile concrete

In order to test the application properties of the positioning aids and to examine the effects on the load-bearing capacity of the textile concrete, carbon concrete slabs including single-layer textile grids with and without fixation were produced (see Figure 1). The dimensions of the slabs were 50 cm x 50 cm. The slabs for the Wo-PC positioning aids included solidian GRID Q85/85-CCE-21 and had a height of 2 cm, whereas the slabs for the MFP elements included solidian GRID Q142/142-CCE-25 and had a height of 4 cm. The concrete mixture is summarised in Table 2. It was mixed using an EIRICH R05/T intensive mixer.

Four-point bending (4PB) tensile test samples with LxW=50 cmx10 cm were cut from the hardened slabs using a tile cutting machine. The tests were carried out on a ZwickRoell Z250 in accordance with DIN EN 12390-5 at a test speed of 2 mm/min. The distance between the supports and the span width were 45 cm and 15 cm, respectively. Six samples, each with two MFP or six Wo-PC

Component	kg/m ³
CEM I 52.5	449
SFA	150
Silica Fume	47
Quartz sand 0/2	1267
Dolomite powder	150
Water	196
Superplasticizer	12
w/b	0.39
w/c	0.44

Table 2: Concrete mixture

positioning aids in the load area were tested. In addition, samples without positioning aids in the load area were tested, too. After failure, the fracture surfaces were examined by light microscopy in the area of the interface between concrete and positioning aids in order to assess the connection.

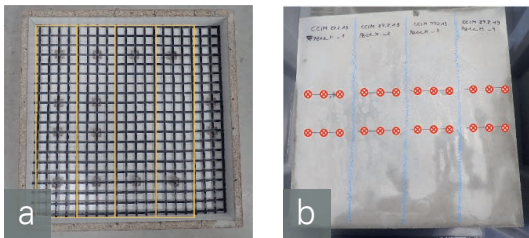


Figure 1: (a) Prepared formwork for MFP carbon concrete slab indicating the positions of the 4PB samples with and without positioning aids in the load area and (b) Wo-PC carbon concrete slab indicating the location of the 4PB samples and of the positioning aids | graphic: K. Mandel

4 Results and discussion

4.1 Material properties

Material and processing properties of Wo-PC depend heavily on temperature and pressure during the entire processing procedure. The results of the rheological measurements of Wo-PC mixtures of raw and calcined powder are presented in Figure 2. The diagram shows that the pot life can be adjusted from minutes to seconds by using special powder compositions with specific amounts of calcined powder and/or with the help of specific temperature control. At temperatures above 40 °C the flowability of the calcined Wo-PC is completely lost and a very fast setting of the cement can be expected.

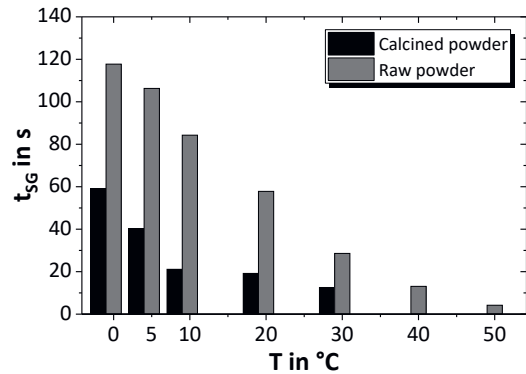


Figure 2: Pot life t_{SG} of different Wo-PC mixtures at different processing temperatures T | graphic: K. Mandel

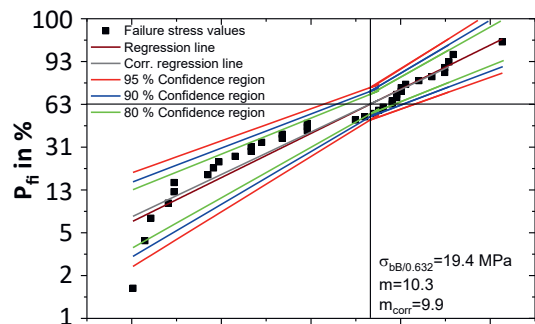


Figure 3: Weibull distribution of the bending strength of the Wo-PC samples - failure probability P_{fi} at different stresses σ_{fb} | graphic: K. Mandel

Figure 3 shows the results of strength tests of Wo-PC with a mixture of 50% raw and 50% calcined powder. The characteristic bending strength is $\sigma_{bB/0.632} = 19.4 \text{ MPa}$ with a Weibull modulus of $m_{corr} = 9.9$, which is a typical value for brittle materials. However, the determined bending strength roughly corresponds to that of concrete. The density of the material is, with $\rho_{geo} = 1.73 \text{ g/cm}^3$ for the geometrical density and $\rho_{true} = 2.6 \text{ g/cm}$ for the true density, slightly lower than that of concrete.

All **MFP** mixtures showed good compoundability. The MFR measurements (see Figure 4) revealed good flow properties in the range of $73 \leq \text{MFR} \leq 110 \text{ g/10min}$ for all MFP compounds. This indicates good processability in the injection moulding process. Barytes as filler material led to even higher flow rates than the marble powders, both at the same mass and volume fraction. Additionally, with regard to the durability of compounding and injection moulding tools, barytes should be preferred as filler material due to its lower abrasiveness in comparison to marble powders.

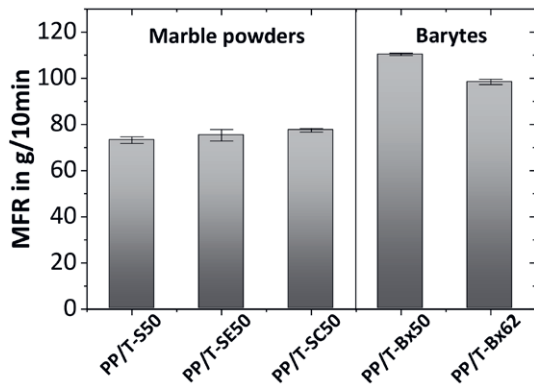


Figure 4: Melt Flow Rate MFR of the MFP (mean values and standard deviations) | graphic: K. Mandel

Selected results of the tensile tests of the MFP are shown in Figure 5. In general, the tensile strength σ_m decreases and the tensile modulus increases with an increasing proportion of filler and increasing particle size of the powder. The marble powder compound PP/T-S50 delivers the highest tensile modulus with up to $E_t=3330\pm36$ MPa. The compound with a similar volume content of barytes PP/T-Bx62, $E_t=3280\pm16$ MPa shows a slightly lower mean value. The impact strengths of the MFP compounds with marble powders are in the range of $6.4 \text{ kJ/m}^2 \leq a_{cu} \leq 8 \text{ kJ/m}^2$ and therefore comparatively low. In contrast, the MFPs with barytes show higher values in the range of $10.6 \text{ kJ/m}^2 \leq a_{cu} \leq 14.2 \text{ kJ/m}^2$. Hence, a less brittle composite behaviour can be expected and barytes filled MFP should be favoured. In order to achieve a high degree of filling and appropriate material properties, the compound PP/T-Bx62 was selected for the production of positioning aids.

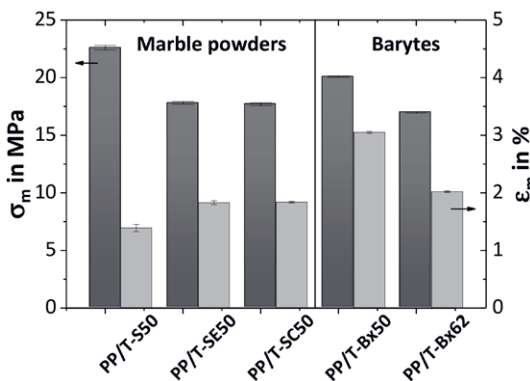


Figure 5: Influence of filler type and proportion on tensile strength σ_m and strain at tensile strength ϵ_m (mean values and standard deviations) | graphic: K. Mandel

4.2 Design and production processes

The different designs of the **Wo-PC** positioning aids considered are shown in Figure 6. In practice, they were produced with specially manufactured plastic tools. The production process was initially carried out by manual injection moulding (design (a)). Due to the difficulties encountered, such as inadequate mould filling and material leakage at undesired locations, the further development was switched to a transfer moulding process (designs (b) and (c)). The ring-shaped variants (a) and (b) should allow undisturbed concreting of the grid intersection and are free of undercuts. However, there was a lack of fixation of the grid and an extreme susceptibility to breakage of the Wo-PC elements. The probability of fracture, which is due to the brittle behaviour of the Wo-PC, can be reduced by using small and compact shapes, see variants (c) and (d). Small series of these positioning aids were produced in a partially automated process using a temperature-controlled PEEK mould. Variant (c) showed good performance characteristics, but required a tool with slides. The final design (d) can be produced with a slide-free tool and is also break-resistant due to its compact shape. Furthermore, it is possible to use this mould in an infiltration process for the production of Wo-PC elements.

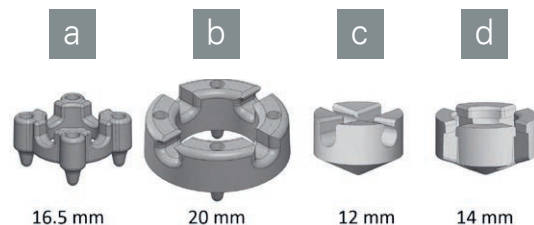


Figure 6: Mould designs for the Wo-PC positioning aids | graphic: H. Strobel, K. Mandel

The development of the mould designs of the MFP positioning aids is shown in Figure 7. 3D printed models enabled the evaluation and initial application tests of the design variants. After the last iteration, all defined criteria were met and the final design was established as shown in Figure 7, right image. A small series of 10,000 pieces of these positioning aids was produced by injection moulding on an Arburg 270 C with a double-cavity mould using the composite material PP/T-Bx62. The injection pressure was 650 bar at 250/500 bar holding pressure, the nozzle temperature 240 ± 10 °C and the cycle time 25 s.

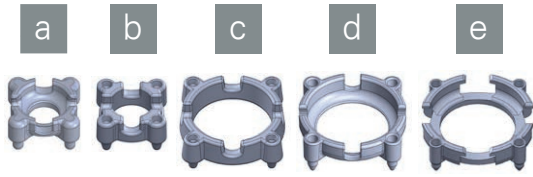


Figure 7: Selected design steps for the MFP positioning aids | graphic: H. Strobel, K. Mandel

A **comparison** of the developed positioning aids is shown in Table 3. Both the Wo-PC and the MFP positioning aids can be fixed to the textile grid via a snap mechanism, the shape is free of undercuts. The Wo-PC elements exhibit one point of contact to the concrete surface and a compact round shape in order to enable an even concrete flow. In contrast, the MFP elements exhibit four contact points and a large circular opening in the middle to allow for undisturbed concrete areas.

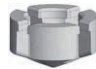

	Wo-PC	MFP
Image		
Outside dimension	Ø 14 mm	33 mm diagonal
Roving width	2-3 mm	6-8 mm
Concrete coverage	6.48 mm	5.8 mm
Production process	Infiltration	Injection moulding
Special advantage	Temperature resistance	Cost efficiency Flexibility

Table 3: Design and production features of the developed positioning aids

4.3 Integration behaviour

The developed positioning aids could be easily integrated into carbon concrete and showed good handling and fixing properties. The results of the strength tests are summarised in Table 4.

	f_{ct} in MPa	f_b in mm
Slab height 20 mm		
Wo-PC	11.7±2.0	20.1±1.7
Without positioning aids	9.9±0.3	20.0±3.5
Slab height 40 mm		
MFP	27.2±1.5	8.5±1.4
Without positioning aids	22.9±1.7	6.6±1.4

Table 4: Results of the 4BP tensile tests of the carbon concrete slabs

As expected, the thicker plates show higher strength values f_{ct} and lower deflection f_b than the thin plates. An increase in strength can be seen for both the Wo-PC and MFP variants, including positioning aids. Thus, the positioning aids seem to have a favourable influence on the load-bearing capacity of the concrete. Indeed, the differences are in the range of the standard deviation for Wo-PC. In contrast, the MFP concrete slabs show a significant increase in strength. This is probably due to the favourable combination of properties of the MFP, especially toughness, and the good adhesion to the concrete, which results from the high mineral filler content. Nevertheless, a larger number of samples should be tested for both variants to prove these tendencies.

Figure 8 shows sections of the optical deflection analysis with Aramis on typical 4PB samples shortly before the final failure. In addition to the absolute values of deflection, the analysis clarified the crack initiation points in the tensile zone of the samples and the crack deflection through the reinforcement grid.

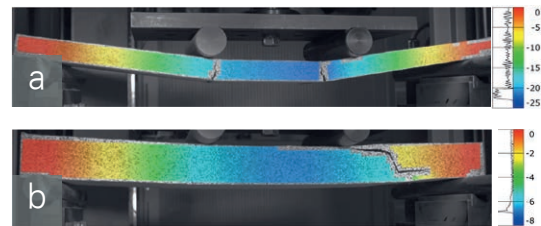


Figure 8: (a) Deflection in mm and failure of carbon concrete slabs with (a) Wo-PC and (b) MFP positioning aids in the 4PB tensile test | graphic: T. Albrecht, K. Mandel

With regard to the fracture behaviour, all Wo-PC positioning aids failed due to the break through the Wo-PC, see Figure 9 (a). The MFP elements failed due to a mixed fracture characterized by detachment from the concrete matrix and fracture through the positioning aids, see Figure 9 (b). Figure 10 shows photo-optical micrographs of the interface between positioning aids and concrete. The pictures illustrate that there is no gap between the two materials, which suggests good adhesion of the elements to the concrete. This is due to the comparatively rough surface on the one hand and the chemical and structural similarity of the materials on the other. While the Wo-PC is completely inorganic like concrete, the MFP is partly organic, but has a high mineral filler content and the coupling agent improves the adhesion.

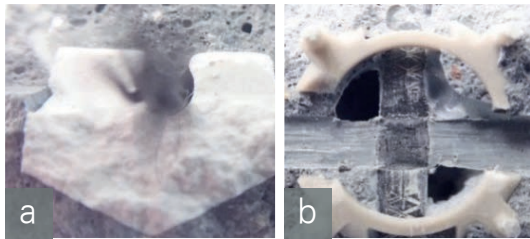


Figure 9: Positioning aids in carbon concrete after fracture (a) Wo-PC and (b) MFP | photos: K. Mandel

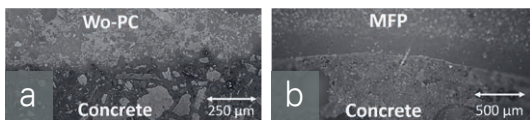


Figure 10: Photo-optical micrographs of the interfaces between concrete and (a) Wo-PC and (b) MFP | photos: K. Mandel

5 Conclusions

In this study, positioning aids made of two different materials were developed and examined in detail. For this purpose, an extensive construction development was carried out and the material as well as the application properties were comprehensively characterised. As a result, positioning aids made of Wo-PC as well as positioning aids made of MFP are now available with adapted properties for different applications.

6 Acknowledgements

This work was supported by the development fund provider AiF Projekt GmbH. Great thanks go to the Federal Ministry for Economic Affairs and Energy and also to the German Research Foundation. Special thanks go to the project partner HPF GmbH & Co. KG, who provided significant support for the development and production.

7 References

- [1] Curbach, M.; Michler, H.; Weiland, S.; Jesse, D.: Textilbewehrter Beton – Innovativ! Leicht! Formbar! Z. BetonWerk International. 11. (2008), Nr. 5, pp. 62-72.
- [2] Raupach, M.: Textile-reinforced concrete: Selected case studies. CM Cruz - Textile Fibre Composites in Civil Engineering, 2016 – Elsevier.
- [3] Zhou, F.; Liu, H.; Du, Y.; Liu, L.; Zhu, D.; Pan, W.: Uniaxial Tensile Behavior of Carbon Textile Reinforced Mortar. Materials 2019, 12, 374.
- [4] Scheerer, S.; Chudoba, R.; Garibaldi, M.P.; Curbach, M.: Shells Made of Textile Reinforced Concrete – Applications in Germany. Journal of the International Association for Shell and Spatial Structures, Vol. 58 (2017) No. 1 March n. 191, pp. 79-93(15).
- [5] Cibulka, T.; Musil, L.; Vodicka, J.: The Lightweight Textile Reinforced Concrete for Thin-walled Structures. Acta Polytechnica CTU Proceedings, 2019, Vol. 22, pp. 17-21.
- [6] Holschemacher, K.: Application of Textile Reinforced Concrete in Precast Concrete Industry. MS&E, 2020, Vol. 753, No. 4, p. 042086.
- [7] Gelbrich, S.: Funktionsintegrierte Leichtbaustrukturen für Tragwerke im Bauwesen. Universitätsverlag Chemnitz, Habilitation 2016, ISBN 978-3-96100-005-0.
- [8] Käseberg, S.; Holschemacher, K.; Mende, K.: Innovations in Construction of Carbon Concrete Composite Members. Structural Engineering, EASEC-15, Xi'an, China, 2017.
- [9] Mandel, K.; Funke, H.; Lindner, M.; Gelbrich, S.; Kroll, L.; Schwarz, T.: Recipe development of low-cost wollastonite-based phosphate cements. In: Forde, M. C. (Ed.): Construction and Building Materials. Vol. 189 (2018), pp. 86-94.

Strut-and-Tie Models for Carbon Reinforced Concrete Members

Jan Philip Schulze-Ardey, M.Sc.

Institute of Structural Concrete, RWTH Aachen University (IMB), Aachen, Germany

✉ jschulze@imb.rwth-aachen.de

Mr Schulze-Ardey is research assistant at IMB in the field of carbon reinforced concrete since two years.

Sven Bosbach, M.Sc.

Institute of Structural Concrete, RWTH Aachen University (IMB), Aachen, Germany

✉ sbosbach@imb.rwth-aachen.de

Mr Bosbach is research assistant at IMB in the field of carbon reinforced concrete since three years.

Dr.-Ing. Norbert Will

Institute of Structural Concrete, RWTH Aachen University (IMB), Aachen, Germany

✉ nwill@imb.rwth-aachen.de

Dr. Will is senior engineer at IMB since twenty years. He managed many carbon concrete research projects and is Convenor for committee "Nichtmetallische Bewehrung" from DAfStb.

Contact: jschulze@imb.rwth-aachen.de

1 Abstract

Due to the continuous development of the innovative composite material carbon reinforced concrete, the knowledge of design models in the ultimate limit state is of great importance. In this context, deficits have been identified especially in the subject of verification of discontinuity areas.

Hence, experimental investigations on nodes of deep beams of carbon reinforced concrete members were carried out and evaluated. The test results and first conclusions are presented in this paper.

Keywords: Strut-and-Tie-Models, CCT-Nodes, Carbon fibre reinforced polymer (CFRP), Experimental investigation, Discontinuity area.

2 Introduction

Experimental investigations presented in the paper are related to Strut-and-Tie-Models in carbon reinforced concrete members. The research findings were obtained in context of investigations from the research project C3-L6. In this context, deficits in knowledge have been identified especially in the subject of verification and design of discontinuity areas [1].

In general, Strut-and-Tie-Models have a great importance in the context of design equations in the ultimate limit state (e.g. shear design, punching, torsion) as well as generally for design of components with no continuous flow of forces in discontinuity areas (e.g. support area) [2].

3 Strut-and-Tie-Models

Structures can be divided into continuous and discontinuity areas. Areas with nonlinear strain distributions are known of discontinuity areas [2]. For these areas design models based on Strut-and-Tie-Models exist, whereby stress fields are combined

to resultant forces [2,3]. This simplification allows a simple design and has several advantages.

Strut-and-Tie-Models can be divided into three components: Compression struts, tension ties and nodes. These elements can be designed by different formulas. Steel reinforced concrete members can be designed by Eurocode 2 [3]. For compression struts, Eurocode 2 uses a reduction factor that depends on the crack formation [3]. Nodes are representing highly stressed areas and are divided into compression nodes (CCC), tension nodes (TTT) and combined nodes (CCT or CTT) [4,5]. The CCT node in context of investigations of anchorage behavior occurs in several structural elements. Results of anchorage failure without lateral stresses of carbon fibre polymer reinforcement exist so far [6,7].

In the CCT node stress peaks occur in the support area, whereby a complicated force flow occurs in the anchorage area due to the transverse pressure of the support [8,9]. Figure 1 shows a typical CCT-Node.

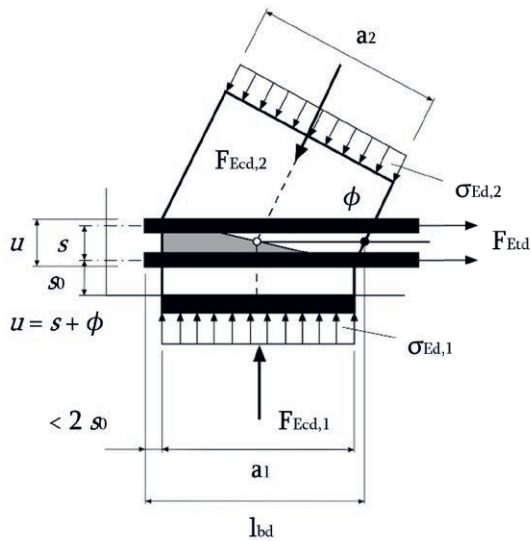


Figure 1: Example of a CCTNode | graphic: Schulze-Ardey

4 Experimental Investigation

Experimental investigations on ten test specimen are done to investigate the load-bearing behaviour of nodes of deep beams. The results of mentioned tests help to understand strut-and-tie models of carbon reinforced concrete members. Due to the chosen depth to length ratio, the test body can be characterized as a deep beam and therefore an investigation of discontinuity regions can be explored. There is no specific anchorage length prescribed by manufacturer for each specific concrete strength but it is known from other experimental investigations that the estimated anchorage length is bigger than the available anchorage length in the experimental test described in this paper.

4.1 Test Setup

4.1.1 Test Program

The ten test specimens with identical dimensions (height/length/width: 30 cm / 60 cm / 10 cm) differ in the number of reinforcement bars and in the reinforcement material. Five test specimens are concrete members reinforced by Thyssen Krupp Carbon4ReBAR carbon fibre polymer bars $\varnothing_{\text{core}}$ 8,5 mm. Five test specimens are reinforced by steel bars \varnothing 14 mm (B500) reinforcement for comparison. The test matrix of the test specimens V1-V10 is shown in Table 1.

Test [-]	Bar material [-]	No. of Bars [-]	Bar- \varnothing [mm]
V1-V3	Steel	1	14
V4-V5	Steel	2	14
V6-V8	Carbon	1	8,5
V9-V10	Carbon	2	8,5

Table 1: Test Program

4.1.2 Test Setup and Measuring Systems

Each test specimen is a simple span deep beam with a span length of 55 cm. The two supports are given by roller bearings with steel plates (50 mm x 100 mm). An image of a test specimen is shown in Figure 2.



Figure 2: Image of test setup | photo: Schulze-Ardey

The load is transmitted by a steel plate (100 mm x 100 mm) on the top of the test specimen and the test load is applied in the middle of the beam by a single force through a deformation-controlled servo-hydraulic cylinder. In addition to the load from the cylinder, the deflection in the middle of the field and the slip of the reinforcement bars are measured with linear variable displacement transformers (LVDT). The slip is measured on the projection of the reinforcement bar against the head side of the concrete specimen. Each reinforcement bar has a vertical concrete cover of 30 mm.

The schematic test setup and the position of the reinforcement bars are shown in Figure 3.

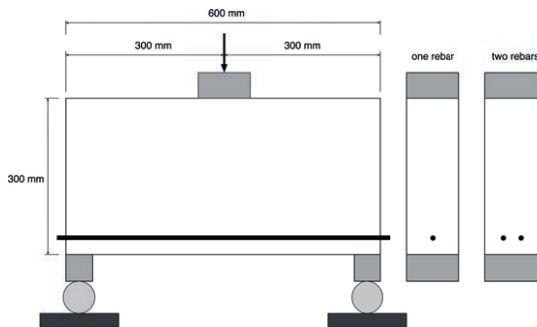


Figure 3: Dimension of specimens | graphic: Schulze-Ardey

4.2 Materials

According to the manufacturer the carbon fibre reinforced polymer bars Thyssen Krupp Carbon4ReBar have a maximum tensile strength of 1650 N/mm² [10]. Carbon bars are shown in Figure 4.



Figure 4: Carbon reinforcement bar | photo: Schulze-Ardey

Each test specimen uses the same concrete mix. The concrete mix has a ratio of water to cement (CEM I 32,5 R) of $w/z = 0.4$ with a maximum grain size of 8 mm. All test specimen as well as the concrete material samples were stored in a dry place at room temperature (20 °C). The material properties of concrete on the day of testing is shown in Table 2.

Test [-]	$f_{ct,flexural}$ [MPa]	$f_{cm,cube}$ [MPa]	E_{cm} [MPa]
V1-V5	8,2	47,7	29.200
V6-V10	7,9	46,2	29.100

Table 2: Concrete Strength and Stiffness

4.3 Test Results

To illustrate the connection between forces and slip only the larger slip of one head side of test body is presented in this chapter (2 bars: mean value of slip of two bars on one head side).

The number of bars and the maximum load as well as the maximum slip at maximum load level for V1-V5 (steel bars) are shown below.

Test [-]	F_{max} [kN]	No. of Bars [-]	Slip at F_{max} [mm]
V1	97,7	1	0,36
V2	114,6	1	0,37
V3	92,9	1	0,01
V4	187,2	2	0,37
V5	189,9	2	0,33

Table 3: Test Results V1-V5 (steel bars)

The maximum load, slip value at maximum load and number of carbon bars are shown in Table 4.

Test [-]	F_{max} [kN]	No. of Bars [-]	Slip at F_{max} [mm]
V6	71,8	1	0,00
V7	62,2	1	0,01
V8	88,0	1	0,08
V9	121,3	2	0,02
V10	97,9	2	0,47

Table 4: Test Results V6-V10 (carbon bars)

The ratio of mean values of maximum loads between tests with two and those with one bar is higher for steel bars (185%) as for carbon bars (148%). The standard deviation of tests with carbon bars is higher than for tests with steel bars.

The force-slip relationship of the steel reinforcement of V1-V5 is shown in Figure 5, the relationships of the carbon reinforced members are shown in Figure 6.

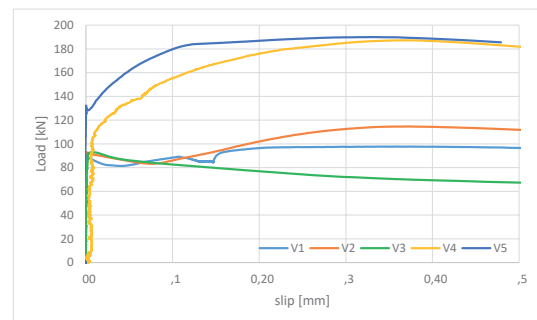


Figure 5: Force-slip relationship of V1-V5 | graphic: Schulze-Ardey

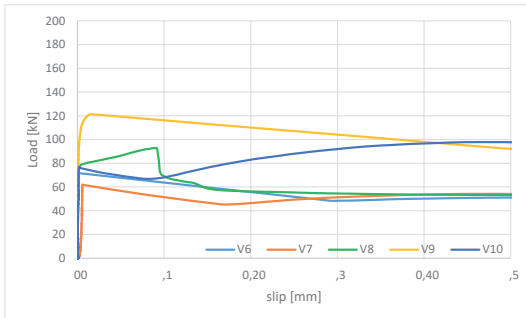


Figure 6: Force-slip relationship of V6-V10 | graphic: Schulze-Ardey

It can be observed that all test specimens have a diagonal crack through the test specimen on at least one side. An exemplary image of a crack pattern is shown in Figure 7.

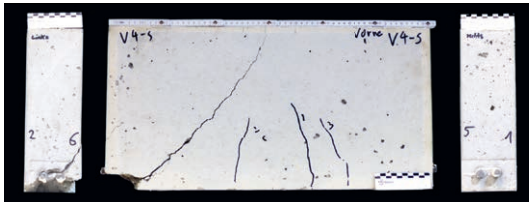


Figure 7: Image of crack pattern from side and head side view of V4 (steel bars) | photo: Schulze-Ardey

4.4 Discussion

The goal of the experimental investigations is a comparison between concrete members with steel and those with carbon fibre reinforced polymer reinforcement depending on number of reinforcement bars.

The maximum load in each type of reinforcement material exceeds for 2 bars the values of the tests with one bar. Therefore, it can be assumed that there is a connection between the reinforcement ratio and the maximum force.

Based on the force-slip-relationship it can be seen that the behavior of steel reinforced specimen with two bars differ from the behavior of those with 1 steel rebar. The increase of the slip in the tests with two steel bars differ from the force-slip-curves of tests with one bar where the load also decreases between a slip of 0 mm - 0.1 mm.

The force-slip-curves of the test with carbon reinforcement with one and two rebars don't show a difference in the form of the force-slip-relationship in comparison to the tests with steel bars. Due to the higher force and the different force-slip-relationship it can be assumed that the tests show the influence of dowelling effect of the

rebars. It seems that the effect of dowelling in steel reinforcement is greater in specimens with steel bars than with carbon bars.

Due to the fact that no reinforcement bar in each test specimen is broken during the tests a tie failure can be excluded. In each test specimen at least one diagonal shear crack as well as vertical or horizontal cracks above the support of one head side occurred (see Figure 7). It can be concluded that large lateral stresses are present in the compression strut as well as in the CCT node of the test specimen. Relating to the cracking pattern of the test specimens and the slippage of bars a combined strut and anchorage failure can be assumed.


Based on to the different effect of dowelling action of steel bars in comparison to carbon bars, the theory of strut-and-tie models cannot simply be adopted to design carbon concrete members without any modifications with current design equations.

Due to the fact that the force doesn't decrease suddenly to zero after reaching the maximum bearing capacity and that the measured slip value was higher than 0.4 mm it can be assumed that in the tests with steel reinforcement as well as in the tests with carbon bars a combined concrete and anchorage failure mode occurred.

5 Conclusions and Acknowledgements

So far there is a deficit of knowledge in the field of Strut-and-Tie-Models of carbon reinforced concrete. In this paper the main results of experimental investigations on deep beams are presented. On the one hand, a comparison is made between reinforcement of carbon bars and conventional steel reinforcement and, on the other hand, the difference in load transfer due to different number of bars has been investigated.

It is not yet possible to derive a design model from the tests, but the work provides a first step in the design of discontinuity areas in carbon reinforced concrete construction and delivers initial results. For an investigation of all components (tension strut, compression strut and nodes) further experimental tests are necessary to develop a design model.



In the future, the load-bearing behavior in detail should be analyzed with more tests and in further work the failure of tension strut, compression strut and nodes should also be investigated in general.

The authors would like to thank the Federal Ministry of Education and Research (BMBF) for funding the project C³-V-L6 "Bemessung und bauliche Durchbildung" within the research program "C³-Carbon Concrete Composite" Nr 03ZZ0336A.

6 References

- [1] J. Schulze-Ardey, S. Bosbach, „Bemessung und bauliche Durchbildung von Carbonbeton“. Tagungsband der 11. Carbon- und Textilbetontage: S. 110-111, 2019.
- [2] K. Zilch, G. Zehetmaier, „Bemessung im konstruktiven Betonbau“. Springer Verlag (2009).
- [3] Eurocode 2, "Design of concrete structures – Part 1-1: General rules and rules for buildings; German version EN 1992-1-1:2004 + AC:2010". European Committee for Standardization, Brussels, Belgium, 2011.
- [4] M. Thompson et al, "CCT Nodes Anchored by Headed Bars-Part 1: Behavior of Nodes", ACI Journal (Title No 102-S81), 2005.
- [5] J. Jirsa, J. Breen, K. Bergmeister, "Experimental studies of nodes in strut-and-tie models", IABSE report, Issue 62, 1991.
- [6] J. Bielak, A. Spelter, N. Will, M. Claßen, „Verankerungsverhalten textiler Bewehrungen in dünnen Betonbauteilen“. Beton- und Stahlbetonbau 113 (7), 2018.
- [7] A. Schumann, M. May, M. Curbach, „Carbonstäbe im Bauwesen“. Beton- und Stahlbetonbau 113 (7), 2018.
- [8] W. Schlaich, K. Schäfer, „Konstruieren im Stahlbetonbau“, Betonkalender, 2001.
- [9] W. Sundermann, K. Schäfer, „Tragfähigkeit von Druckstreben und Knoten in D-Bereichen“, Deutscher Ausschuss für Stahlbeton Heft 478, Beuth Verlag GmbH, Berlin, 1997.
- [10] www.thyssenkrupp-carbon-components.com (abgerufen am 27.05.2020)

Tenax[®] CARBONFASERN DARAUF BAUT DIE ZUKUNFT

Parkhaus Hirschberg
© GOLDBECK GmbH

Leicht, stabil, dünn – eben ein echter Hightech-Werkstoff. Carbonfasern von Teijin werden in innovativen Bauprojekten eingesetzt, sowohl bei aufwändigen Sanierungen als auch für zukunftsweisende Neubauprojekte. Teijin Carbon Europe ist weltweiter Marktführer für Carbonfaserprodukte im Bauwesen und produziert als einziger Hersteller seit über 30 Jahren in Deutschland. Wirtschaftlich und nachhaltig entwickelt Teijin gemeinsam mit seinen Kunden Projekte für eine lebenswerte Zukunft!



Hyparschale Magdeburg
© Wilhelm Kneitz Solutions in Textile GmbH



Fußbodensanierung
© Hitexbau



Altenzentrum Neuer Gehren
© solidian GmbH



Bond behavior of carbon rebars and concrete

Alexander Schumann

Dipl.-Ing., CARBOCON GmbH, Dresden, Germany

✉ schumann@carbocon-gmbh.de

Is managing director of CARBOCON GmbH. Before that, he was research assistant and research group leader of the group “carbon reinforcement concrete for strengthening” at the Institute of Concrete Structures (TU Dresden)

Frank Schladitz

Dr.-Ing., Technische Universität Dresden, Institute of Concrete Structures Dresden, Germany

✉ frank.schladitz@tu-dresden.de

Schladitz is research group leader at the Institute of Concrete Structures at the Technical University of Dresden and representative of the board of the C³ - Carbon Concrete Composite e.V.

Manfred Curbach

Prof. Dr.-Ing Dr.-Ing. E. h., Technische Universität Dresden, Institute of Concrete Structures Dresden, Germany

✉ manfred.curbach@tu-dresden.de

Manfred Curbach is head of the Institute of Concrete Structures at the TU Dresden. He has been dealing with carbon reinforced concrete as a material for over 20 years.

Contact: schumann@carbocon-gmbh.de

1 Abstract

The material carbon reinforced concrete finds more and more acceptance in construction. Comprehensive research results are at hand already for the use of carbon reinforcements in the form of mats concerning their tensile and bond behavior. However, many research activities are still urgently required regarding the use of carbon rebars, particularly in view of the bond behavior of the bars in concrete. For this reason, different carbon rebars with varying surface profiles have been tested in a number of experimental tests for their bond behavior. The influence of the concrete strength on the bond behavior was additionally tested at a preferred rebar.

Keywords: carbon rebars, bond behavior, carbon reinforced concrete

2 Introduction

The material carbon reinforced concrete has experienced an astonishing development. Carbon reinforced concrete has become more than an alternative to traditional steel-reinforced concrete. In particular, comprehensive research results and practice projects have been made for the use of carbon mats, e.g. [1]. However, this statement does regrettably not apply to components reinforced by carbon rebars. Although there are a few publications in hand concerning the tensile strength of carbon rebars, e.g. [2], or about carbon-concrete components with mixed reinforcement (carbon rebars and mats), e.g. [3]-[5], but no sufficient knowledge has been obtained regarding the general bond behavior between the rebars and the concrete. For safe and efficient designing, calculation and dimensioning however, the bond behavior and its influencing factors must be known.

For this reason, experimental bond tests have been made for carbon rebars with varying surface profiles in concrete, as described in the following. The influence of the concrete strength on the bond behavior was additionally tested for a selected preferred rebar.

3 Materials used

The materials used in the experimental tests are described below. For more details, please refer to [6]-[9].

3.1 Carbon rebars and steel rebar

Eight different carbon bars (fig. 1) and a conventional steel bar (fig. 2) were used as reinforcing bars. The carbon bars used were made of differed source materials, in particular their impregnation, and had varying surface profiles.



Figure 1: Used carbon rebars | graphic: Alexander Schumann



Figure 2: Used steel rebar (rebar 9) | graphic: Alexander Schumann

3.2 Concretes

In the first test series (touch test series), a high-strength concrete developed in the C³ project, maximum grain size 5 mm and compressive strengths >90 N/mm², was applied. For further details to the concrete used, please refer to [7].

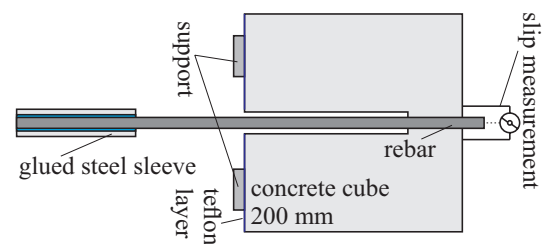
To investigate the influence of the concrete strength on the bond behavior, two normal-strength concretes (NC 1 und NC 2) and an ultra-high strength concrete (UHPC) were applied in addition to the high-strength concrete (HC). The mixture formulations of the regarding concretes are given in [9].

3.3 Test setup

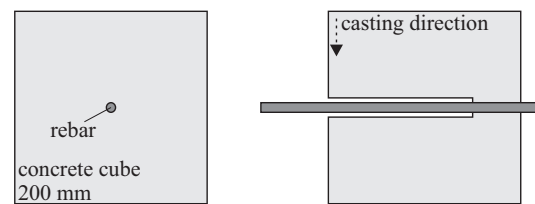
The tests were prepared in the Otto-Mohr-Laboratory of the Technische Universität Dresden. Two different test specimens were used for the touch test series. Fig. 3 b) shows the specimen defined as standard for the touch test series. It was used for almost all tests. Just for the investigation of the bond behavior of rebar configuration 6, the smaller specimen showed in figure 3 c) had to be applied, caused by the length of the carbon rebar, which was limited because of production reasons. Furthermore, when compared to specimen 1, the bond zone had to be positioned in the center of specimen 2, because of technological manufacturing aspects for this geometry.

In the second test series, the specimen shown in figure 3 d) was generally applied.

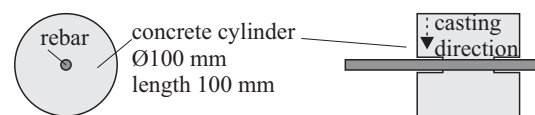
In all tests, the bond length uniformly corresponded to the five-fold of the rebar diameter ($5 d_v$). Only in the test series using the steel rebar, the bond length had to be reduced to $2 d_v$ to avoid any yielding of the steel rebar in the bonding test, as high-strength concrete was used in it. To introduce the test force into the carbon rebar without damaging the bar, steel sleeves were glued to the end of the carbon rebars, see figure 3.



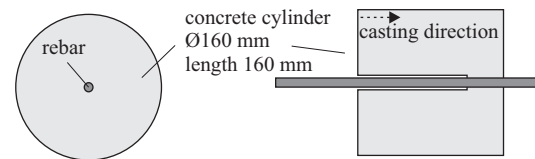
a) Test setup



b) Specimen 1



c) Specimen 2



d) Specimen 3

Figure 3: Used test setup and specimens | graphic: Alexander Schumann

In test series 1 (touch tests), the bond test specimens were fabricated in recumbent position, and in test series 2 in upright position. After manufacture, the specimens remained covered in their shuttering for three days. Afterwards the specimens were stripped and stored at room temperature and 65% relative humidity under a plastic membrane until the date of the test. In the touch test series, the tests were made after approx. 14

days, and in the test series 2 after approx. 28 days. During the execution of the tests, the slip of the rebar at the unloaded bar end and also the tool path and the test force were permanently measured. The force was applied deformation-controlled at a test speed of 0.01 mm/sec.

For each test series, three concrete prisms of the dimensions 40 x 40 x 160 mm³ were additionally fabricated in accordance with DIN EN 196-1 [10], and tested on the bond testing date to determine the bending tensile strength and the compressive strength. Deviating from DIN EN 196-1 [10], the prisms were stored analogously to the bond test specimens.

4 Results of the touch test series

The individual test series for the different rebar variants have been evaluated and compared by means of the bond-stress–slip ratio. For traceability reasons, table 1 shows a list of all relevant parameters.

A rebar configuration to be applied for further bond investigations shall be determined by means of the tests made. To determine a preferred variant, fig. 5 shows a comparison of the mean value curves of the regarding rebar variants.

It can be seen from figure 4 that the transferable bond stresses significantly depend on the surface profile. It is further shown that the steel rebar (rebar configuration 9) reaches the highest bond stresses. Additionally, the steel rebar has the highest bond rigidity, best demonstrated in fig. 4 b). Based on the experimental bond tests, it can be further stated that rebar configuration 7 (profiling by milling) can transfer maximum bond stresses, reaching the ones of the steel rebar. Concerning the comparison of the two variants, it has to be mentioned that the bond tests with the steel rebar had to be carried out with a bond length of 2 d_v to avoid any yielding of the reinforcement; whereas all carbon rebars had a bond length of 5 d_v; indicating that the bond stresses at the steel

Term	Rebar	l _b m	d _v mm	A d	τ _{max} MPa	s _{o,max} mm	f _{cm} MPa	f _{ctm,fl} MPa
V-1-1	1	40	8	10	4.3	0.2	107.3	10.4
V-1-2	1	40	8	10	4.3	0.3	107.3	10.4
V-2-1	2	40	8	14	8.1	0.2	108.2	11.2
V-2-2	2	40	8	14	6.9	0.2	108.2	11.2
V-2-3	2	40	8	14	10.7	0.3	108.2	11.2
V-3-1	3	45	9	11	6.0	10.9	108.7	10.0
V-3-2	3	45	9	11	7.4	10.8	108.7	10.0
V-3-3	3	45	9	11	5.8	5.7	108.7	10.0
V-4-1	4	30	6	12	20.0	5.7	112.4	9.8
V-4-2	4	30	6	12	21.5	4.2	112.4	9.8
V-4-3	4	30	6	12	19.9	10.2	112.4	9.8
V-4-4	4	40	8	12	21.2	6.1	112.4	9.8
V-4-5	4	40	8	12	21.1	5.3	112.4	9.8
V-4-6	4	40	8	12	21.2	6.7	112.4	9.8
V-5-1	5	30	6	11	21.5	6.5	108.7	10.0
V-5-2	5	30	6	11	28.9	2.6	108.7	10.0
V-6-1	6	50	10	12	29.1	1.1	112.4	9.8
V-6-2	6	50	10	12	26.8	1.4	112.4	9.8
V-6-3	6	50	10	12	28.9	0.9	112.4	9.8
V-7-1	7	40	8	13	36.0	0.5	115.0	10.1
V-7-2	7	40	8	13	38.1	0.6	115.0	10.1
V-8-1	8	46	9.3	12	11.7	2.3	111.5	9.9
V-8-2	8	46	9.3	12	11.0	1.7	111.5	9.9
V-8-3	8	46	9.3	12	11.2	1.8	111.5	9.9
V-9-1	9	20	10	11	38.0	0.3	108.7	10.0
V-9-2	9	20	10	11	40.1	0.4	108.7	10.0
V-9-3	9	20	10	11	40.0	0.3	108.7	10.0

l_b ... bond length; A ... specimen age at test day; τ_{max} ... max. bond strength

s_{o,max} ... slip at τ_{max}

f_{cm} ... mean compression strength tested at prism

f_{ctm,fl} ... mean flexural tensing strength tested at prism

Table 1: Results of Serie 1:

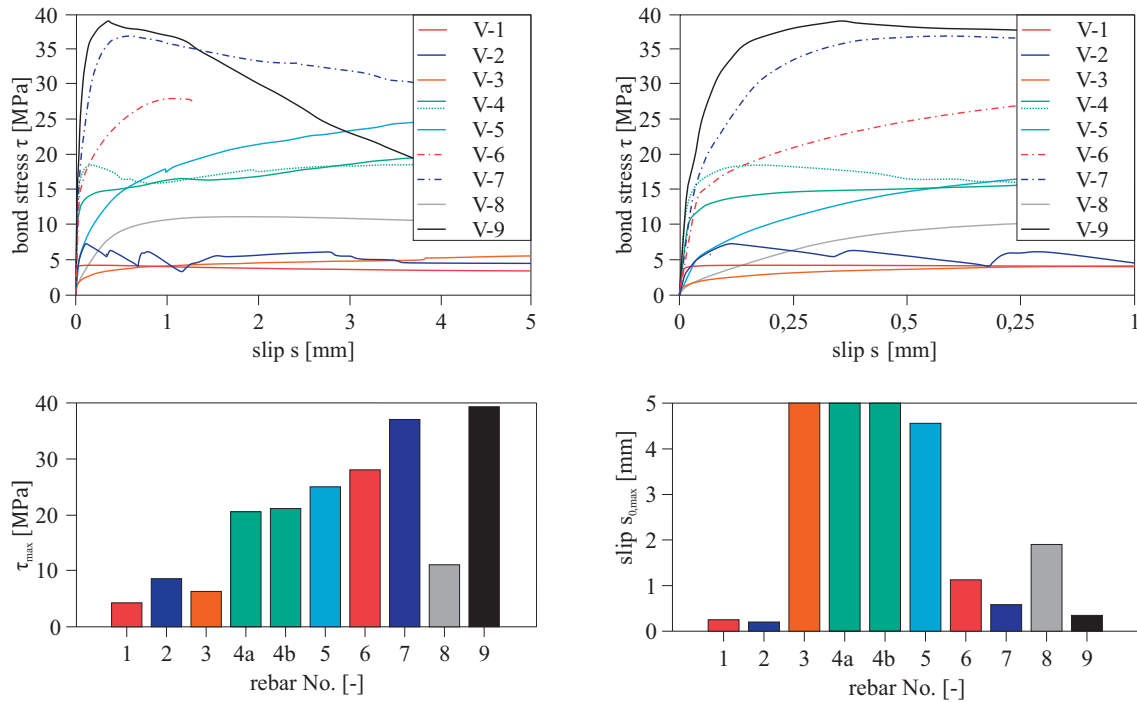


Figure 4: Results of series 1 | graphic: Alexander Schumann

rebar of $2 d_v$ are overestimated in comparison to $5 d_v$. Thus, when applying the formulae of [11], this results in a decrease of approx. 15% for the conversion of the bond values from $2 d_s$ to $5 d_s$, so that the maximum bond stresses of rebar configurations 7 and 6 are already in the range of the steel rebar or even above. As in construction, the bond rigidity and thus also the slip development are of essential importance, fig. 4 d) additionally shows the slip values $s_{0,max}$ related to the maximum bond stress τ_{max} . Because the maximum bond stresses in some rebar configurations occur at slip values of higher than 5 mm only, and these ranges are of minor importance in construction, the x axis of the diagram has been limited to the value of 5 mm for simplified presentation. Based on figure 5 d), it can be concluded that all rebar configurations that have a distinct form closure or no profiling at all (smooth bar, rebar configuration 1) reach maximum bond stresses below the slip value of 1 mm, indicating good bond rigidity. For the other rebar variants, the bond stresses rise continuously with increasing slip value up to the maximum bond stress at a very large slip $s_{0,max}$. For in contrast to the rebars with a high bond rigidity, the rebars with a low bond rigidity do not show a distinct form closure, with the result that the failure of these carbon rebars in the bond test happens successively and finally at high slip values only.

Further evaluations for finding a preferred variant are given in [9]. Here, end anchoring lengths and derived from them mean bond stresses were calculated for each rebar configuration by applying gradual integration on the basis of the experiments. Based on this and on fig. 4, the rebar configuration 7 (fig. 5) was determined as preferred variant for further bond tests.



Figure 5: Selected preferred variant | photo: Alexander Schumann

5 Results of test series 2

The influence of the concrete strength on the bond behavior was studied in the second test series. Four different concretes were used for this purpose, which shall cover a possible application range of the carbon rebars. For this reason, concrete No. 1 (NC 1) should purposefully have low strengths, as it can be considered as the lower limit, and concrete No. 4 (UHPC) should have extremely high strengths to represent a possible upper limit. Below, the two other concretes (NC 2 and HC) should reflect the strength ranges in between. In the following, the obtained bond re-

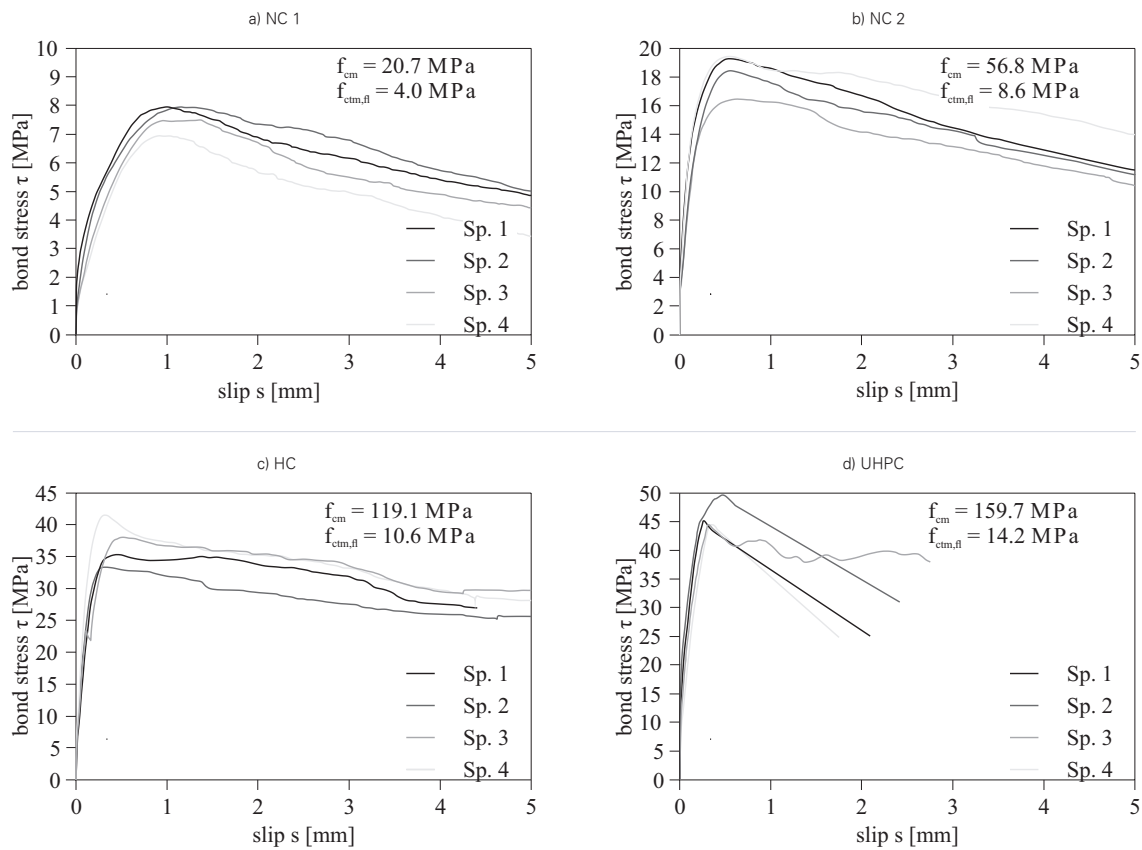


Figure 6: Bond-strain-slip relations for different concrete strengths | graphic: Alexander Schumann

sults in dependence on the concrete strength are shown and compared to each other.

Figure 6 a) - d) shows the bond-strain-slip curves for the different concretes. The diagrams additionally contain the mean values of the bending tensile and compressive strength tests obtained at the mortar prism after approx. 28 days.

As can be seen from the diagrams, the maximum bond stresses rise with increasing concrete strength. For example, the test series with the lowest concrete strength (NC 1, fig. 6 a)) shows the lowest bond stresses, and the test series with the highest concrete strength (UHPC, see fig. 6 d)) the highest maximum bond stresses. In the test series with the normal-strength and high-strength concretes (NC 1, NC 2 and HC), the failure was marked by the extraction of the carbon rebar from the specimen. When UHPC was used, the specimen was split after the maximum bond stress had been exceeded (see fig. 7), as can be seen from the steep drop in the bond-stress-slip curve in fig. 6 d) As the splitting happened after the maximum bond stress was exceeded only, the values can be used for the comparisons given below. After the tests had been made, the specimens of all series

were split to measure the real bond length and to determine the failure mechanism. Fig. 8 shows pictures of the failures after the end of the tests.

In this connection, it could be stated that the failure in concrete 1 (NC 1) was caused by a complete shearing of the concrete consoles between the FRP ribs (see fig. 8 b)).



Figure 7: Splitting failure at UHPC | photos: Frank Schladitz

But fig. 8 a) also shows that some slight traces of scratching from the carbon rebar can be seen at the concrete. With rising strength, the failure changes from a pure shearing of the concrete consoles to a combined failure, a shearing of the concrete consoles and a shearing of the FRP profiles. This is shown in fig. 8 c) - d) and 8 e) - f) by the larger carbon residuals at the concrete. In the test series with UHPC, the failure is clearly characterized by a full-surface shearing of the FRP profiles from the carbon rebar (see fig. 8 g) and h)).

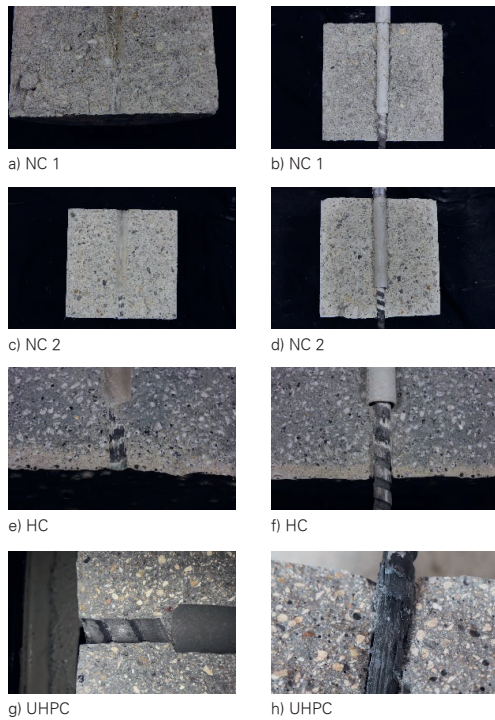


Figure 8: Failure mechanisms in dependence on the concrete strength; 1st line: NF, 2nd line: NF 2; 3rd line: HF; 4th line: UHPC | photos: Alexander Schumann

Caused by the complete shearing of the FRP profiling from the rebar core when applying UHPC, the splitting of the specimen can be traced back to the high bond stresses, on the one hand, and on the famous „wedging effect“, which happens only in the case of a complete shearing of the FRP reinforcement.

Figure 9 a) shows the mean value curves of the bond-stress–slip relations obtained in the different series. Analogously to steel-reinforced construction, the carbon rebars develop higher bond values and a more rigid bond behavior with increasing concrete strength. For better comparability of the test results, the curves in fig. 9 b) and c) are related to the mean concrete compressive strength f_{cm} and the bending tensile strength $f_{ctm,fl}$.

The bond curves related to the concrete compressive strength show similar values, with decreasing maximum related bond stresses at increasing concrete compressive strength. In contrast to that, no definite dependence can be seen for the related bond stresses with regard to the bending tensile strength (see fig. 9 c)). These findings can be substantiated by fig. 9 d) and e).

As shown in fig. 9 d), an almost linear connection between the maximum bond stress and the concrete compressive strength can be proven for the reference rebar up to the compressive strength of approx. 160 N/mm² tested in this study. When a quadratic regression function is applied instead of the linear connection, the influence of the concrete compressive strength on the maximum bond stresses can be described more exactly, as the maximum bond values proportionally decrease at high concrete strengths. When the maximum bond stresses are applied in relation to the tensile strength of the concrete (see fig. 9 e)), no clear tendency can be derived from the test results. To characterize the bond rigidity in dependence on the concrete strength, fig. 9 f) includes the slip values $s_{u,max}$ related to the maximum bond stress. It can be seen that the slip values $s_{u,max}$ decrease with increasing concrete strength, caused by the higher bond rigidity at a higher concrete compressive strength. Fig. 9 g) and h) additionally show the bond stresses at a slip of 0.1 mm ($\tau_{0,1}$) and 0.2 mm ($\tau_{0,2}$) in relation to the compressive strength and the bending tensile strength of the concrete. They can be applied to prove the statements made above that the description of the influence between the concrete compressive strength and the bond behavior leads to more conclusive results, as there is an almost linear relation between the concrete strength and the bond values $\tau_{0,1}$ and $\tau_{0,2}$.

6 Discussion, conclusions and acknowledgements

In this study, several carbon rebars with different surface profiles were tested for their bond behavior in concrete. By means of the first test series (touch tests), it could be proven that the surface profiling has a significant influence on the bond behavior and the maximum transferable bond stresses. In conclusion of the test results, the milled carbon rebar was chosen as the preferred variant for further bond investigations. In a second test series with the milled rebar, the influence of the concrete strength on the bond behavior was studied. It was found that, for this carbon rebar, the concrete strength has a significant influence on the maximum bond stresses and the bond rigidity. It was further stated that the concrete strength at the carbon rebar also has an influence on the form of the failure. With low-strength concretes, the concrete consoles between the

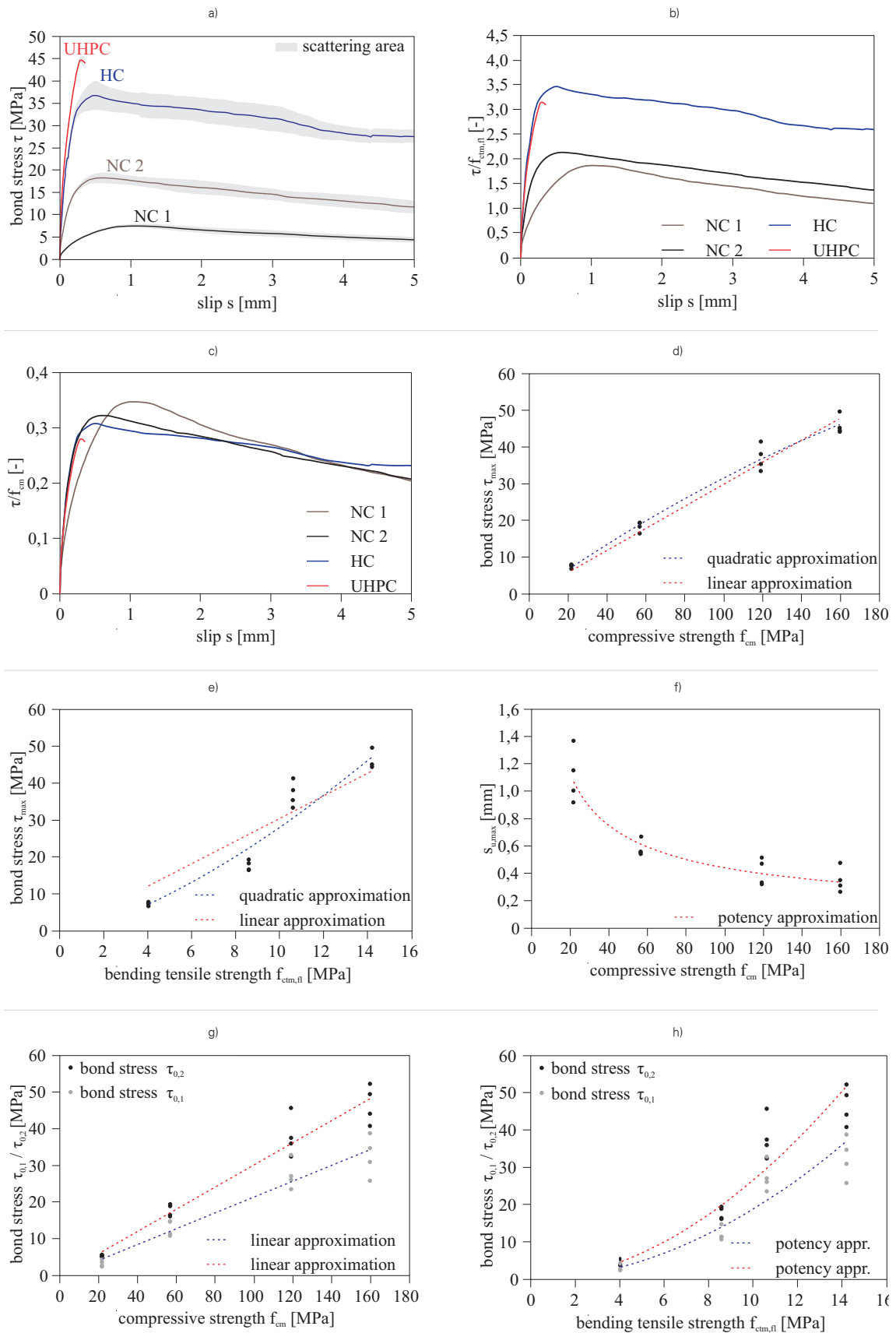


Figure 9: Comparison of the test results | graphic: Alexander Schumann

carbon ribs were sheared off, whereas the carbon ribs were completely destroyed when UHPC was used. In the range between the failure forms, mixed failures occur, a partial destroy of the carbon ribs and a shearing of the concrete consoles. The results obtained show that for the carbon rebar the maximum bond stresses increase with increasing concrete strength, as it is known from steel-reinforced concrete. Therefore the findings obtained are transferable, when sufficient data quantities are at hand.

Based on these results it is intended to study further factors of influence on the bond behavior, including the rebar batch, the bond length and the maximum grain size as well as the composition of the concrete. The results shall be used to develop a number of approaches for the description of the influence factors, to describe the bond behavior of structural components made of carbon concrete in greater detail.

7 References

- [1] Schütze, E.; Bielak, J.; Scheerer, S.; Hegger, J.; Curbach, M.: Einaxialer Zugversuch für den Carbonbeton mit textiler Bewehrung. *Beton- und Stahlbetonbau*. 2018;113, Vol. 1:33-47.
- [2] May, M.; Riegelmann, P.; Schumann, A.; Curbach, M.: Carbonstäbe im Bauwesen – Teil 3: Bestimmung der Zugtragfähigkeit. *Beton- und Stahlbetonbau*, submitted. 2020.
- [3] Schmidt, A.; Bielak, J.; Hegger, J.: Large-Scale Tests on the Structural and Deformation Behaviour of I-Beams with Carbon Reinforcement. In.: *International Institute for FRP in Construction (FRPRCS-14)*, Belfast 2019.
- [4] Schumann, A.; May, S.; Curbach, M.: Design and Testing of various Ceiling Elements made of Carbon Reinforced Concrete. *Proceedings (2018)*, Vol. 2:1-6.
- [5] Kromoser, B.; Preinstorfer, P.; Kollegger, J.: Building lightweight structures with carbon-fiber-reinforced polymer-reinforced ultra-high-performance concrete: Research approach, construction materials, and conceptual design of three building components. *Structural Concrete* 20 (2018), Vol. 2:730-744.
- [6] Schumann, A.; May, M.; Schladitz, F.; Curbach, M.: Carbonstäbe im Bauwesen. Teil 2: Verbundverhalten – Verbundversuche an unterschiedlichen Carbonstäben. *Beton- und Stahlbetonbau*. Submitted. 2020.
- [7] Schneider, K.; Butler, M.; Mechtcherine, V.: Carbon Concrete Composites C3 – Nachhaltige Bindemittel und Betone für die Zukunft. *Beton- und Stahlbetonbau* 112 (2017), Vol. 12.
- [8] Böhm, R.; Thieme, M.; Wohlfahrt, D.; Wolz, S. S. J.; Richter, B.; Jäger, H.: Reinforcement Systems for Carbon Concrete Composites Based on Low-Cost Carbon Fibers. *Fiber* 6 (3) (2018), Vol. 56:1-21.
- [9] Schumann, A.: Experimentelle Untersuchungen des Verbundverhaltens von Carbonstäben in Betonmatrices. TU Dresden, Dissertation. Submitted 2020.
- [10] DIN EN 196-1:2016-11: Prüfverfahren für Zement – Teil 1: Bestimmung der Festigkeit; Deutsche Fassung EN 196-1:2016. 2016.
- [11] Ritter, L.: Der Einfluss von Querkzug auf den Verbund zwischen Beton und Stahl. Technische Universität Dresden, Diss., 2014.

What can we learn from sustainability assessment: the case of carbon concrete composite structures

Christoph Scope

Technische Universitaet Dresden,
Dresden, Germany
✉ christoph.scope@tu-dresden.de
Researcher at TU Dresden with focus on life cycle based decision-making and sustainability assessments

Julia Schütz

LCEE Life Cycle Engineering Experts GmbH,
Darmstadt, Germany
✉ j.schuetz@lcee.de
Project engineer at LCEE GmbH with expertise on sustainable buildings and life cycle assessment (LCA)

Torsten Mielecke

LCEE Life Cycle Engineering Experts GmbH,
Darmstadt, Germany
✉ t.mielecke@lcee.de
Director at LCEE GmbH with expertise on sustainable buildings, DGNB certification, and LCA

Contact: christoph.scope@tu-dresden.de

Eric Mündecke

Ingenierbüro Grassl GmbH, Berlin, Germany
✉ emuendecke@grassl-ing.de
Senior project engineer at Grassl GmbH with expertise on structural design and implementation planning

Konstantin Schultze

Ingenierbüro Grassl GmbH, Berlin, Germany
✉ ksultze@grassl-ing.de
Project engineer at Grassl GmbH with expertise on structural design and BIM

Peter Saling

BASF S.E., Ludwigshafen, Germany
✉ peter.saling@basf.com
Director Sustainability Methods at BASF S.E. with expertise on sustainability assessments, LCA, standardization, and CSR

1 Abstract

Sustainable construction plays a significant role for minimizing negative effects on planetary boundaries. New materials like carbon concrete composites (CCC) may offer options of integral design or remedial maintenance to improve SDGs #9 to #13. For the built sector, a variety of approaches to sustainability assessments exists thanks to intensive research, building certificates, international standards, and stakeholder pressure. We conceptualized a sustainability assessment framework and applied it to variants of prefabricated wall systems made of CCC. Preliminary results signal current hotspots in material and technology choices along the entire value chain to initiate suitable iterative redesign strategies.

Keywords: Sustainability assessment, Life cycle assessment, Life cycle costing, Carbon concrete composite, Cement-based composite, Textile reinforced concrete, Sandwich wall

2 Introduction

The European construction industry including buildings contribute to 9 percent in European Union's GDP [1], but is also held accountable for 90 percent of used mineral resources, 40 percent of consumed primary energy, and 35 percent carbon emissions [2]. A dedicated pathway to sustainable construction, built materials, and design is thus essential to diminish negative effects on the nine planetary boundaries [3], in particular in cities [4]. Currently, climate change and circular economy is attracting the most attention, e.g. European Parliament announcing its "Green Deal" following its call for a "climate neutral Europe by 2050" [5].

Circular economy allows environmental strategies along nine "Rs" [6] e.g. with options for raw material savings ("R2 Reduce"), remedial maintenance ("R0 Refuse") or closed material loops ("R8 Recycle"). For decision-makers in the built industry, the question is to what extent innovative building materials can help achieving Sustainable Development Goals #9 to #13 [7].

In this article, carbon concrete composite (CCC) is examined as new type of textile reinforced concrete with promising beneficial raw material savings [8,9] surpassing the "existing range of application specific properties" [10] of mature 'top dog' technologies like steel reinforced concrete

(SRC). CCC is hereby understood as cement-based carbon fiber reinforced composite using a fine-grained concrete [11] and mesh-like textile reinforcements or carbon fiber rods [12]. We will use 'carbon concrete', respectively CCC, as synonym for similar types in this article.

Two German collaborative research centers in Dresden and Aachen, 528 and 532, [13] and the succeeding joint research project "C³ – Carbon Concrete Composite" [14] have intensively studied and tested its mechanical behavior. However, little is known about its impacts on dimensions of sustainability over its entire life cycle. CCC still needs to showcase whether its application is environmentally, socially and financially viable [15]. In case of significant benefits, regulators might reduce impeding market entry barriers to accelerate its dissemination [16].

To close that research gap, we developed a sustainability assessment framework and applied it to variants of a partly or fully prefabricated sandwich wall system of either CCC or SRC. Our research aims to identify hotspots for carbon concrete from a sustainability perspective. Our research is guided by:

1. What impacts (hotspots) are characterizing compared wall systems?
2. What level of energy and resource depletion is embodied in the CCC life cycle?
3. Is substitution of SRC with CCC an eligible economic measure?

An initial systematic review revealed that, to the best of our knowledge, this study adds to the empirical research landscape with an unprecedented sustainability assessment of wall systems made of carbon concrete including company data (see Sect. 3). There is, furthermore, a lack of coherent knowledge about single assessment tools, e.g. life cycle assessment (LCA), applied to building components made of CCC.

For scholars, this article will add insights to existing research dialogues on sustainability assessments in the built industry. For practitioners, signaled hotspots along the value chain of CCC should direct attention to iterative redesign strategies [17]. For civil engineers, material or technology choices within the design process are suggested to improve sustainability at early stage. For city planners, the feasibility and scale for climate mitigation strategies is relevant. The next section

describes applied methods and used material. Results and discussion follow in Sect. 4. Conclusions are drawn in Sect. 5.

3 Material and methods

We began our scoping stage with a systematic literature review following Fink [18] to safeguard rigor evidence-based research practices (Tranfield et al., 2003) and to identify comparable datasets. We then modelled an LCA using GaBi software and a spreadsheet based LCC approach.

3.1 Scoping stage

First, we applied a systematic literature review to explore and synthesize relevant standards, guidelines, and studies on sustainability assessments for CCC or the construction industry in general. Methodological details cannot be presented here. We conclude that a holistic sustainability assessment methodology based on the triple bottom line concept is well established in national and international standards. Recommended practice covers the environmental, economic, and social dimension of sustainability based on technical/functional equivalence, e.g. DIN EN 15643-1:2010 or ISO 15392:2008. Common assessment tools encompass LCA, life cycle costing (LCC), and social life cycle assessment (S-LCA). Nevertheless, the application of complex sustainability assessment frameworks is not trivial: academic research is engaged in discussing aggregation schemes, understanding impact paths, and evaluating trade-offs between all dimensions [19–23].

Second, we systematically screened previous studies for pertinent cases on sustainability, LCA, LCC or S-LCA with respect to CCC or related fiber reinforced composites within construction. For LCA, the majority refers to automotive or railway lightweight design based on thermoplastics, i.e. carbon fiber reinforced plastics (CFRPs) [24–26], different to our understanding of CCC. LCC is often applied to bridges [15] often only including user costs as type of social impact.

In an attempt close to our research objectives, Williams Portal et al. [27] studied various reinforcement technologies, among them SRC and CCC. They quantified its "environmental sustainable potential" with cradle-to-gate LCA. CCC yielded the lowest total environmental impacts. Other projects use glass fibers as base material instead but add economic assessment: Hülsmeyer et al.

Parameter	Variants A-A' (SRC)	Variants B-B' (CCC)	Unit
N.x (outer shell)		- 15 -	kN
M.y (-)		- 0.8 -	kNm/m
U-value		- 0.27 -	W/mK
Sound insulation	76-77	71-73	dB

Table 1: The functional unit for the four sandwich wall variants (own illustration) | graphic: E. Mündecke und K. Schultze

compare design variants of unwearing façade elements made of glass fiber-reinforced concrete, SRC, wood and brick by means of cradle-to-grave LCA [28]. CCC performed better than SRC in terms of global warming (-13 kg CO₂-eq/m²), but worse than a wood framed construction (+115 kg CO₂-eq/m²).

They also showed that an optimized multifunctional vacuum-insulated façade element made of glass fiber-reinforced concrete was outperforming the standard CCC panel (-74 kg CO₂-eq/m²). Our study close these research gaps with non-disclosed company data, updated materials for CCC, and integrating data from cases on recycling potentials of CCC or related recycling processes e.g. pyrolysis [29,30].

3.2 System boundaries

We initially started dimensioning four variants of sandwich wall systems: two each made of SRC (Variants A-A'), respectively CCC (Variants B-B').

They were designed as non-stiffening sandwich outer walls with load-bearing inner shell, thermal insulation, and non-load-bearing outer shell with total dimensions 6x2.8 meters for a 3-storied building. For SRC, the inner shell was supplemented by in situ concrete according to a commercially available Syspro thermowall. Variant A used C25/30, Variant A' C50/60 resulting in slightly different thickness of the wall layers. For CCC, Variant B was fully prefabricated, Variant B' used in

situ concrete supplement C80/95. Our reference functional unit was defined as 1 m² of such partly prefabricated sandwich wall. Functional equivalence had high priority (see Table 1); only sound insulation differed slightly.

A glance at the material weight of all 4 variants reveals: concrete fraction is reduced with CCC (max. -192 kg/m²). Weight of steel reinforcement is 16-22 times that of carbon fiber fabric. Net total weights of SRC variants differ by up to 242 kg/m² (max. +37%).

3.3 LCA approach

The system boundaries of our cradle-to-grave LCAs encompass all life cycle stages except the use phase. We followed the nomenclature of DIN EN 15804:2014 for life cycle stages. For base scenario, service life is assumed 50 years as suggested by German regulatory bodies [31]. Currently, there is no long-term service life scenario above 50 years implemented – that is an opportunity for further research. For use phase, no conversion scenarios, no replacement cycles or maintenance activities were expected. Component layers subject to wear (e.g. paint coats) are not considered, too. As base scenario for end-of-life, we assumed that the building is somewhere in a German major city, the wall is demolished, the building materials are separated and transported to dedicated plants for further processing with pyrolysis. Based on large-scaled experimental data in research sub-project V1.5 of C³ [32,33], we assumed that 95

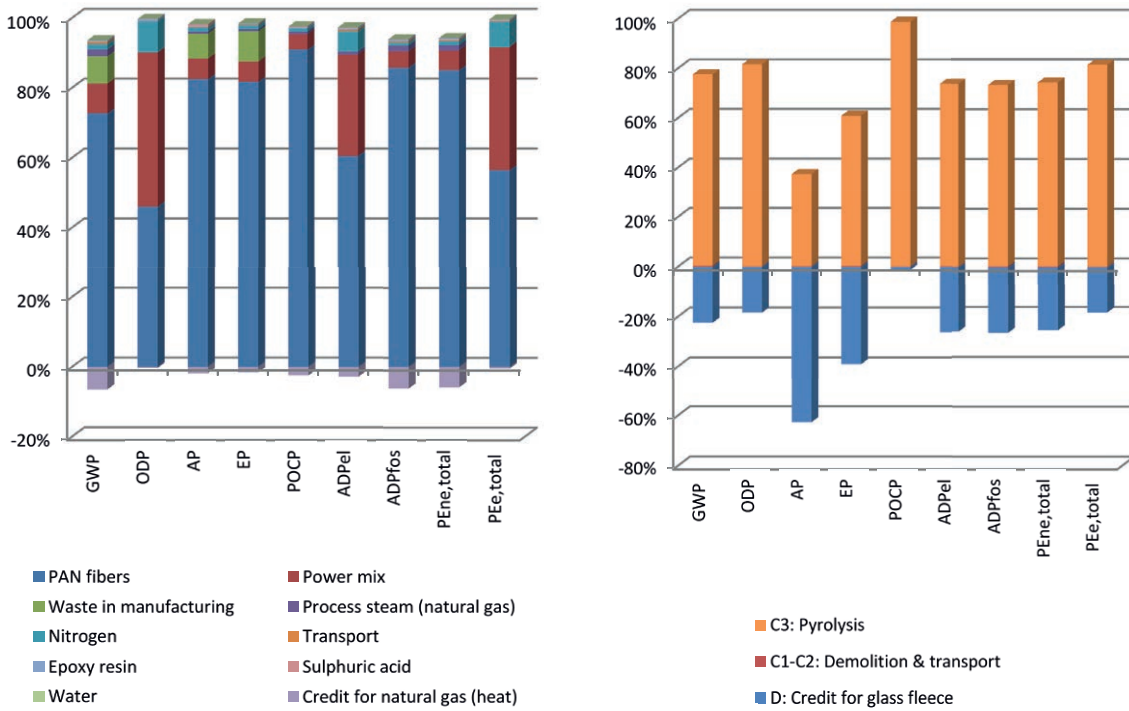


Figure 1: Hotspot analysis for the manufacturing stage of carbon fibers (left) and the end-of-life stage of CCC (right) in (PE = primary energy consumption, PEne = ~ non-renewable, PEe = ~ renewable) | graphic: J. Schütz und C. Scope

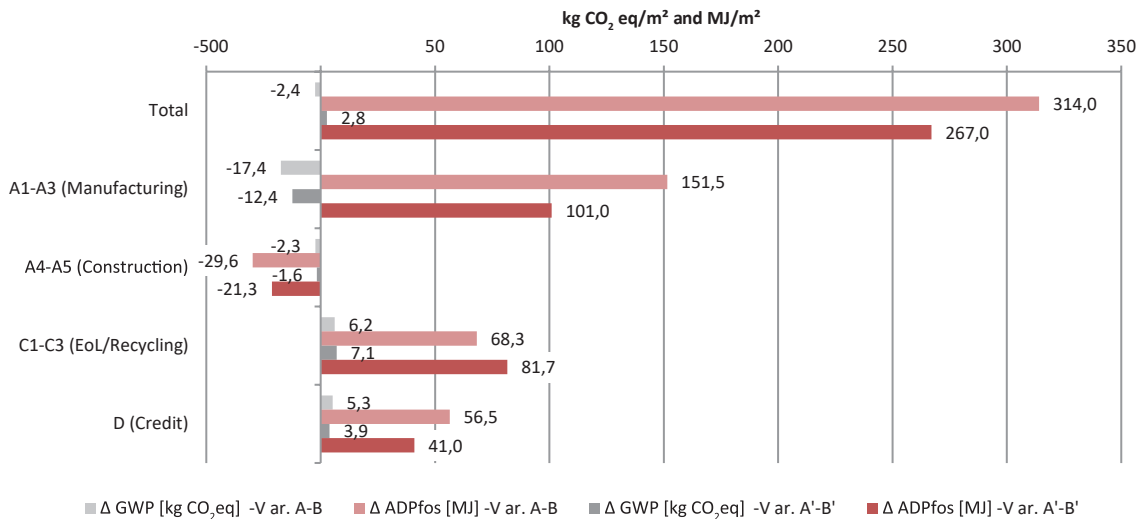


Figure 2: Cradle-to-grave analysis for all wall variants SRC and CCC: differences in global warming (GWP) and abiotic depletion (ADPfos) | graphic: J. Schütz und C. Scope

percent of initial carbon fiber fabric was reclaimed after separation for material reuse in glass fleece production [34]. We credited avoided production of primary glass fleece for the recycled carbon fibers.

Regarding cut-offs, we excluded plants, machines, and infrastructure necessary for manufacturing and construction. The LCA was mostly set-up for

reference area Germany. We used GaBi software and different datasets of GaBi databases. The dataset for special fine-grained concrete mix "C3-B2-HF-2-145-5" similar to C80/95 and carbon fiber rovings was based on research subprojects within C³ [35]. We used non-disclosed data of a manufacturer of carbon fiber fabrics and concrete plants. The dataset for reinforcing steel was based on pub-

lished EPD-BS-10.2 [36], data for stainless steel was sourced from GaBi. We are aware that different data sets exist for reinforcing steel – that is an opportunity for further research. The life cycle impact assessment was based on CML2015 method. LCA follows DIN EN ISO 14040:2009 [49] and DIN EN ISO 14044:2018 [50], respectively recommendations of DIN EN 15643-2:2011 and DIN EN 16757:2017.

4 Preliminary results

We discuss preliminary results of cradle-to-grave LCA, then its economic pendant LCC, and our limitations.

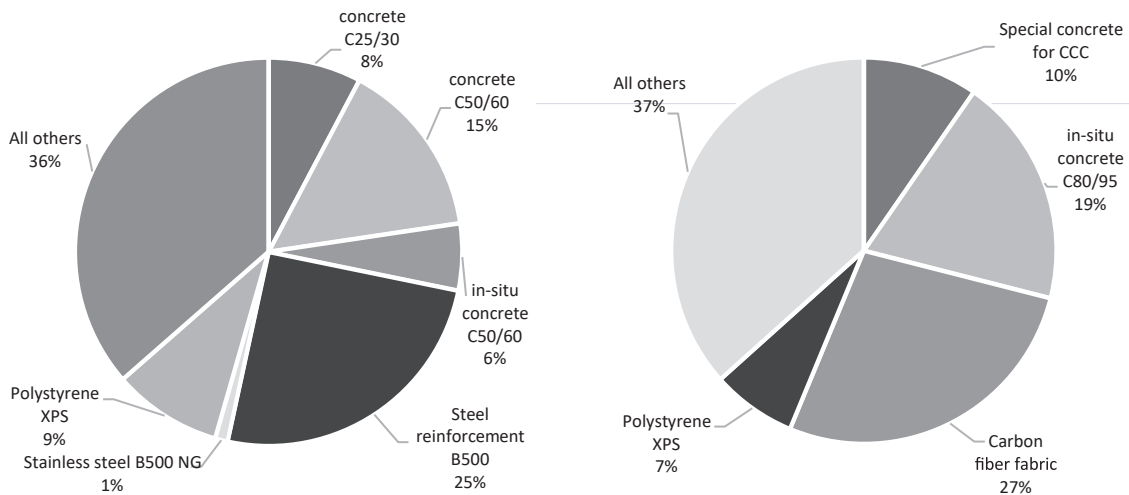


Figure 3: Cost assigned to basic materials over the life cycle for two wall variants A (SRC left) and B' (CCC right) | graphic: K. Schultze und C. Scope

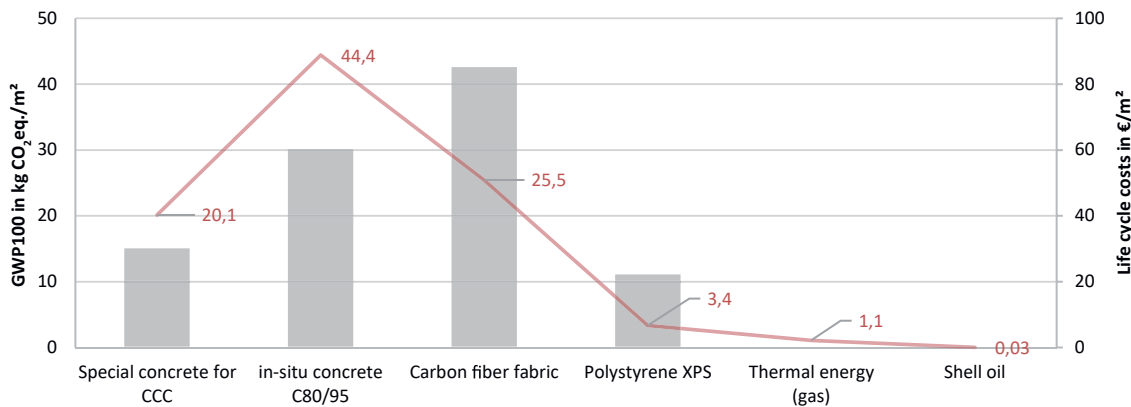


Figure 4: Cost and carbon emissions combined for wall variant B' made of CCC | graphic: C. Scope

3.4 LCC approach

We follow the review of Ilg et al. [15] and DIN EN 15643-4:2012 by assorting costs and revenues along harmonized life cycle stages for described wall variants. We apply a building contractor's perspective: procurement of base materials covers the life cycle stage A1-A2, currently neglecting external costs there. We collected costs data directly from manufacturers and databases [37]. At present, discounting is not included.

4.1 LCA hotspots

First, we refer only to base materials starting with carbon fibers (see Figure 1): the precursor and its succeeding production processes, e.g. oxidation, carbonization and graphitization annealing (named "PAN fiber"), are by far the largest influencing factor with only a mass fraction of approximately 50 percent. Power mix used follows second place. Manufacturing companies should strengthen efficiency programs and increase the share of renew-

ables in their power mix along all upstream activities [26] fostering circular economy strategies “R2 Reduce” [6]. Alternatives to petroleum-based PAN, e.g. lignin, is another valuable strategy for “R0 Refuse” [6]. Low-carbon transition paths for concrete, the other main driver of our LCA results, are published [38,39].

At first glance: current recycling technologies for carbon fiber fabric in CCC offers a true circular economy “R8 Recycle” [6] path. At second sight, the results are dissatisfying: pyrolysis is dominating the total environmental impacts due to its energy intensity. In all but one (i.e. AP, acidification potential) impact category, the crediting for the glass fleece production has a negative net effect. From an environmental point of view, this is far from ideal though better than current difficulties faced for wind turbines [40].

When looking at embodied carbon emissions (only life cycle stages A1-A5), CCC shows better environmental performance: between 13.9-19.7 kg CO₂-eq./m² less than SRC variants. Results of the cradle-to-grave life cycle impact assessment illustrate a close-up race between CCC and SRC. Exemplary, we illustrate the difference in ADPfos (abiotic depletion potential), and GWP scores for each considered life cycle stage (see Figure 2). We state: it depends. Each square meter of variants made of CCC (B and B') either leads to slightly lower or higher carbon emissions (-2.4 or +2.8 kg/m²) compared to SRC. Effects of modelled alternative scenarios could increase the environmental advantage to 9.3-24.3 kg CO₂-eq/m². In any case, CCC is characterized by higher abiotic depletion (+267-314 MJ/m²). Apparently, the value chain of CCC and its carbon fiber fabric uses low-carbon power generation as compared to steel. When calculating specific carbon emissions, CCC performs better with regard to M.x (outer shell): 6.6 versus of 6.8 CO₂-eq./kN/m² for SRC.

4.2 LCC hotspots

Current preliminary economic hotspot analyses show the impact of each base material for total life cycle costs (see Figure 3). A fair third of total costs cannot be directly linked to material choices (category “All others”). This include transport, wages, etc. For companies, this refers to organizational or technological efficiency along the value chain.

Most surprisingly, the share of costs assigned to reinforcement materials differ not so much between CCC and SRC: roughly a quarter of total costs refer to either steel or carbon fiber fabric. The concrete fraction is responsible for 29%. Above all, purchasers could improve contractual agreements to lower purchasing prices, e.g. for special fine-grained or C80/95 concrete, and carbon fiber fabric, as those are driving the overall costs.

Absolute life cycle costs and related carbon emissions are illustrated in Figure 4. For non-disclosure purposes, these costs are neither complete nor correct in size. We observe that, currently, materials with high specific carbon emissions are not sanctioned with market prices. The latter do not reflect externalities related to global warming. For carbon fiber fabric, one spends 3.35 €/kg CO₂-eq. as compared to 1.36 €/kg CO₂-eq. for in-situ concrete C80/95.

4.3 Limitations

Although we applied a scientifically rigor methodology, (model) choices were made with effects on overall results. Subsequently, we present selected limitations.

First, we did not quantify the use of lignin-based PAN to substitute for high purity PAN. There is promising research that illustrates lignin as future, more sustainable sourcing of PAN for thermoplastics [41]. Other alternatives to PAN, e.g. based on algae or waste cotton linter are rather at an experimental stage [42,43] but could also lower geopolitical risks in the value chain. Second, natural fiber materials, e.g. flax, jute or bamboo are not examined as alternative [44]. Third, green concrete [45] encompassing strategies of reducing the share of cement, namely Portland clinker, was not separately modelled in scenarios within our LCA. The special fine-grained concrete applied is an already optimized mix [35]; all other types of concrete are standard industry averages. Fourth, recycled aggregate concrete [46] or other types of concretes with recycle materials were not explicitly modelled in our end-of-life scenarios. This could be a feasible option for both comparing wall systems. So we did not consider that. Fifth, we did not model effects of digitalization, e.g. 3D printing or additive manufacturing [47] although results partly support precasting structural elements of CCC. Sixth, the choice of sandwich wall systems as object of analysis was based on mar-

ket analyses within C³ [14]. Other structural elements with specific environmental circumstances might be more eligible for the deployment of CCC: in cities close to seaside, where a combination of high salt content and steady moisture triggers severe corrosion in SRC. Seventh, our assessment is preliminary in nature. We further add uncertainty analyses. Scenarios are the only but yet unsatisfactory measure. We are planning to apply uncertainty propagation [15,48]. Eight and at last, this article did not yet present results of assessing the social dimension.

5 Conclusions

In this article, the sustainability potential of carbon concrete in comparison to conventional SRC was assessed. Sustainability was hereby limited to assessing the environmental and economic dimension by applied comparative LCA and LCC. Our research aimed to identify existing comparative advantages for new, innovative building materials like carbon concrete from these two perspectives.

This article was guided by three research questions. First, we show that the manufacturing stage, in particular of carbon fiber and concrete, as well as recycling technologies in end-of-life stage are dominating the environmental impacts for both wall systems. Second, we quantified embodied carbon emissions for each material life cycle. In base scenario, difference amounts to 13.9-19.7 kg CO₂-eq./m² in manufacturing and construction stages. Results for cradle-to-grave carbon emissions are much closer: intervall varies between -2.4 or +2.8 kg CO₂-eq/m². Alternative scenarios may increase the environmental advantage for CCC up to 9.3-24.3 kg CO₂-eq/m². Third, we illustrated economic feasibility for two variants. Currently, CCC faces challenges in its cost structure typical for innovations with little economies of scale in comparison to mature technologies like SRC. Market prices also do not reflect externalities, therefore not sanctioning the use of materials like concrete in SRC variants.

In summary, our assessment indicates that the carbon concrete uses less material that could lead to lower total carbon emissions, but depends on design variants for CCC itself. Thus, carbon concrete may improve the climate mitigation potential of buildings. Building professionals and planners should study the new material CCC and start piloting building projects, in particular in exposed environments. This study's limitations were exten-

sively discussed in Sect. 4.3. Above all, we recommend to apply presented method to other building components of CCC and to extend the scope to all dimensions of sustainability. In short-term, future research will improve the existing LCA and LCC model by adding uncertainty analyses and analyzing data quality effects. In the long run, we would love to engage in a dialogue with a wider scholarly community for a more holistic sustainability assessment and plausibility checks with practitioners. Carbon concrete faces the challenge of non-selection ("overlooked" [27]) because of comparing higher upfront research and development and manufacturing costs with respect to technological incumbents like SRC.

6 Acknowledgements

The authors thank the German Federal Ministry of Education and Research for funding the program "Twenty20 — Partnership for Innovation" and the entailed project "Carbon Concrete Composite".

7 References

- [1] European Commission (EU-COM) 2019 Construction Intern. Mark. Ind. Entrep. SMEs
- [2] Abergel T, Dean B, Dulac J, Hamilton I, Wheeler T and International Energy Agency (IEA) 2018 Towards a zero-emission, efficient, and resilient buildings and construction sector: Global Status Report 2017 (United Nations Environment Programme (UNEP))
- [3] Rockström J 2015 Bounding the Planetary Future: Why We Need a Great Transition Gt. Transit. Initiat. 14
- [4] Randers J, Rockström J, Stoknes P E, Golüke U, Collste D and Cornell S 2018 Transformation is feasible. How to achieve the Sustainable Development Goals within Planetary Boundaries (Stockholm, SE: Stockholm Resilience Centre)
- [5] European Commission (EU-COM) 2018 The Commission calls for a climate neutral Europe by 2050 Clim. Action - Eur. Comm.
- [6] Potting J, Hekkert M, Worrell E and Hanemaaijer A 2017 Circular economy: measuring innovation in the product chain (The Hague, NL: Netherlands Environmental Assessment Agency (PBL))
- [7] United Nations 2019 About the Sustainable Development Goals U. N. Sustain. Dev.
- [8] Frenzel M, Lieboldt M and Curbach M 2014 Concrete light: Balcony slabs with carbon reinforcement Beton- Stahlbetonbau 109 713–25
- [9] Curbach M, Schladitz F, Weselek J and Zobel R 2017 Eine Vision wird Realität: Der Betonbau der Zukunft ist nachhaltig, leicht, flexibel und formbar - dank Carbon. Für Sanierung oder Neubau sind jetzt Decken und Wände, Fuß- und Radwegbrücken, Bögen [only in German] Prüfingenieur 51 20–35
- [10] Curbach M and Jesse F 2009 Eigenschaften und Anwendung von Textilbeton [only in German] Beton- Stahlbetonbau 104 9–16
- [11] Anon 2006 State-of-the-Art Report of RILEM TC 201-TRC: Textile reinforced concrete (Bagneux, FR: RILEM Publications S.A.R.L.)
- [12] Kulas C, Karle R, Hegger J and Goralski C 2014 A sustainable pedestrian bridge made of textile-reinforced concrete Bridge Maintenance, Safety, Management and Life Extension ed Chen, A and Frangopol, DM and Ruan, X (Boca Raton, US-FL: CRC Press) pp 2100–7
- [13] Ehlig D, Schladitz F, Frenzel M and Curbach M 2012 Textilbeton – Ausgeführte Projekte im Überblick [only in German] Beton- Stahlbetonbau 107 777–85

- [14] C³ – Carbon Concrete Composite e. V. 2019 About C³ - Carbon Concrete Composite
- [15] Ilg P, Hoehne C and Guenther E 2016 High-performance materials in infrastructure: a review of applied life cycle costing and its drivers – the case of fiber-reinforced composites *J. Clean. Prod.* 112 926–45
- [16] Naor M, Bernardes E S, Druhl CT and Shifan Y 2015 Overcoming barriers to adoption of environmentally-friendly innovations through design and strategy *Int. J. Oper. Prod. Manag.*
- [17] Millet D, Bistagnino L, Lanzavecchia C, Camous R and Poldma T 2007 Does the potential of the use of LCA match the design team needs? *J. Clean. Prod.* 15 335–46
- [18] Fink A 2019 *Conducting Research Literature Reviews: From the Internet to Paper* (Los Angeles, US-CA: Sage Publications)
- [19] Sala S, Ciuffo B and Nijkamp P 2015 A systemic framework for sustainability assessment *Ecol. Econ.* 119 314–25
- [20] Villares M, İşildar A, Giesen C van der and Guinée J 2017 Does ex ante application enhance the usefulness of LCA? A case study on an emerging technology for metal recovery from e-waste *Int. J. Life Cycle Assess.* 22 1618–33
- [21] Helbig C, Gemechu E D, Pillain B, Young S B, Thorenz A, Tuma A and Sonnemann G 2016 Extending the geopolitical supply risk indicator: Application of life cycle sustainability assessment to the petrochemical supply chain of polyacrylonitrile-based carbon fibers *J. Clean. Prod.* 137 1170–8
- [22] van Breugel K 2018 How models can make a difference for a sustainable future of the building industry *Mater. Struct.* 51 161
- [23] Panesar D K, Seto K E and Churchill C J 2017 Impact of the selection of functional unit on the life cycle assessment of green concrete *Int. J. Life Cycle Assess.* 22 1969–1986
- [24] Das S 2011 Life cycle assessment of carbon fiber-reinforced polymer composites *Int. J. Life Cycle Assess.* 16 268–82
- [25] Albrecht S, Baumann M, Brandstetter C P, Horn R, Krieg H, Fischer M and Ilg R 2013 Environmental aspects of lightweight construction in mobility and manufacturing *Green Design, Materials and Manufacturing Processes* ed Bartolo, HM and Bartolo, PJD and Alves, NMF and Mateus, AJ and Almeida, HA and Lemos, ACS and Craveiro, F and Ramos, C and Reis, I and Durao, L and Ferreira, T and Duarte, JP and Roseta, F and Costa, ECE and Quaresma, F and Neves, JP (Boca Raton, US-FL: CRC Press) pp 185–90
- [26] Hohmann A, Albrecht S, Lindner J P, Voringner B, Wehner D, Drechsler K and Leistner P 2018 Resource efficiency and environmental impact of fiber reinforced plastic processing technologies *Prod. Eng.-Res. Dev.* 12 405–17
- [27] Williams Portal N, Lundgren K, Wallbaum H and Malaga K 2015 Sustainable Potential of Textile-Reinforced Concrete. *J. Mater. Civ. Eng.* 27 1–12
- [28] Hülsmeier F, Kahnt A, Grauer O, Huth S, Kirmse S and Tietze M 2013 vakutex - Vacuum-insulated textile concrete facade elements (Leipzig, DE: University of Applied Sciences)
- [29] Kimm M, Gerstein N, Schmitz P, Simons M and Gries T 2018 On the separation and recycling behaviour of textile reinforced concrete: an experimental study *Mater. Struct.* 51 122
- [30] Meng F, Olivetti E A, Zhao Y, Chang J C, Pickering S J and McKechnie J 2018 Comparing Life Cycle Energy and Global Warming Potential of Carbon Fiber Composite Recycling Technologies and Waste Management Options *ACS Sustain. Chem. Eng.* 6 9854–65
- [31] Federal Institute for Research on Building, Urban Affairs and Spatial Development (BBSR) 2017 Nutzungsdauern von Bauteilen für Lebenszyklusanalysen nach Bewertungssystem Nachhaltiges Bauen (BNB) [only in German] (Berlin, DE: BBSR)
- [32] C³ – Carbon Concrete Composite e. V. and Kortmann J 2019 C3-V1.5 Abbruch, Rückbau und Recycling von C3-Bauteilen [only in German]
- [33] Kopf F, Kortmann J and Jehle P 2019 Recycling an reuse of carbon fiber reinforcement *Proceedings of the Seventh International Conference on Structural Engineering, Mechanics and Computation 2019 SEMC2019, September 02-04 2019 (Cape Town, ZA)* pp 1543–7
- [34] STFI e. V. Chemnitz 2020 *Textile recycling Research*
- [35] Schneider K, Butler M and Mechtcherine V 2017 Carbon Concrete Composites C3 - Sustainable binders and concretes for the future *Beton- Stahlbetonbau* 112 784–94
- [36] Badische Stahlwerke GmbH (BSW) 2018 *Betonstahl (EPD-BS-10.2). Umweltproduktdeklaration nach ISO 14025 und EN 15804* [only in German] (Rosenheim, DE: ift)
- [37] f:data GmbH 2020 *Baupreislexikon für Architekten und Planer*
- [38] Becke A, Reiners J and Sülün C 2014 *Erläuterungen zu den Umweltproduktdeklarationen von Beton* [only in German] (Erkrath, DE: InformationsZentrum Beton GmbH)
- [39] Kisić M, Ferguson C, Clarke C and Smyth J 2018 *Building pressure. Which cement companies will be left behind in the low-carbon transition?* (London, UK: CDP)
- [40] Hao S, Kuah AT H, Rudd C D, Wong K H, Lai N Y G, Mao J and Liu X 2020 A circular economy approach to green energy: Wind turbine, waste, and material recovery *Sci. Total Environ.* 702 135054
- [41] Souto F, Calado V and Pereira N Jr 2018 Lignin-based carbon fiber: a current overview *Mater. Res. EXPRESS* 5
- [42] Zhou X, Wang P, Zhang Y, Zhang X and Jiang Y 2016 From Waste Cotton Linter: A Renewable Environment-Friendly Biomass Based Carbon Fibers Preparation *ACS Sustain. Chem. Eng.* 4 5585–93
- [43] Arnold U, Brück T, De Palmenaer A and Kuse K 2018 Carbon Capture and Sustainable Utilization by Algal Polyacrylonitrile Fiber Production: Process Design, Techno-Economic Analysis, and Climate Related Aspects *Ind. Eng. Chem. Res.* 57 7922–33
- [44] Carvalho H, Raposo A, Ribeiro I, Kaufmann J, Goetze U, Pecas P and Henriques E 2016 Application of Life Cycle Engineering approach to assess the pertinence of using natural fibers in composites - the rocker case study 23rd CIRP Conference on Life Cycle Engineering *Procedia CIRP* vol 48, ed Seliger, G and Kruger, J (Amsterdam, NL: Elsevier Science BV) pp 364–9
- [45] Limbachiya M, Bostanci S C and Kew H 2014 Suitability of BS EN 197-1 CEM II and CEM V cement for production of low carbon concrete *Constr. Build. Mater.* 71 397–405
- [46] Akhtar A and Sarmah A K 2018 Construction and demolition waste generation and properties of recycled aggregate concrete: A global perspective *J. Clean. Prod.* 186 262–81
- [47] Tian X, Liu T, Wang Q, Dilmurat A, Li D and Ziegmann G 2017 Recycling and remanufacturing of 3D printed continuous carbon fiber reinforced PLA composites *J. Clean. Prod.* 142 1609–18
- [48] Groen E A, Heijungs R, Bokkers E A M and de Boer I J M 2014 Methods for uncertainty propagation in life cycle assessment *Environ. Model. Softw.* 62 316–25
- [49] DIN EN ISO 14040:2009-11 – Umweltmanagement – Ökobilanz – Grundsätze und Rahmenbedingungen (ISO 14040:2006) [only in German]
- [50] DIN EN ISO 14044:2018-05 – Umweltmanagement – Ökobilanz – Anforderungen und Anleitungen (ISO 14044:2006 + Amd 1:2017) [only in German]
- [51] DIN EN 15643-2:2011-05 – Nachhaltigkeit von Bauwerken – Bewertung der Nachhaltigkeit von Gebäuden – Teil 2: Rahmenbedingungen für die Bewertung der umweltbezogenen Qualität (EN 15643-2:2011) [only in German]
- [52] DIN EN 16757:2017-10 – Nachhaltigkeit von Bauwerken – Umweltproduktdeklarationen – Produktkategorieregeln für Beton und Betonelemente (EN 16757:2017) [only in German]

Meister des Mischens

Jahrzehntelange Erfahrung mit dem Mischen, Dosieren und Fördern von unterschiedlichsten Materialien und Zuschlägen vereint zu höchster Qualität und Produktivität in KNIELE Mischanlagen.

Innovation

Die innovativen Produkte der KNIELE GmbH finden Einzug in unterschiedlichste Industriezweige mit immer wachsenden Anforderungen und wir sind Teil dieser rasanten und aufregenden Entwicklung.

KNIELE Konusmischer

Unser patentierter Konusmischer KKM meistert jede Herausforderung und ist ein wahrer „Meisters des Mischens“.

Von Hochleistungsbetonen über selbstverdichtende Betone bis hin zu Faserbetonen - Der Intensivmischer KKM liefert herausragende Mischergebnisse.

Durch seine konische Bauform bringt der KKM weitere Vorteile mit sich:

Sie ermöglicht das Mischen von Kleinstmengen, eine restlose Entleerung innerhalb weniger Sekunden, eine einfache und schnelle Reinigung von Hand oder automatisiert sowie schnelle Produktwechsel wie zum Beispiel Farbwechsel. Weiter kann die Mischgeschwindigkeit stufenlos geregelt und somit optimal an die erforderliche Mischqualität angepasst werden.

Mit Anlagen in über 35 Ländern weltweit ist KNIELE Ihr kompetenter Partner in Sachen Mischen, Dosieren und Fördern.

Besuchen Sie uns online auf kniele.de und kontaktieren Sie uns noch heute.

Wir freuen uns auf Sie!



blending • dosing • conveying - Made in Germany



FON: +49 7582 9303 - 0

Mail: info@kniele.de

www.kniele.de



kniele.de

Kniele GmbH • Gemeindebeunden 6 • 88422 Bad Buchau

Ihre Zufriedenheit durch unsere Qualität
und Zuverlässigkeit.

Seit mehr als vier Jahrzehnten bestimmt die Firma PAGEL® Spezial-Beton GmbH & Co. KG, Essen, die Entwicklung von Verguss-, Reparatur- und Spezialmörteln. Dabei sind insbesondere die PAGEL® Verguss-Mörtel-systeme mit der bekannten Marke V1® sowie die PAGEL® Betoninstandsetzungs-Mörtel für ihre gleichbleibende und stets höchste Qualität bekannt - und das weltweit seit mehr als 45 Jahren!

Verguss

- › Standardverguss
- › Schnellverguss
- › Hochfestverguss
- › Sonderanwendungen

Betoninstandsetzung

- › Korrosionsschutz und Haftbrücke
- › Konstruktive Instandsetzung
- › Instandsetzung
- › Abwasser
- › Trinkwasser
- › Oberflächenschutz

Industrieböden und Verkehrsflächen

- › Industrieboden-Haftbrücke
- › Industrieboden
- › Reparaturbeton

Bauprodukte

- › Blitzmörtel

Reaktionsharze

- › Epoxidharz-Mörtel

PAGEL®
Spezial-Beton

VERGUSS
BETONINSTANDSETZUNG
INDUSTRIEBÖDEN & VERKEHRSFLÄCHEN
BAUPRODUKTE
REAKTIONSHARZE



PAGEL Spezial-Beton GmbH & Co. KG

Tel. +49 201 68504 0
Fax +49 201 68504 31

Wolfsbankring 9 · 45355 Essen
www.pagel.com · info@pagel.com



Übersicht der > C³-Partner

- **Adolf Würth GmbH Co. KG**
Reinhold-Würth-Straße 12, 74653 Künzelsau
- **AIB GmbH**
Liselotte-Herrmann-Straße 4, 02625 Bautzen
- **Albani Group GmbH & Co. KG**
Steinerne Furt 44, 86167 Augsburg
- **ALHO Systembau GmbH**
Hammer 1, 51598 Friesenhagen
- **Assmann Beraten + Planen AG**
Reichenbachstraße 55, 01069 Dresden
- **Augel GmbH**
Windkaulweg 1, 56745 Weibern
- **BARG Betontechnik u. -instandsetzungs GmbH & Co. KG**
Potsdamer Straße 23/24, 14163 Berlin
- **Bauhaus-Universität Weimar, F. A. Finger-Institut für Baustoffkunde**
Coudraystraße 11, 99423 Weimar
- **Baustoffprüflabor Müller & Lobisch GmbH**
Am Gewerbepark 8, 04860 Süptitz
- **Bauunternehmen Torsten Sperling**
In der Lache 11, 63697 Hirzenhain
- **Bautenschutz Müller GmbH**
An der Jägerbäk 2, 18069 Rostock
- **Bauwerke – Management – Systeme AG**
Sohlweg 76, 41372 Niederkrüchten
- **BCS Natur- und Spezialbaustoffe GmbH**
Hammerweg 25, 01127 Dresden
- **Betonwerk Oschatz GmbH**
Mühlberger Straße 17–19, 04758 Oschatz
- **BNB Beton- und Naturstein Babelsberg GmbH**
Walter-KLauschstraße 17a, 14482 Cottbus
- **Brandenburgische Technische Universität Cottbus-Senftenberg, Lehrstuhl Massivbau**
Konrad-Wachsmann-Allee 2, 03046 Cottbus
- **Bundesanstalt für Wasserbau – Referat Baustoffe**
Kußmaulstraße 17, 76187 Karlsruhe
- **CARBOCON GmbH**
Ammonstraße 72, 01067 Dresden
- **CHT Germany GmbH**
Postfach 1280, 72002 Tübingen
- **Clement Germany GmbH**
Grubenstraße 48, 18055 Rostock
- **DBF Deutsche Basalt Faser GmbH**
Carl-Rabe-Straße 11, 06526 Sangerhausen
- **Deutscher Ausschuss für Stahlbeton e. V. (DAfStb)**
Budapester Straße 31, 10787 Berlin
- **Deutscher Beton- und Bautechnik-Verein e. V.**
Kurfürstenstraße 129, 10785 Berlin
- **Deutsches Zentrum für Luft- und Raumfahrt e. V. – Institut für Bauweisen und Strukturtechnologie**
Pfaffenwaldring 38–40, 70569 Stuttgart
- **Dipl. Ing. H. Bendl Hoch- und Tiefbau GmbH & Co. KG Sebnitz**
Kreuzstraße 3a, 01855 Sebnitz

- **Diubal Software GmbH**
Am Zellweg 2, 93464 Tiefenbach
- **dresden | exists**
01062 Dresden
- **Dreßler Bau GmbH**
Müllerstraße 26, 63741 Aschaffenburg
- **DuraPact 2.0 Kompetenzzentrum Faserbeton GmbH**
Büssingstraße 4, 42781 Haan
- **DYWIDAG-Systems International GmbH**
Siemensstraße 8, 85716 Unterschleißheim
- **EBF Dresden GmbH**
Clara-Zetkin-Straße 31, 01159 Dresden
- **EIPOS GmbH**
Freiberger Straße 37, 01067 Dresden
- **EK Bauwerkabdichtung von Glasenapp GmbH**
Salmdorfer Straße 1, 85540 Haar
- **EurA AG**
Am Köhlersgehäu 60, 98544 Zella-Mehlis
- **Evonik Ressource Efficiency GmbH**
Rodenbacher Chaussee 4, 63457 Hanau
- **Fachhochschule Münster**
Corrensstraße 25, 48149 Münster
- **Fachvereinigung Deutscher Betonfertigteilebau e. V. (FDB)**
Postfach 21 02 67, 53157 Bonn
- **Filmaton**
Karl-Liebknecht-Straße 133, 04275 Leipzig
- **Fischer Bauabdichtung GmbH**
Bahnhof Frauendorf 3, 04654 Frohburg
- **Fraunhofer-Institut für Angewandte Polymerforschung IAP, Forschungsbereich Polymermaterialien und Composite PYCO**
Kantstraße 55, 14513 Teltow
- **Fraunhofer-Zentrum für Internationales Management und Wissensökonomie Gruppe Geschäftsmodelle: Engineering und Innovation**
Städtisches Kaufhaus, Neumarkt 9-19, 04109 Leipzig
- **GINKGO Projektentwicklung GmbH**
An der Pikardie 6, 01277 Dresden
- **Goldbeck Ost GmbH**
Zum Bahndamm 18, 08233 Treuen
- **GQ Quadflieg Bau GmbH**
Schumannstraße 18, 52146 Würselen
- **Groz-Beckert KG**
Parkweg 2, 72458 Albstadt
- **Grötz GmbH & Co. KG**
Jahnstr. 19, 76571 Gaggenau
- **Gustav Gerster GmbH & Co. KG, Geschäftsbereich Gerster TechTex**
Memminger Straße 18, 88400 Biberach/Riss
- **Halfen GmbH**
Liebigstraße 14, 40764 Langenfeld
- **HÄNDLE GmbH Maschinen und Anlagenbau**
Industriestraße 47, 75417 Mühlacker
- **HEBAU GmbH**
Postfach 1308, 87517 Sonthofen
- **HeidelbergCement AG**
Oberklamweg 6, 69181 Leimen
- **Hentschke Bau GmbH**
Zeppelinstraße 15, 02625 Bautzen
- **Hering Bau GmbH & Co. KG**
Neuländer 1, 57299 Burbach
- **HFB Engineering GmbH**
Zschortauer Straße 42, 04129 Leipzig
- **Hitexbau GmbH**
Steinerne Furt 44, 86167 Augsburg
- **Hochschule für Technik und Wirtschaft Dresden, Fakultät Bauingenieurwesen/ Architektur**
Friedrich-List-Platz 1, 01069 Dresden
- **Hochschule für Technik, Wirtschaft und Kultur Leipzig**
Karl Liebknecht Straße 132, 04277 Leipzig
- **Holcim (Deutschland) GmbH**
Willy-Brandt-Straße 69, 20457 Hamburg
- **Hörnig Bauwerkssanierung GmbH**
Magnolienweg 5, 63741 Aschaffenburg
- **HUESKER Synthetic GmbH**
Fabrikstraße 13-15, 48712 Gescher
- **IAB – Institut für Angewandte Bauforschung Weimar gGmbH**
Über der Nonnenwiese 1, 99428 Weimar
- **ICL Ingenieur Consult Dr.-Ing. A. Kolbmüller GmbH**
Diezmannstraße 5, 04207 Leipzig
- **Implenia Construction GmbH, Baustofftechnik**
Martin-Luther-Ring 13, 04109 Leipzig
- **Implenia Instandsetzung GmbH**
Zielstattstraße 19, 81379 München
- **InformationsZentrum Beton GmbH**
Hannoversche Straße 21, 31319 Sehnde
- **Ingenieurbüro Grassl GmbH**
Hertzstraße 20, 13158 Berlin
- **Ingenieurbüro Roland Fink**
Blumenstraße 16, 01445 Radebeul
- **Ingenieurbüro Säbisch**
Spinnereistraße 7, 04179 Leipzig
- **INROS LACKNER SE**
Sachsendorfer Straße 2, 03051 Cottbus
- **Institut für Korrosionsschutz Dresden GmbH**
Gostritzer Straße 65, 01217 Dresden
- **Johne & Groß GmbH**
Kamenzer Straße 18, 01936 Schwepnitz
- **JORDAHL GmbH**
Nobelstraße 51, 12057 Berlin
- **kahnt und tietze ug (haftungsbeschränkt)**
Anna-Kuhnnow-Straße 39, 04317 Leipzig
- **KARL MAYER Technische Textilien GmbH**
Mauersbergerstraße 2, 09117 Chemnitz
- **Klaus Raps Beteiligungs GmbH**
Hohenmarkstraße 116a, 61440 Oberursel (Taunus)
- **Klebl GmbH**
Köthener Straße 40, 06388 Südliches Anhalt
- **Kniele GmbH**
Köthener Straße 40, 06388 Südliches Anhalt
- **Kordes + Ziegenhorn Partner**
Emil-Ueberall-Straße 5, 01159 Dresden

- **Laumer Bautechnik GmbH**
Bahnhofstraße 8, 84323 Massing
- **Lefatex Chemie GmbH**
Stiegstraße 64, 41379 Brüggen
- **Leibniz-Institut für Polymerforschung Dresden e. V.**
Hohe Straße 6, 01069 Dresden
- **Leichtbau-Zentrum Sachsen GmbH**
Marschnerstraße 39, 01307 Dresden
- **LISt Gesellschaft für Verkehrswesen und ingenieurtechnische Dienstleistungen GmbH**
Ernst-Thälmann-Str. 5, 09661 Hainichen
- **Materialforschungs- und -prüfanstalt an der Bauhaus-Universität Weimar**
Postfach 2310, 99404 Weimar
- **Max Bögl Bauservice GmbH & Co. KG**
Max-Bögl-Str. 2, 07546 Gera
- **maxit Baustoffwerke GmbH**
Brandensteiner Weg 1, 07387 Krölpa
- **Meißner Hoch-, Tief- und Straßenbau GmbH**
Ölbergstraße 4-6, 53840 Troisdorf
- **MFPA Leipzig GmbH**
Postfach 74 11 06, 04323 Leipzig
- **Müller Fugensysteme GmbH**
Niederdorfstraße 57, 01877 Rammenau
- **NU Informationssysteme GmbH**
Bahnhofstraße 4, 01587 Riesa
- **OPTERRA Karsdorf GmbH**
Straße der Einheit 25, 06638 Karsdorf
- **PAGEL Spezial-Beton GmbH & Co. KG**
Wolfsbankring 9, 45355 Essen
- **PAULSBERG OHG**
Loschwitzer Straße 56, 01309 Dresden
- **Photonion GmbH**
Hagenower Straße 73, 19061 Schwerin
- **Planning GmbH**
Eichertstraße 10, 56745 Weibern
- **pmp Projekt GmbH, Gesellschaft für Projektentwicklung und Generalplanung mbH**
Domlinden 21, 14776 Brandenburg
- **Podobnik Bohr und Säge GmbH**
Elly-Beilhorn-Str. 2, 69214 Eppelheim
- **Prignitz Mikrosystemtechnik GmbH**
Margarethenstraße 61, 19322 Wittenberge
- **Qpoint Composite GmbH**
Breitscheidstraße 78, 01237 Dresden
- **Reisch Ingenieure GmbH**
Pröllstraße 14, 86157 Augsburg
- **Rekers Betonwerk GmbH & Co. KG**
Portlandstraße 15, 48480 Spelle
- **Ruhr-Universität Bochum, Fakultät Bau- und Umweltingenieurwissenschaften, Lehrstuhl Baustofftechnik**
Universitätsstraße 150, 44801 Bochum
- **RWTH Aachen, Institut für Massivbau**
Mies-van-der-Rohe-Straße 1, 52074 Aachen
- **RWTH Aachen University, Institut für Bauforschung, Lehrstuhl für Baustoffkunde**
Schinkelstraße 3, 52062 Aachen
- **Sächsisches Textilforschungsinstitut e. V. (STFI)**
Annaberger Straße 240, 09125 Chemnitz
- **SAERTEX GmbH & Co. KG**
Brochterbecker Damm 52, 48369 Saerbeck
- **SCALE GmbH**
Donaustraße 7, 85049 Ingolstadt
- **Schill + Seilacher „Struktol“ GmbH**
Moorfleeter Straße 28, 22113 Hamburg
- **schlaich bergemann und partner.sbp gmbh**
Schwabstraße 43, 70197 Stuttgart
- **Schlatter Deutschland GmbH & Co. KG**
Dahlweg 105, 48163 Münster
- **Schöck Bauteile GmbH**
Vimbucher Straße 2, 76534 Baden-Baden
- **SC Tiefbau GmbH**
Austr. 6, 72320 Kirchheim unter Teck
- **SGL Carbon GmbH**
Werner-von-Siemens-Straße 18, 86405 Meitingen
- **Sika Deutschland GmbH**
Kornwestheimer Straße 103-107, 70439 Stuttgart
- **SKZ-KFE gGmbH**
Friedrich-Bergius-Ring 22, 97076 Würzburg
- **Solidian GmbH**
Sigmaringer Straße 150, 72458 Albstadt
- **Specht Kalleja & Partner GmbH**
Keplerstraße 8-10, 10589 Berlin
- **Stäubli GmbH**
Theodor-Schmidt-Straße 19, 95448 Bayreuth
- **steinbeisser GmbH**
Max-Planck-Ring 8, 06188 Landsberg/OT Queis
- **STL Heizsysteme GmbH**
Florian-Geyer-Straße 7, 01307 Dresden
- **Synthomer Deutschland GmbH**
Werrastraße 10, 45768 Marl
- **Syspro-Gruppe Betonbauteile e. V.**
Hanauer Straße 31, 63526 Erlensee
- **T A R K U S IngenieurSanierung GmbH**
Hochbergweg 2, 12207 Berlin
- **Technische Universität Berlin, Fachgebiet Entwerfen und Konstruieren – Massivbau**
Gustav-Meyer-Allee 25, 13355 Berlin
- **Technische Universität Chemnitz, Fakultät Maschinenbau, Institut für Strukturleichtbau, Professur Strukturleichtbau und Kunststoffverarbeitung**
Reichenhainer Straße 31/33, 09126 Chemnitz
- **Technische Universität Darmstadt, Ernst-Berl-Institut für Technische und Makromolekulare Chemie**
Alarich-Weiss-Straße 8, 64287 Darmstadt
- **Technische Universität Darmstadt, Fachgebiet Massivbau**
Franziska-Braun-Straße 3, 64287 Darmstadt
- **Technische Universität Dresden, Fakultät Bauingenieurwesen, Institut für Massivbau**
01062 Dresden
- **Technische Universität Dresden, Fakultät Bauingenieurwesen, Institut für Statik und Dynamik der Tragwerke**
01062 Dresden

- **Technische Universität Dresden, Fakultät Bauingenieurwesen, Institut für Baustoffe – IfB**
01062 Dresden
- **Technische Universität Dresden, Fakultät Bauingenieurwesen, Institut für Baubetriebswesen**
01062 Dresden
- **Technische Universität Dresden, Fakultät Architektur, Institut für Bauklimatik**
01062 Dresden
- **Technische Universität Dresden, Fakultät Wirtschaftswissenschaften, Lehrstuhl für Betriebliche Umweltökonomie**
01062 Dresden
- **Technische Universität Dresden, Fakultät Maschinenwesen, Institut für Textilmaschinen und Textile Hochleistungswerkstofftechnik – ITM**
01062 Dresden
- **Technische Universität Dresden, Fakultät Maschinenwesen, Institut für Leichtbau und Kunststofftechnik – ILK**
01062 Dresden
- **Technische Universität Dresden, Fakultät Maschinenwesen, Institut für Verfahrenstechnik und Umwelttechnik, Arbeitsgruppe Mechanische Verfahrenstechnik**
01062 Dresden
- **Technische Universität Dresden, Fakultät Maschinenwesen, Institut für Werkzeugmaschinen und Steuerungstechnik – IWM**
01062 Dresden
- **Technische Universität Dresden, Fakultät Elektrotechnik und Informationstechnik, Institut für Nachrichtentechnik, Lehrstuhl Hochfrequenztechnik**
01062 Dresden
- **Teijin Carbon Europe GmbH**
Kasinostraße 19-21, 42103 Wuppertal
- **texton e. V.**
Alte Dresdner Straße 99, 01108 Dresden
- **thones® Dichtungstechnik GmbH**
Zeppelinstraße 15, 01665 Klipphausen
- **thyssenkrupp Carbon Components GmbH**
Frankenring 1, 01723 Kesselsdorf
- **ToPAS GmbH**
Oskar-Röder-Straße 12, 01237 Dresden
- **TORKRET GmbH**
Langemarckstraße 39, 45141 Essen
- **TUDAG**
Freiberger Straße 37, 01067 Dresden
- **TUDALIT e. V.**
Freiberger Straße 37, 01067 Dresden
- **TUDATEX GmbH**
Freiberger Straße 37, 01067 Dresden
- **UNGER Bau-Systeme GmbH**
Donauwörther Straße 2, 09114 Chemnitz
- **Universalbeton Heringen GmbH & Co. KG**
Nordhäuser Straße 2, 99765 Heringen
- **Universität Rostock, Institut für Chemie, Abteilung Analytische und Technische Chemie**
Dr.-Lorenz-Weg 1, 18059 Rostock
- **Universität Stuttgart, Institut für Leichtbau, Entwerfen und Konstruieren – ILEK**
Pfaffenwaldring 14, 70569 Stuttgart
- **VDZ gGmbH**
Postfach 30 10 63, 40410 Düsseldorf
- **VETRA Betonfertigteilwerke GmbH**
Industriestraße 6, 26802 Neermoor
- **Weber Betonwerk GmbH**
Industriestraße 3-5, 97258 Ippesheim
- **WILHELM KNEITZ Solutions in Textile GmbH**
Holzwiesenweg 17, 95028 Hof/Saale
- **Wilhelm Wallbrecht GmbH & Co. KG**
Adelheidstraße 24, 30171 Hannover
- **WTM Engineers GmbH**
Johannisbollwerk 6-8, 20459 Hamburg
- **Zeisberg Carbon GmbH**
Voltmerstraße 65, 30165 Hannover
- **Ziegelwerk Arnach GmbH & Co. KG**
Ziegeleistraße 1, 88410 Bad Wurzach

Stand: August 2020



solidian

Wegweiser für den Baustoff der Zukunft.



build solid.

Wir sind Experten für nicht-metallische Bewehrungen aus Carbon-, Glas-, oder Basaltfasern. Mit einem eigenen Entwicklungslabor und der engen Zusammenarbeit mit führenden universitären Forschungseinrichtungen arbeiten wir an innovativen Lösungen für die Baubranche.

solidian steht für Innovation, Technologie und erstklassigen Service. Mit einem Team, bestehend aus 270 Mitarbeitern an zwei Standorten, erarbeiten wir für unsere Kunden praxisrelevante Lösungen für Bauwerke und Konstruktionen von Morgen.



Unsere nicht-metallischen Bewehrungen haben zahlreiche Vorteile:



Leicht



bis zu 7x stärker
als Stahl



Nicht
ätzend



Starke
Verbindung



Niedrigere
Transportkosten



Einfache
Handhabung



Niedrigere
Instandhaltungskosten



Chlorid
beständig

solidian GmbH

📍 Sigmaringer Straße 150
72458 Albstadt, Deutschland

✉ info@solidian.com

🌐 www.solidian.com

☎ P +49 7431 10-3135

☎ F +49 7431 10-63135

Kelteks d.o.o.

📍 Dr. Slavka Rozgaja 3
47000 Karlovac, Croatia

✉ info@solidian-kelteks.com

🌐 www.solidian.com

☎ P +385 47 693 300

☎ F +385 47 434 203



Impressum

Herausgeber

C³ – Carbon Concrete Composite e. V.
Ammonstraße 72
01067 Dresden
Tel. +49 351 484 567-00
Fax +49 351 484 567-10
post@bauen-neu-denken.de
www.bauen-neu-denken.de

TUDALIT e. V.
Freiberger Str. 37
01067 Dresden
Tel. +49 351 404 704-10
Fax +49 351 404 703-10
info@tudalit.de
www.tudalit.de

Redaktion

TUDALIT e. V. und C³ – Carbon Concrete Composite e. V. übernehmen keinerlei Gewähr für die Aktualität, Korrektheit, Vollständigkeit und/oder Qualität der bereitgestellten Informationen.

Inhaltliche Prüfung

Kerstin Schön | TUDALIT e. V.
Dr.-Ing. Frank Schladitz | C³ – Carbon Concrete Composite e. V.

Korrekturen

Kerstin Schön | TUDALIT e. V.

Design, Layout, digitale Bildbearbeitung, Druckvorstufe

Stefan Gröschel

Druck

Addprint AG | Gewerbegebiet Am Spitzberg 8a, 01728 Bannechwitz/Possendorf

Stand

September 2020

Fotos/Bildnachweis

Stefan Gröschel, Iurii Vakaliuk

Auflage

100 Exemplare

Herzlichen Dank an unsere Unterstützer:





www.bauen-neu-denken.de



www.tudalit.de